Title
The mechanistic role of the clathrin light chain subunits in cell function

Permalink
https://escholarship.org/uc/item/9cj4b9dx

Author
Majeed, Sophia Rafaa

Publication Date
2015

Peer reviewed|Thesis/dissertation

The mechanistic role of the clathrin light subunits in cell function

by

Sophia R. Majeed

DISSERTATION

Submitted in partial satisfaction of the requirements for the degree of

DOCTOR OF PHILOSOPHY

in

Pharmaceutical Sciences and Pharmacogenomics

in the

GRADUATE DIVISION

of the

UNIVERSITY OF CALIFORNIA, SAN FRANCISCO

Acknowledgements

I would like to thank my PhD thesis advisor, Dr. Frances Brodsky, for all of her support and scientific guidance throughout my time in graduate school. Frances has provided me with mentorship when I needed it, and has given me the freedom to think independently and pursue my own scientific ideas. She has constantly challenged me to think creatively and tackle big problems that don't have simple answers. As a woman and as a scientist, Frances has inspired me to persevere in the face of challenges. She has taught me that even the most insurmountable difficulties can be overcome with the right combination of diligence, passion and determination. Thank you for providing me with the tools to become a critical and creative independent researcher.

I would like to thank my other mentors who have had a profound impact on me, both on a scientific and personal level, during my time at UCSF. I would like to thank Drs. Mike Bishop and Mark von Zastrow for serving on my thesis committee and providing me with mentorship and scientific direction. They encouraged me to think about the larger implications of my research and provided me with invaluable feedback. I would also like to thank Drs. Deanna Kroetz, Bill Weiss and Diane Barber for serving on my qualifying exam committee. My mentors in the PSPG graduate program have had a significant impact on my trajectory and development as a scientist, and have enriched my graduate experience over the last five years. Thank you Drs. Deanna Kroetz, Steve Hamilton and Leslie Benet for your generous mentorship and advice. I would also like to thank Debbie Acoba-Idelbi for seamlessly handling everything related to PSPG, and for being a wonderful source of support during my time in the graduate program.

I would like to thank all of the members of the Brodsky lab who have been instrumental to both my scientific and personal development. I can honestly say that I have loved every moment of my PhD, and this was because I was fortunate enough to be surrounded by

Contributions to presented work

Chapter 2 of this dissertation contains work that was published in *Nature Communications*:

Majeed, S.R., L. Vasudevan*, C.Y. Chen*, Y. Luo*, J.A. Torres, T.M. Evans, A. Sharkey, A.B. Foraker, N.M. Wong, C. Esk, T.A. Freeman, A. Moffett, J.H. Keen, and F.M. Brodsky. 2014. Clathrin light chains are required for the gyrating-clathrin recycling pathway and thereby promote cell migration. *Nat Commun* 5:3891.
*equal contribution

This was a long-term project under the guidance of Frances Brodsky, initiated by Jean Chen and Lavanya Vasudevan, who performed biochemical experiments and 2D cell migration experiments, respectively. I generated stable cell lines, performed biochemical, 2D cell migration, chemotaxis and fixed-cell imaging experiments in which levels of CLCs and CLC mutants were manipulated. Yi Luo and Jim Keen contributed live imaging studies and interpretation of these studies. Theresa Freeman contributed analytical tools. Andrew Sharkey and Ashley Moffett contributed sample material and performed the gene expression analysis. Timothy Evans generated CLC-Hip binding mutants. Jorge Torres, Nicole Wong, Christopher Esk and Amy Foraker contributed to the generation of stable cell lines.

Chapter 3 of this dissertation contains unpublished material in preparation for submission to The Journal of Experimental Medicine:

Shuang Wu*, Sophia R. Majeed*, Timothy M. Evans, Marine Camus+, Nicole M.L. Wong+, Yvette Schollmeier, Minjong Park, Jagen R. Muppidi, Peter Parham, Jason G. Cyster[#]

and Frances M. Brodsky[#]. Elevated IgA phenotype resulting from clathrin light chains

role in cargo selection.

*,+equal contribution, #co-corresponding author

The mechanistic role of the clathrin light chain

subunits in cell function

Sophia R. Majeed

Abstract

Clathrin is a coat protein that mediates membrane traffic by capturing and transporting cargo between different cellular compartments. It is composed of heavy and light chain subunits, which coat membranes of budding vesicles involved in receptor-mediated endocytosis and organelle biogenesis. Clathrin-mediated endocytosis (CME) of many cargoes can occur in the absence of CLCs, however recent studies have demonstrated that they are required for specialized clathrin functions that require actin assembly through binding the actin-organizing huntingtin-interacting proteins (Hip). Since cell migration requires both clathrin and actin, we investigated the role of the CLCs in this pathway. Inhibition of CLC function by siRNA-mediated depletion and by expression of a dominant negative CLC decrease cell migration and recycling of inactive β1 integrin. These CLC functions occur through Hip binding. CLC depletion and expression of a dominant negative CLC also reduce the appearance of gyrating (G)-clathrin structures, which mediate rapid recycling of transferrin receptor, implicating G-clathrin in these pathways. These results demonstrate that CLCs' ability to link clathrin to actin is necessary for important cellular functions like cell migration and led us to ask which CLC functions are physiologically relevant *in vivo*. We addressed this question by genetically engineering mice lacking the CLCa isoform. Murine tissue analyses indicated that lymphoid tissues express predominantly CLCa, which prompted a detailed investigation of these cell types in the CLCa mutant mice. Immunoglobulin class switch recombination between IgA and IgG is impaired in the germinal center B cells of the CLCa-deficient mice, which stems from CLCs' role in mediating TGFβR2 endocytosis. CLCs are also necessary for CME of CXCR4 and the delta

opioid receptor but not the β2 agonist receptor or CXCR5, indicating that CLCs exhibit differential cargo selectivity. Thus, our results reveal that CLCs play an important role in CME for a subset of signaling receptors *in vivo*. Moreover, these studies demonstrate that CLCs influence a broad range of physiological functions including cell migration and adaptive immune responses through their regulation of clathrin coat dynamics*.*

Table of Contents

List of Figures

1. Chapter 1: Introduction

Part 1: Clathrin structure, biology, and function

1. Clathrin biology and function

Cells interact with their external environment by signaling through the numerous and varied receptors on their surface. Once these receptors are activated, they are internalized from the plasma membrane and shuttled to endosomes, where they can be sorted for recycling back to the surface or further transported to lysosomes for degradation. This process allows cells to quickly respond to their changing environment by regulating the composition of receptors and other signaling proteins on their surface. Bacteria and large virus particles can also take advantage of this internalization pathway in order to evade immune surveillance and promote infection (Bonazzi et al. 2011; Bonazzi et al. 2012; Cureton et al. 2010). The predominant mechanisms through which these processes occur involve clathrin.

Eukaryotic cells have membrane-bound organelles that perform specialized functions, and thus they require vesicle trafficking to transport proteins, metabolites and other cellular molecules between these compartments. Clathrin was the first transport protein to be identified and consequently its biochemistry, cellular functions and interactions with adaptor proteins have been extensively characterized (Brodsky et al. 2001; Pearse 1976; Roth and Porter 1964; Kadota and Kaneseki 1969). In addition to clathrin, cells have two other types of coat proteins that facilitate cargo selection for membrane traffic. The COPII-coated vesicles mediate cargo selection for export from the endoplasmic reticulum (ER) through the Golgi apparatus and COPI-coated vesicles capture cargo from the Golgi and traffic them back to the ER (Barlowe 2000).

Clathrin is a self-assembling coat protein that forms a lattice around budding vesicles during receptor-mediated endocytosis at the plasma membrane and during protein sorting at the

trans-Golgi network during lysosomal biogenesis. During clathrin-mediated endocytosis (CME), adaptor proteins target clathrin to membranes and induce the formation of the clathrin lattice around the emerging clathrin-coated vesicle (CCV). Three clathrin heavy chain (CHC) subunits trimerize into a triskelion (3-legged), which serve as the building blocks of the clathrin polyhedral lattice coat. The predominant CHC isoform, CHC17, associates with the clathrin light chain (CLC) subunits in a 1:1 stoichiometric ratio (Brodsky et al. 2001).

2. Clathrin light chain characteristics and function

Vertebrates have two isoforms of CLCs that are encoded by separate chromosomes in humans, CLCa and CLCb, while yeast, insects and invertebrates have only a single CLC. Mammalian CLCs share ~60% protein sequence identity and both undergo alternative splicing. CLCa has four splice variants, while CLCb has two. The CLC isoforms have characteristic tissue-specific expression patterns, and clathrin triskelia are heterogeneously composed of CLCa and CLCb depending on their relative levels in the cell. The CLCs bind CHC through a central domain and both have a calcium-binding site near the N-terminus. CLCa also has a binding site for the uncoating protein hsc70, which can promote disassembly of the clathrin coat (Brodsky et al. 2001).

CLCs bind to the hub domain of the clathrin triskelion, which is composed of the C-terminal portion of CHC and formed by their trimerization (Wilbur et al. 2010; Chen and Brodsky 2005). CLCs regulate CME by stabilizing the CHC trimer and prevent spontaneous assembly of the clathrin lattice *in vitro* through a patch of three negatively charged residues near their N-termini (Ybe et al. 1998; Ybe et al. 2007; Wilbur et al. 2010). Structural models of CLCs reveal that they influence clathrin function by holding the "knee" of CHC in a straight conformation, preventing assembly (Wilbur et al. 2010). Regulation of spontaneous coat formation by CLCs makes clathrin susceptible to positive regulation by adaptor proteins within the cell (Brodsky et al. 2001). Given that CLCs have an important role in regulation of clathrin assembly, it is

remarkable that they are dispensable for CME of many classical cargoes, including the epidermal growth factor receptor (EGFR) and transferrin receptor (Huang et al. 2004). However, a recent study implicated the CLCs in the CME of three G-protein coupled receptors (GPCRs), raising the possibility that CLCs may have specialized functions in CME (Ferreira et al. 2012).

3. Hip proteins: the link between CLCs and actin

Both CLCs share a 22-residue consensus sequence near the N-terminus that binds members of the Huntingtin-interacting protein family (referred to as Hip proteins), Hip1 and Hip1R, and Sla2p in yeast (Chen and Brodsky 2005; Legendre-Guillemin et al. 2005). The Hip proteins contain an N-terminal ANTH domain for phospholipid binding, a central coiled-coiled domain that binds CLC, and a C-terminal THATCH domain that binds actin (Legendre-Guillemin et al. 2005; Chen and Brodsky 2005; Engqvist-Goldstein and Drubin 2003; Legendre-Guillemin et al. 2002). The Hip proteins bind clathrin and actin sequentially, and can influence actin assembly during CME. During CCV formation, clathrin-associated Hip proteins on the lattice have low affinity for actin, which negatively regulates actin assembly on the coat. However, Hip proteins near the neck of the budding vesicle can directly bind to the membrane through their ANTH domain and dissociate from CLCs, which increases Hip's affinity for actin and promotes actin filament assembly at that location (Wilbur et al. 2008; Engqvist-Goldstein et al. 2001). Thus, Hip proteins can organize and direct actin assembly for cellular processes that require both clathrin and actin.

4. CLCs and cell migration: a shared connection

Numerous cellular functions require coordination of membrane traffic with actin dynamics. One such process is cell migration, which is crucial for development, wound healing, and immune cell function. If dysregulated, cell migration can contribute to pathologies including cancer and autoimmune diseases. Cell migration consists of several coordinated, spatiotemporally regulated processes, including rapid actin polymerization, trafficking of

3

adhesion proteins and addition of membrane to the leading edge. Further, focal adhesions are disassembled and internalized, and myosin II-dependent contractile events mediate contraction of the cell rear (Reig, Pulgar, and Concha 2014; Vicente-Manzanares 2013). Transport of newly synthesized integrins to the plasma membrane for focal adhesion assembly, uptake of integrins from existing focal adhesions, and recycling of integrins back to the surface all require membrane traffic, and there is emerging evidence that some of these pathways also require actin (Fang et al. 2010; Zech et al. 2011).

Several studies have shown that $\beta 1$ integrin is internalized through a clathrin-dependent pathway, and that CHC17 is required for disassembly of focal adhesions, and thus for cell motility (Chao and Kunz 2009; Ezratty et al. 2009; Nishimura and Kaibuchi 2007; Teckchandani et al. 2009; Teckchandani et al. 2012). However, clathrin may make additional contributions to cell migration through its CLC-Hip actin-organizing function. Once receptors are internalized, they are sorted in endosomes for degradation or recycling. Cargo that is destined for recycling can be sorted into distinct subdomains of the endosome. A subset of these tubular endocytic microdomains are stabilized by local actin polymerization, which allows sequence-specific accumulation of cargo into the recycling tubules (Puthenveedu et al. 2010). Since CHC17 was implicated in integrin recycling, we speculated that this clathrin function was mediated by CLC binding to Hip proteins, which can influence local actin polymerization for cargo selection through recycling tubule stabilization (Li et al. 2007). This speculation was investigated and proved to be correct, as described in Chapter 2 of this thesis.

5. CLC function *in vivo*

Several CLC functions have been characterized in cell lines; however there have been limited studies that dissect CLC function in *in vivo* models. Interestingly, a recent study identified a role for CLCs in Drosophila eye development through interaction with leucine-rich repeat kinase 2 (LRRK2) on endosomes (Schreij et al. 2015). However the physiological functions of

the CLC in the context of an *in vivo* vertebrate model have yet to be addressed. Although there are many benefits of using cell lines to investigate the function of a biomolecule, including feasibility and cost, there are also several disadvantages. One disadvantage is that there are many interacting physiological factors in a whole, intact animal that are needed to produce a biological response. Therefore, when some substances are administered to cells or denervated tissues, no response may be observed if the cognate receptor is not present in the specific cell type, or if the biological response requires tissue innervation. Further, complex physiological regulatory mechanisms and genetic interactions are lost in tissue culture studies, as only regulation at the cellular level can be determined using this method (Murphy 1991). Thus, it is imperative to conduct *in vivo* studies to understand the function of a protein in the context of a whole organism. Chapter 3 of this thesis describes initial efforts to study CLC function in vivo.

Part 2: Objectives of thesis

Clathrin orchestrates numerous membrane traffic pathways in the cell. While the heavy chain subunit is necessary for all clathrin functions identified to date, the light chain subunits are only required for certain specialized clathrin functions, most of which require actin polymerization. The goal of this study was to use molecular and biochemical methods to identify new functions of CLCs and characterize their physiological role in a vertebrate model. In chapter 2, I present work that identifies a key role for CLCs in cell migration through recycling of inactive β1 integrin adhesion proteins. I describe additional biochemical and imaging experiments that were undertaken to assess the contribution of CLC-Hip protein binding to CLC-dependent cell migration and recycling. In chapter 3, I present studies that investigate the dominant phenotypes in a genetically engineered mouse lacking the CLCa isoform. I illustrate a comprehensive murine tissue analysis, which led us to examine the immune compartment of the mice. I further describe molecular and *in vivo* studies to characterize the immune defect in these mice and

define the molecular mechanism for this effect. In chapter 5, I present the major conclusions

resulting from this work, and discuss future directions and implications of these studies.

References

Barlowe, C. 2000. 'Traffic COPs of the early secretory pathway', *Traffic*, 1: 371-7.

Bonazzi, M., A. Kuhbacher, A. Toledo-Arana, A. Mallet, L. Vasudevan, J. Pizarro-Cerda, F. M. Brodsky, and P. Cossart. 2012. 'A common clathrin-mediated machinery co-ordinates cell-cell adhesion and bacterial internalization', *Traffic*, 13: 1653-66.

Bonazzi, M., L. Vasudevan, A. Mallet, M. Sachse, A. Sartori, M. C. Prevost, A. Roberts, S. B. Taner, J. D. Wilbur, F. M. Brodsky, and P. Cossart. 2011. 'Clathrin phosphorylation is required for actin recruitment at sites of bacterial adhesion and internalization', *J Cell Biol*, 195: 525-36.

Brodsky, F. M., C. Y. Chen, C. Knuehl, M. C. Towler, and D. E. Wakeham. 2001. 'Biological basket weaving: formation and function of clathrin-coated vesicles', *Annu Rev Cell Dev Biol*, 17: 517-68.

Chao, W. T., and J. Kunz. 2009. 'Focal adhesion disassembly requires clathrin-dependent endocytosis of integrins', *FEBS Lett*, 583: 1337-43.

Chen, C. Y., and F. M. Brodsky. 2005. 'Huntingtin-interacting protein 1 (Hip1) and Hip1-related protein (Hip1R) bind the conserved sequence of clathrin light chains and thereby influence clathrin assembly in vitro and actin distribution in vivo', *J Biol Chem*, 280: 6109-17.

Cureton, D. K., R. H. Massol, S. P. Whelan, and T. Kirchhausen. 2010. 'The length of vesicular stomatitis virus particles dictates a need for actin assembly during clathrin-dependent endocytosis', *PLoS Pathog*, 6: e1001127.

Engqvist-Goldstein, A. E., and D. G. Drubin. 2003. 'Actin assembly and endocytosis: from yeast to mammals', *Annu Rev Cell Dev Biol*, 19: 287-332.

Engqvist-Goldstein, A. E., R. A. Warren, M. M. Kessels, J. H. Keen, J. Heuser, and D. G. Drubin. 2001. 'The actin-binding protein Hip1R associates with clathrin during early stages of endocytosis and promotes clathrin assembly in vitro', *J Cell Biol*, 154: 1209-23.

Ezratty, E. J., C. Bertaux, E. E. Marcantonio, and G. G. Gundersen. 2009. 'Clathrin mediates integrin endocytosis for focal adhesion disassembly in migrating cells', *J Cell Biol*, 187: 733-47.

Fang, Z., N. Takizawa, K. A. Wilson, T. C. Smith, A. Delprato, M. W. Davidson, D. G. Lambright, and E. J. Luna. 2010. 'The membrane-associated protein, supervillin, accelerates F-actin-dependent rapid integrin recycling and cell motility', *Traffic*, 11: 782-99.

Ferreira, F., M. Foley, A. Cooke, M. Cunningham, G. Smith, R. Woolley, G. Henderson, E. Kelly, S. Mundell, and E. Smythe. 2012. 'Endocytosis of G protein-coupled receptors is regulated by clathrin light chain phosphorylation', *Curr Biol*, 22: 1361-70.

Huang, F., A. Khvorova, W. Marshall, and A. Sorkin. 2004. 'Analysis of clathrin-mediated endocytosis of epidermal growth factor receptor by RNA interference', *J Biol Chem*, 279: 16657-61.

Kadota, K., and T. Kaneseki. 1969. 'Isolation of a synaptic vesicle fraction from guinea pig brain with the use of DEAE-sephadex column chromatography and some of its properties', *J Biochem*, 65: 839-42.

Legendre-Guillemin, V., M. Metzler, M. Charbonneau, L. Gan, V. Chopra, J. Philie, M. R. Hayden, and P. S. McPherson. 2002. 'HIP1 and HIP12 display differential binding to F-actin, AP2, and clathrin. Identification of a novel interaction with clathrin light chain', *J Biol Chem*, 277: 19897-904.

Legendre-Guillemin, V., M. Metzler, J. F. Lemaire, J. Philie, L. Gan, M. R. Hayden, and P. S. McPherson. 2005. 'Huntingtin interacting protein 1 (HIP1) regulates clathrin assembly through direct binding to the regulatory region of the clathrin light chain', *J Biol Chem*, 280: 6101-8.

Li, J., P. J. Peters, M. Bai, J. Dai, E. Bos, T. Kirchhausen, K. V. Kandror, and V. W. Hsu. 2007. 'An ACAP1-containing clathrin coat complex for endocytic recycling', *J Cell Biol*, 178: 453-64.

Murphy, H. Claire. 1991. 'The Use of Whole Animals Versus Isolated Organs or Cell Culture in Research', *Transactions of the Nebraska Academy of Sciences and Affiliated Societies*, XVIII: 105-08.

Nishimura, T., and K. Kaibuchi. 2007. 'Numb controls integrin endocytosis for directional cell migration with aPKC and PAR-3', *Dev Cell*, 13: 15-28.

Pearse, B. M. 1976. 'Clathrin: a unique protein associated with intracellular transfer of membrane by coated vesicles', *Proc Natl Acad Sci U S A*, 73: 1255-9.

Puthenveedu, M. A., B. Lauffer, P. Temkin, R. Vistein, P. Carlton, K. Thorn, J. Taunton, O. D. Weiner, R. G. Parton, and M. von Zastrow. 2010. 'Sequence-dependent sorting of recycling proteins by actin-stabilized endosomal microdomains', *Cell*, 143: 761-73.

Reig, G., E. Pulgar, and M. L. Concha. 2014. 'Cell migration: from tissue culture to embryos', *Development*, 141: 1999-2013.

Roth, T. F., and K. R. Porter. 1964. 'Yolk Protein Uptake in the Oocyte of the Mosquito Aedes Aegypti. L', *J Cell Biol*, 20: 313-32.

Schreij, A. M., M. Chaineau, W. Ruan, S. Lin, P. A. Barker, E. A. Fon, and P. S. McPherson. 2015. 'LRRK2 localizes to endosomes and interacts with clathrin-light chains to limit Rac1 activation', *EMBO Rep*, 16: 79-86.

Teckchandani, A., E. E. Mulkearns, T. W. Randolph, N. Toida, and J. A. Cooper. 2012. 'The clathrin adaptor Dab2 recruits EH domain scaffold proteins to regulate integrin beta1 endocytosis', *Mol Biol Cell*, 23: 2905-16.

Teckchandani, A., N. Toida, J. Goodchild, C. Henderson, J. Watts, B. Wollscheid, and J. A. Cooper. 2009. 'Quantitative proteomics identifies a Dab2/integrin module regulating cell migration', *J Cell Biol*, 186: 99-111.

Vicente-Manzanares, M. 2013. 'Cell migration: cooperation between myosin II isoforms in durotaxis', *Curr Biol*, 23: R28-9.

Wilbur, J. D., C. Y. Chen, V. Manalo, P. K. Hwang, R. J. Fletterick, and F. M. Brodsky. 2008. 'Actin binding by Hip1 (huntingtin-interacting protein 1) and Hip1R (Hip1-related protein) is regulated by clathrin light chain', *J Biol Chem*, 283: 32870-9.

Wilbur, J. D., P. K. Hwang, J. A. Ybe, M. Lane, B. D. Sellers, M. P. Jacobson, R. J. Fletterick, and F. M. Brodsky. 2010. 'Conformation switching of clathrin light chain regulates clathrin lattice assembly', *Dev Cell*, 18: 841-8.

Ybe, J. A., B. Greene, S. H. Liu, U. Pley, P. Parham, and F. M. Brodsky. 1998. 'Clathrin self-assembly is regulated by three light-chain residues controlling the formation of critical salt bridges', *EMBO J*, 17: 1297-303.

Ybe, J. A., S. Perez-Miller, Q. Niu, D. A. Coates, M. W. Drazer, and M. E. Clegg. 2007. 'Light chain C-terminal region reinforces the stability of clathrin heavy chain trimers', *Traffic*, 8: 1101-10.

Zech, T., S. D. Calaminus, P. Caswell, H. J. Spence, M. Carnell, R. H. Insall, J. Norman, and L. M. Machesky. 2011. 'The Arp2/3 activator WASH regulates alpha5beta1-integrin-mediated invasive migration', *J Cell Sci*, 124: 3753-9.

2. Chapter 2: Clathrin light chain subunits promote cell migration

Cell motility requires spatiotemporal coordination of several complex processes, including actin polymerization at the leading edge, focal adhesion assembly and disassembly, and myosin II-dependent contractile events (Reig, Pulgar, and Concha 2014). It is becoming increasingly clear that membrane trafficking of integrins plays a crucial role in cell motility. Integrins are heterodimeric adhesion receptors composed of non-covalently associated α and β subunits (Jacquemet, Humphries, and Caswell 2013). Several studies have established clathrin-mediated endocytosis (CME) as the major route of internalization for integrins, which mediates disassembly of focal adhesions and promotes cell migration (Chao and Kunz 2009; Nishimura and Kaibuchi 2007; Ezratty et al. 2009; Teckchandani et al. 2009; Teckchandani et al. 2012). Once integrins are internalized, they can be sorted for degradation or recycling back to the plasma membrane. Since integrins turnover at a relatively slow rate, recycling plays a major role in determining the availability of integrins at the cell surface (Jacquemet, Humphries, and Caswell 2013). Recent studies have demonstrated that recycling of integrins is critical for the formation of focal adhesion complexes and cell migration (Bridgewater, Norman, and Caswell 2012; Steinberg et al. 2012; Bottcher et al. 2012). As an example, sorting nexin-17 (SNX17) can rescue $\beta 1$ integrin and its associated α subunit from lysosomal degradation, leading to integrin recycling and cell motility (Bottcher et al. 2012; Steinberg et al. 2012). Further, siRNA depletion of CHC17 reduces recycling of $\beta 1$ integrin, however the contribution of CLCs was not assessed in these studies (Li et al. 2007).

There is increasing evidence that the clathrin light chain (CLC) subunits contribute to clathrin functions by linking the clathrin coat to the actin cytoskeleton. While they are not required for CME of several classical cargoes in mammals, CLCs are necessary for many clathrin pathways that require actin (Huang et al. 2004; Poupon et al. 2008). CLCs can influence actin polymerization through interactions with the actin-binding Hip proteins, Hip1 and Hip1R,

and contribute to actin recruitment during cell-cell contact formation and CME when the plasma membrane is under tension (Bonazzi et al. 2011; Bonazzi et al. 2012; Boulant et al. 2011). Likewise, integrin recycling pathways have also been shown to exhibit actin dependence, which raised the possibility that these pathways may also require CLCs (Fang et al. 2010; Zech et al. 2011; Duleh and Welch 2012).

To characterize the role of the CLCs in cell migration, we performed functional 2D migration studies in CLC and Hip-depleted cells. To further understand the mechanistic role of CLCs and their interaction with Hip proteins in this process, I performed biochemical and immunofluorescence-based recycling experiments in cells in which CLC protein levels and their Hip-binding abilities were manipulated. These results define a new function for the CLCs in cell migration and cargo recycling. Further, it broadens the range of CLCs' actin-organizing functions and showcases their importance in mediating physiological clathrin functions.

The rest of this chapter is comprised of work that was published in *Nature Communications* (Majeed et al. 2014). Below is the full text of the manuscript that was accepted for submission, and was modified slightly upon publication.

CLATHRIN LIGHT CHAINS ARE REQUIRED FOR THE GYRATING-CLATHRIN RECYCLING PATHWAY AND THEREBY PROMOTE CELL MIGRATION

Sophia R. Majeed[1,2,3,4], Lavanya Vasudevan*[1,2,3,4], Chih-Ying Chen*[1,2,3,4], Yi Luo*[5],

Jorge A. Torres[1,2,3,4], Timothy M. Evans[1,2,3,4], Andrew Sharkey[7], Amy B. Foraker[1,2,3,4], Nicole

M.L. Wong[1,2,3,4], Christopher Esk[1,2,3,4], Theresa A. Freeman[6], Ashley Moffett[7], James H. Keen[5]

and Frances M. Brodsky[1,2,3,4]

*equal contribution

[1]Department of Bioengineering and Therapeutic Sciences, [2]Department of

Pharmaceutical Chemistry, [3]Department of Microbiology and Immunology, [4]The G.W. Hooper

Foundation, University of California San Francisco, San Francisco, CA 94143, USA,

[5]Department of Biochemistry and Molecular Biology, Thomas Jefferson University, Philadelphia,

PA, 19107, [6]Department of Orthopedic Surgery, Thomas Jefferson University, Philadelphia, PA,

19107, USA, [7]Department of Pathology and Centre for Trophoblast Research, University of

Cambridge, Cambridge, UK

Corresponding author address:

Frances M. Brodsky

The G. W. Hooper Foundation, HSW 1529, Box 0552

University of California San Francisco

513 Parnassus Avenue

San Francisco, CA 94143-0552, USA

Phone: +1-415-476-6406; Fax: +1-415-476-6185

Email: Frances.Brodsky@ucsf.edu

Abstract

The clathrin light chain (CLC) subunits participate in several membrane traffic pathways involving both clathrin and actin, through binding the actin-organizing huntingtin-interacting proteins (Hip). However, CLCs are dispensable for clathrin-mediated endocytosis of many cargoes. Here we observe that CLC depletion affects cell migration through Hip binding and reduces surface expression of $\beta 1$ integrin by interference with recycling following normal endocytosis of inactive $\beta 1$ integrin. CLC depletion and expression of a modified CLC also inhibit the appearance of gyrating (G)-clathrin structures, known mediators of rapid recycling of transferrin receptor from endosomes. Expression of the modified CLC reduces $\beta 1$ integrin and transferrin receptor recycling, as well as cell migration, implicating G-clathrin in these processes. Supporting a physiological role for CLC in migration, the CLCb isoform of CLC is upregulated in migratory human trophoblasts during uterine invasion. Together, these studies establish CLCs as mediating clathrin-actin interactions needed for recycling by G-clathrin during migration.

Clathrin plays a key role in intracellular membrane traffic by polymerizing into a membrane-associated latticed coat that captures cargo during receptor-mediated endocytosis and organelle biogenesis (Brodsky 2012). The lattice-forming clathrin triskelion is composed of trimerized clathrin heavy chain (CHC) subunits, which comprise the determinants for self-assembly. The major CHC isoform (CHC17) is bound by clathrin light chain (CLC) subunits that extend half way along the triskelion leg. There are two CLCs in vertebrates (CLCa and CLCb) with characteristic tissue-specific expression. Though their cellular functions have yet to be fully defined, CLCs stabilize CHC17 trimerization and regulate lattice formation *in vitro* (Ybe et al. 2013; Wilbur et al. 2010). While depletion of CHC17 globally impairs clathrin-mediated endocytosis (CME), the only known cargos affected by CLC depletion are certain G-protein-coupled receptors (Hinrichsen et al. 2003; Huang et al. 2004; Poupon et al. 2008; Ferreira et al. 2012). Uptake of transferrin receptor, epidermal growth factor (EGF) receptor, cation-independent-mannose-6-phosphate receptor and low-density lipoprotein receptor occur in the absence of CLC (Huang et al. 2004; Poupon et al. 2008). However, depletion of CLC effectively inhibits internalization of cargo such as bacteria and virus particles that are too large for conventional CME but require clathrin and actin for uptake (Bonazzi et al. 2011; Cureton et al. 2010). CLCs are also required for internalization from villous membranes under tension on mammalian cells and from the yeast plasma membrane under turgor pressure, processes that likewise require actin (Boulant et al. 2011; Boettner et al. 2011). These actin-dependent clathrin pathways involve the actin-binding proteins huntingtin-interacting protein 1 (Hip1), its related homologue Hip1R or Sla2p in yeast, all of which bind to CLCs (Brodsky 2012). The 22-residue Hip-binding region is the only conserved sequence completely shared by CLCa and CLCb and is conserved in yeast CLC, suggesting a key biological function (Aghamohammadzadeh and Ayscough 2009; Chen and Brodsky 2005; Legendre-Guillemin et al. 2005; Gottfried, Ehrlich, and Ashery 2010; Wilbur et al. 2008).

Cell migration represents a different process involving coordination of clathrin and actin

activity. Migration requires trafficking of the integrins that bind extracellular matrix through endocytic, as well as fast and slow recycling pathways (Jones, Caswell, and Norman 2006; Ezratty et al. 2009; Teckchandani et al. 2009; Bridgewater, Norman, and Caswell 2012; Arjonen et al. 2012). Clathrin has been implicated in cell migration, since siRNA targeting CHC17 or CLC overexpression affect cell motility (Ezratty et al. 2009; Shieh et al. 2011; Saffarian, Cocucci, and Kirchhausen 2009; Nishimura and Kaibuchi 2007). However, distinct roles for CHC and CLC were not addressed in these studies. The rapid recycling pathways for integrins during cell migration depend on actin and actin-modulating proteins (Zech et al. 2011). Rapid endosomal recycling can be mediated by intracellular peripheral clathrin-coated structures termed 'gyrating clathrin' (G-clathrin), characterized by live cell imaging of fluorescent CLC or GGA1 adaptors (Zhao and Keen 2008; Hsu, Bai, and Li 2012; Parachoniak et al. 2011). The potential coincidence of these pathways inspired the investigation of a role for the CLC-actin connection during the rapid recycling that occurs in cell migration that we report here.

We observe that complete loss of both clathrin subunits (CHC17 depletion) or of CLC alone impedes cell migration, but resulting actin morphologies and focal adhesion characteristics suggest distinct roles for the clathrin subunits. Analysis of integrin trafficking reveals that CLC-Hip interactions are needed for recycling of inactive β1 integrin, while CHC17 but not CLC is needed for its internalization. Furthermore, disruption of CLC function significantly reduces G-clathrin structures marked by Golgi-localized gamma-adaptin ear containing Arf-binding protein 1 (GGA1), and attenuates transferrin receptor recycling. In support of a key role for CLC in cell migration, we observe upregulation of CLCb, along with other proteins involved in migration and adhesion, in trophoblast cells that invade the uterus during fetal implantation. Our combined results establish that the clathrin-actin interactions mediated by the CLC subunits are important for G-clathrin recycling of β1 integrin during cell migration and have potential significance for Hip1 upregulation in metastatic cancers.

Results

Actin and focal adhesions differ upon CLC or CHC depletion

Following up our published observation that overexpression of the Hip-binding CLC fragment (residues 1-44) dramatically alters cortical cellular actin distribution, we characterized the effects of CLC depletion on actin organization at the cell periphery (Chen and Brodsky 2005). Cells were depleted of CLCs using siRNA targeting both CLCa and CLCb, or of total clathrin using siRNA targeting CHC17. During depletion, cells were co-transfected with either mutant CLCa (I38A, D25A) that does not bind Hip proteins but does bind CHC17 or with WT CLCa (both siRNA-resistant and HA-tagged), or with the empty expression vector (Chen and Brodsky 2005). Consistent with previous studies, CLC depletion generated short, disorganized actin structures characterized by the presence of cortactin at the tips (Poupon et al. 2008). This phenotype was rescued by WT CLCa, but not by mutant CLCa (Fig. 1a). CHC17-depleted cells had a completely different actin phenotype characterized by increased long actin fibers at the cell periphery. This phenotype was not reversed by expression of CLCs, which depend on CHC17 for membrane recruitment. No phenotype was seen in cells expressing the mutant CLCa without endogenous CLC depletion. These results show distinct effects of CHC17 and CLC depletion on actin morphology and extend our previous findings that CLC's influence on actin is mediated through Hip binding.

The changes in actin upon depletion of either clathrin subunit suggested potential correlative changes in focal adhesions resulting from these perturbations. Compared to control-treated cells, bright patches stained for the focal adhesion marker paxillin were more obvious in CHC17-depleted cells, while paxillin patches appeared duller and were reduced in CLC-depleted cells (Fig. 1b). Quantitative analysis revealed that 32% of the cell periphery in CHC17-depleted cells was occupied with paxillin-containing focal adhesions, compared to 17% of control and less than 10% of CLC-depleted cells (Fig. 1c). Thus, our data suggest that CLCs play a unique role in influencing focal adhesion morphology distinct from the pathway affected

17

by depletion of both clathrin heavy and light chain subunits upon CHC17 targeting (Fig. 1d).

Loss of CLC-Hip coupling impairs cell migration

Clathrin has been implicated in cell migration and this has been attributed to a role in endocytosis at focal adhesions, a role in plaque formation and SCAR-WAVE binding by CHC17 (Ezratty et al. 2009; Shieh et al. 2011; Saffarian, Cocucci, and Kirchhausen 2009; Nishimura and Kaibuchi 2007; Gautier et al. 2011). Although CLC depletion has variable effects on endocytosis, our observations (Fig. 1) that CLC influences actin and focal adhesions led us to address CLC's role in cell migration (Huang et al. 2004; Poupon et al. 2008; Ferreira et al. 2012). HeLa cells depleted of CLC or CHC17 were grown to confluency and migration was assessed in a wound-healing assay. Depletion of CHC17 impaired HeLa cell migration as measured by displacement by 35% relative to control-treated cells (Fig. 2a,b,c), consistent with previous reports without affecting cell speed (Ezratty et al. 2009; Nishimura and Kaibuchi 2007). Migration of a HeLa cell derivative expressing SNAP-tagged CLCa, in which whole clathrin was acutely inactivated by drug-induced crosslinking of the SNAP tag, was similarly impaired (Supplementary Fig. 1a; (Foraker et al. 2012). Notably, CLC depletion reduced HeLa cell migratory displacement by 22%, also without affecting speed (Fig. 2a,b,c). Depletion of the second CHC isoform CHC22, which does not influence CLC or CHC17 levels or participate in endocytosis had no effect on HeLa cell migration (Supplementary Fig. 1b,c; (Vassilopoulos et al. 2009; Esk et al. 2010). Cell proliferation was not significantly altered by siRNA depletion of either clathrin subunit 24-48 hours post cell plating, indicating that wound-healing defects could be ascribed directly to altered migration (Supplementary Fig. 2a,b,c).

In H1299 lung cancer cells, which migrate faster than HeLa cells, CHC17 depletion only reduced migration by 17%, whereas CLC depletion reduced migration by 41% relative to control cells (Fig. 2d,e,f), validating that CLC's contribution to cell migration is independent of the associated decrease in CHC17 stability upon CLC depletion. As seen for HeLa, CHC or CLC

18

depletion mainly affected displacement, though double depletion also affected speed (Fig. 2f) and CHC22 depletion had no effect (Supplementary Fig. 2d,e). However, Hip depletion from H1299 cells decreased cell migration by 27% (Fig. 2d,e,f), while having a marginal effect on HeLa cell migration. This suggests that CLC-Hip protein interaction plays a greater role in regulation of cell migration in H1299 cells compared to HeLa cells. Interestingly, H1299 cells express more Hip1 protein relative to CHC17 than HeLa cells.

To address whether CLC's role in migration requires association with Hip proteins, we generated H1299 and HeLa cell clones stably expressing siRNA-resistant mutant CLCa or CLCb that do not bind Hip proteins or siRNA-resistant WT CLCa or CLCb, using the non-coding vector as a control (Chen and Brodsky 2005). Each stable transfectant was depleted of endogenous CLCa and CLCb or treated with control siRNA, and migration was compared between these two conditions for each clone. Migration defects following CLC depletion were obvious in H1299 clones with siRNA-resistant mutant CLCa or CLCb but did not occur in the clones expressing WT CLCa or WT CLCb (Fig. 3). These results were replicated in HeLa cell lines stably expressing siRNA-resistant WT or Hip-binding-deficient CLCb (Supplementary Fig. 3). We were unable to establish HeLa clones that stably express WT CLCa or mutant CLCa. These data demonstrate that CLC plays a role in cell migration that requires its binding to Hip. Migration defects caused by depletion of both CLCs were rescued by expression of WT CLCa or WT CLCb, indicating that the role in migration is a shared property of the CLC isoforms, consistent with their identical Hip-binding sequences (Chen and Brodsky 2005).

Inactive β1-integrin recycling involves CLC and G-clathrin

Focal adhesions and cell migration are affected by surface integrin levels, so we assessed if these were altered by CLC depletion using cell-surface biotinylation (Jones, Caswell, and Norman 2006). We focused on β1 integrin, the dominant β integrin subunit in HeLa cells, which heterodimerizes with different α subunits to alter specificity for extracellular

matrix ligands (Hynes 2002). Biotinylated surface molecules were isolated by streptavidin binding from solubilized cells treated with siRNA, and then identified by immunoblotting. Consistent with inhibition of endocytosis, CHC17 depletion resulted in slightly increased levels of surface proteins, including β1 integrin (~13% increase) and transferrin receptor (~19% increase) (Fig. 4a,b,c). In contrast, CLC depletion reduced levels of several cell surface proteins, including the mature form of β1 integrin (58% reduction of upper band, note lower band is immature form), transferrin receptor (59% reduction), EGF-receptor, major histocompatibility complex (MHC) class I, and Na/K ATPase (Fig. 4a,b,c). CLC depletion also decreased total protein levels of β1 integrin.

The CLC depletion phenotype was consistent with normal endocytosis coupled with impaired endosomal recycling and consequent degradation in lysosomes. Given the relevance of β1 integrin to cell migration, we focused on understanding the role of CLC in β1 integrin traffic. We performed internalization and recycling assays in control and CLC-depleted cells that were surface-labeled with biotin using a reducible crosslinker. In this assay, proteins are internalized followed by stripping of residual surface biotin. Then proteins are allowed to recycle, followed by a second surface-stripping treatment. Internalized surface proteins that do not recycle remain biotinylated. While CLC depletion reduced overall levels of β1 integrin, internalization of β1 integrin was not affected. However, after stripping, more internal β1 integrin remained in CLC-depleted cells compared to control-treated cells, indicating impaired recycling (Fig. 4d,e, and see Supplementary Fig. 4 for later time points).

There is growing evidence that inactive and active integrins are trafficked through different pathways in the cell (Teckchandani et al. 2009; Arjonen et al. 2012). We therefore used an antibody-based internalization and recycling assay to specifically analyze trafficking of the inactive and form of β1 integrin following CLC depletion, as endocytosis of this form has been shown to be clathrin-dependent (Ezratty et al. 2009; Teckchandani et al. 2009). Surface-bound antibody against inactive β1 integrin was internalized, and visualized after cell permeabilization.

20

Or, residual antibody was stripped from the surface after internalization and internalized antibody allowed to recycle, followed by a second stripping step. Antibody bound to inactive β1 integrin was taken up by CLC-depleted cells or control-treated cells (Fig. 5a), with reduced signal for the CLC-depleted cells reflecting decreased total amounts of β1 integrin. Notably, internalized antibody remained inside CLC-depleted cells, while internalized antibody was recycled and lost by stripping from control treated cells within 30 min (Fig. 5b). Thus, CLCs are not necessary for CME of inactive β1 integrins, but are involved downstream in their recycling. No antibody to inactive β1 integrin was internalized upon CHC17 depletion, as expected, so recycling could not be assessed (Ezratty et al. 2009; Teckchandani et al. 2009).

Following depletion of endogenous CLCs from HeLa clones expressing WT or mutant CLCb (Fig. 5c), antibody to inactive β1 integrin was internalized (Fig. 5d). A recycling defect was observed for cells expressing the mutant CLCb but rescued in cells expressing WT CLCb (Fig. 5e). Thus, recycling of inactive β1 integrin involves CLC-Hip interactions. Internalization of inactive β1 integrin was partially impaired in the cells expressing the mutant CLCb (Fig. 5d), but internalized antibody was not recycled in these cells upon depletion of endogenous CLC.

Integrins transit through rapid and slow recycling pathways during cell migration. A role for clathrin in recycling to the plasma membrane from endosomes has been much debated, but it is clear that one of the pathways for rapid recycling of transferrin receptor involves G-clathrin (Zhao and Keen 2008). G-clathrin has been visualized using fluorescent protein fusions with CLCs or with GGA1 adaptors, with which it is associated in the cell periphery, and its recruitment to endosome-derived structures is ADP-ribosylation factor 6 (ARF6)-dependent (Zhao and Keen 2008; Parachoniak et al. 2011; Luo, Zhan, and Keen 2013). Many ARF6-dependent pathways involve actin, thus suggesting a role for CLCs in G-clathrin. To visualize G-clathrin under CLC depletion conditions, HeLa-M cells (a flat subclone of HeLa cells) were simultaneously transfected with siRNA and GGA1 coupled to yellow fluorescent protein (YFP) (Luo, Zhan, and Keen 2013; Zhao and Keen 2008). Live transfected cells were imaged using

continuous 30 ms exposures (Supplementary Movie 1) and it was obvious that the peripheral, highly mobile GGA1-containing structures were significantly reduced in cells treated with siRNA targeting CLC. These structures were also absent from cells co-transfected with CLCa coupled to DsRed1 (CLCa-DsRed1).   GGA1 in G-clathrin structures was quantified by comparing segmented maximum projection images (comprising both highly mobile G-clathrin and stable clathrin structures) to summed projection images (emphasizes relatively stationary structures, not G-clathrin). Upon CLC depletion, there was a ~60% reduction in G-clathrin structures compared to cells treated with control siRNA (Fig. 6a,b,d), and an ~85% reduction in G-clathrin in cells expressing CLCa-DsRed1 (Fig. 6a,c,d). Though in other respects (i.e., labeling of plasma membrane coated pits and trans-Golgi network (TGN) clathrin), CLCa-DsRed1 appears to be similar to GFP-CLC and has been used for live cell imaging of clathrin, here it acts as a dominant negative CLC mutant that specifically affects G-clathrin (Engqvist-Goldstein et al. 2001; Rappoport and Simon 2003; Rappoport, Benmerah, and Simon 2005). Consistent with its effect on G-clathrin, CLCa-DsRed1 expression attenuated recycling of the known G-clathrin cargo transferrin receptor and it reduced β1 integrin recycling, as assessed by the biotinylation-based recycling assay (Fig. 6e,f and Supplementary Fig. 5a). Linking this G-clathrin recycling pathway to migration, expression of CLCa-DsRed1 impaired migration of H1299 cells towards a gradient of EGF, visualized by tracking transiently transfected fluorescent cells in a Dunn chamber assay (Fig. 6g and Supplementary Fig. 5b). The effect of CLCa-DsRed1 expression was similar to the effect of CLC depletion in the same Dunn chamber assay, where transfected cells were visualized by co-transfection of mCherry and siRNA (Fig. 6h and Supplementary Fig. 5c). HeLa cells expressing CLCa-DsRed1 or depleted of CLCs demonstrated a reduction in speed as well as displacement, compared to control cells (Fig. 6i,j,k,l). This migration behavior on matrigel in the Dunn chamber contrasted with the marginal reduction of speed observed in the wound-healing assay upon CLC depletion (Figs. 2,3). Matrigel contains ligands for several integrins including β1 integrin, therefore migration on this substrate could be more sensitive to

an integrin recycling defect. Together these results implicate CLC as an active component of the G-clathrin rapid recycling pathway for β1 integrin as well as transferrin receptor, and demonstrate the importance of this pathway in cell migration.

CLCb expression increases in migratory trophoblast cells

Villi of the placenta are covered by villous trophoblast (VT) cells of fetal origin. Specialized anchoring villi form where the placenta contacts the uterine wall from where migratory extravillous trophoblast (EVT) cells invade the uterine lining. This infiltration results in remodeling of maternal arteries, leading to placental vascularization (King and Loke 1997). In search of a physiological correlate for CLC's role in migration, we queried available data from a microarray analysis comparing gene expression in VT vs EVT cells (Apps et al. 2011). As expected, several genes involved in cell adhesion and migration were upregulated in the migratory EVT cells compared to non-migratory VT cells (Fig. 7a). Strikingly, we noted that non-neuronal CLCb was one of the top genes upregulated in invasive EVT cells (Fig. 7a). No such increase in expression was observed for non-neuronal or neuronal CLCa, neuronal CLCb or CHC17 transcripts in these cells, suggesting that CLCb may uniquely contribute to the migratory potential of EVT cells.

To establish whether CLCb protein increases in EVT cells as a result of increased gene expression, we analyzed the distribution of clathrin and CLCs in placental tissue sections by tracking the level of immunofluorescence across tissue sections from VT to EVT cells. These trophoblast regions were identified by immunolabeling for standard markers of all trophoblast (cytokeratin) and of EVT cells, which express HLA-G on their surface during invasion (Fig. 7b; (Moffett-King 2002). Consistent with known distribution, cytokeratin expression was observed in cytotrophoblast cell columns and interstitial trophoblast cells present in maternal tissue. The EVT cells showed restricted expression of HLA-G as expected (Fig. 7b). CLCb was barely detectable in the VT cells (Fig. 7b), but labeling increased in EVT cells (indicated by arrowheads

in Fig. 7b) in the vicinity of maternal vessels. In contrast, CLCa and CHC17 expression were uniform across all trophoblast regions (Fig. 7b). These observations were reproduced in other placental sections from an unrelated individual, and agree with the array data. Thus tissue expression analysis suggests a physiological role for CLCb in trophoblast invasion that is consistent with a role for CLC in cell migration.

Discussion

This study establishes a role for clathrin light chain (CLC) subunits and their Hip binding in the recycling of inactive β1 integrin and in cell migration. Moreover, we show that the rapid endosomal recycling pathway mediated by G-clathrin structures depends on CLC function and that a specific inhibitor of G-clathrin attenuates cell migration and β1 integrin recycling, as well as recycling of the known G-clathrin cargo, transferrin receptor. Identification of G-clathrin as a mediator of rapid endosomal recycling during migration and demonstrating its CLC dependence, implicates the CLC-binding Hip proteins as additional actin organizers needed for this pathway, shown previously to also require the actin-organizing proteins Wiskott-Aldrich syndrome protein family homolog (WASH) and actin-related protein 2/3 complex (Arp2/3) (Zech, Calaminus, and Machesky 2012). In support of a key role for CLC-dependent G-clathrin in cell migration, we observed upregulation of CLCb in migrating trophoblast, providing an in vivo correlate for our findings.

Clathrin's role in migration mediated by CLC defined here is distinct from that previously established by depletion of the CHC17 clathrin heavy chain, which revealed a role for clathrin in endocytosis of inactive β1 integrin during migration (Ezratty et al. 2009; Teckchandani et al. 2009). These distinguishable clathrin-mediated trafficking pathways for inactive β1 integrin (Fig. 8) both influence focal adhesions. CHC17 depletion increased focal adhesions, as expected from reduced integrin uptake, while CLC depletion had the opposite effect (Fig. 1), explained by

24

reduced recycling of β1 integrin with persistent internalization. Supporting the concept that clathrin functions in balanced membrane traffic pathways during cell migration, overexpression of a CLCb mutant that reduced actin-associated clathrin plaques at the cell-substrate interface was shown to enhance migration (Saffarian, Cocucci, and Kirchhausen 2009). That particular QQN-CLCb mutant studied is defective for both Hip binding and for regulation of clathrin assembly, so could not distinguish between CLC and CHC17 roles in migration (Chen and Brodsky 2005; Legendre-Guillemin et al. 2005; Ybe et al. 1998). Here, using different mutants, we show that both migration and β1 integrin recycling depend on the minimal CLC-Hip binding residues, without altering the CLC residues involved in clathrin assembly. The CLC-dependent G-clathrin recycling pathway could potentially influence levels of growth factor receptors and affect directional migration, also explaining variable migration phenotypes seen with different cells and interference protocols. We further note that CHC17 has been implicated in lamellipodium formation, and could affect cell migration via recruitment of the Scar-Wave complex to the leading edge of the cell (Gautier et al. 2011). Thus clathrin plays multiple roles in cell motility, expanded by the function of CLC and G-clathrin in β1 integrin recycling established here.

Defining the roles of CLC in cellular clathrin function has been challenging, although in vitro biochemical studies have demonstrated a role for CLC in regulating both clathrin assembly and Hip interactions with actin (Wilbur et al. 2010; Wilbur et al. 2008). The requirement for CLCs in CME is limited to some G-protein-coupled receptors, but dispensable for many common CME cargo (Huang et al. 2004; Poupon et al. 2008; Ferreira et al. 2012). On the other hand, uptake of cargo from membranes under tension and of large pathogen particles depend on CLC interactions with Hip proteins (Bonazzi et al. 2011; Cureton et al. 2010; Boulant et al. 2011; Boettner, Chi, and Lemmon 2012). In these latter situations, clathrin serves an actin organizer, a role that it also plays at certain bacterial-host interfaces and during adherens junction formation (Bonazzi et al. 2012; Bonazzi et al. 2011). Hip1R has been implicated in actin-based

25

movements of *Rickettsia* and clathrin is required for actin polymerization during vaccinia infection, suggesting that CLC may be similarly involved (Humphries et al. 2012; Serio et al. 2010). Here we add to the repertoire of actin-based functions mediated by CLC. Upon CLC depletion, we observe disorganized, branched actin filaments at the cell periphery and reversing the depletion phenotype requires CLC-Hip interaction. We further show that CLC is needed for G-clathrin, as well as migration and recycling, which also depend on CLC-Hip binding. G-clathrin has a characteristic "gyrating" behavior in the cell periphery and represents endosome-associated clathrin-coated tubules that mediate rapid recycling (Zhao and Keen 2008). We propose that CLC is needed for G-clathrin to function in recycling and migration because, through Hip binding, CLC could connect tubule-associated clathrin coats with actin for directional extension from endosomes. Clathrin-coated carriers bound to ADP-ribosylation factor 1 (ARF1) and adaptor protein 1 (AP1) in the TGN form actin-based tubules, and G-clathrin is also nucleated by ARF1 and ARF6 (Luo, Zhan, and Keen 2013; Anitei et al. 2010). CLC depletion was reported to change actin morphology in a perinuclear compartment labeled for the AP1 adaptor, consistent with our finding a function for CLC on endosome-associated clathrin and possibly a further role for CLC on TGN tubule clathrin (Poupon et al. 2008). It is notable that CLCa-DsRed1 acts as a dominant negative mutant in the G-clathrin recycling pathway, though it has been used as a marker for live cell imaging of clathrin and functions normally at the plasma membrane. This is likely a consequence of a unique intolerance of G-clathrin to oligomerization of CLCs, driven by the obligate tetrameric quaternary structure of DsRed1 (Baird, Zacharias, and Tsien 2000). In contrast, either N- or C-terminal-tagged fusions of CLCs with predominantly monomeric GFP, YFP or mCherry proteins all give robust evidence of G-clathrin.

The observation that CLCb is markedly upregulated in invasive trophoblast further strengthens our assignment of an important role for CLC in migration. In our cellular studies, there was no distinction between CLCa and CLCb function in migration or influence on actin organization or recycling, as each CLC isoform seems to substitute for the other in restoring the

26

knockdown phenotypes observed here. Tissue analysis has indicated that the CLCa:CLCb ratio is characteristic of different tissues and that CLCa is usually the more abundant (Brodsky and Parham 1983; Acton and Brodsky 1990). Indeed, the tissue section staining we performed shows ubiquitous expression of CLCa in all placental regions. Currently little is known about clathrin gene regulation, but it may be that CLCb is expression is more subject to transcriptional regulation, allowing its increase during differentiation. Alternatively or additionally, CLCa and CLCb share only 60% sequence identity outside of their identical Hip-binding regions, so it is possible that there are functional differences in flanking sequences that affect Hip-actin interactions required for trophoblast migration, again needing further biochemical evaluation.

Pre-eclampsia occurs when trophoblast invasion of the uterine wall is defective, so CLC expression might be a therapeutic target for women with pregnancy disorders (Moffett-King 2002). Another physiological correlate, not addressed directly here, is the observation that Hip1 expression is upregulated in metastatic breast and prostate cancers as well as other malignancies (Bradley et al. 2007; Rao et al. 2002; Rao et al. 2003). It is conceivable that increased Hip expression enhances migratory behavior. Migration of H1299 cells was more sensitive to CLC and Hip knockdown than migration of the slower-moving HeLa cells, which express less Hip1 protein. Thus, defining the role of CLC in cell migration establishes a potential mechanism for metastasis of cancers with increased Hip expression that might be considered as a molecular target for anti-metastatic strategies.

Methods

siRNAs and plasmids

siRNA duplexes were synthesized by Qiagen. Targeting sequences were published as follows, CHC17, CLCa and CLCb, CHC22, or designed by Qiagen for Hip proteins (5'-CAGGAACTTGCCACAAGCCAA-3', Hip1 and 5'-CTCCGACATGCTGTACTTCAA-3, Hip1R) (Huang et al. 2004; Vassilopoulos et al. 2009). The CLC siRNA-resistant construct (WT, with a silent mutation at serine 88 from AGT to TCA) or CLC Hip-binding resistant mutant (I38A and D25A) of bovine brain CLCa was generated from a 5' HA tagged pcDNA3-based construct, with QuikChange site-directed mutagenesis kit (Stratagene) (Chen and Brodsky 2005). Mutant human CLCa (I43A) and CLCb (I35A) encoding constructs that are siRNA resistant were similarly produced.

Tissue Culture and Transfections

HeLa cells (lab stock) and the H1299 lung cancer cell line (gift of J.M. Bishop, UCSF) were cultured in DMEM and RPMI-1640 respectively, supplemented with 10% FBS (Hyclone) and antibiotics. Cells were trypsinized and transfected at ~30% confluency with siRNA using the HiPerfect reagent (Qiagen), following the manufacturer's protocols. For transient rescue experiments, cells were transfected with plasmid DNA one day after siRNA transfection, using Lipofectamine 2000 (Life Technologies) according to the manufacturer's instructions. Cells were analyzed 72 hours post-siRNA treatments.

HeLa and H1299 clones expressing the empty vector, siRNA-resistant human WT CLCa or CLCb, or human Hip-binding resistant mutant CLCa (I43A) or CLCb (I35A) were established by transfection of plasmids into HeLa and H1299 cells using Lipofectamine 2000 (Life Technologies) as above. G418 (Life Technologies) was added to the cell culture medium at 500 µg ml^{-1} 48 hours post transfection to select clones. Individual G418 resistant colonies were

selected and expanded into cell lines 3 weeks later, followed by confirmation of plasmid expression by immunoblotting.

Antibodies and other reagents

The following monoclonal antibodies were used for immunofluorescence: anti-CHC17 (2 µg ml^{-1}; X22), cortactin (1:500; Millipore, number 05-180), paxillin (1:500; Millipore, number 05-417), anti-HA (1:100; Covance, number MMS-101P). Rat anti-CD29 mAb13 against inactive β1 integrin (5 µg ml^{-1}; BD biosciences, number BDB552828), rabbit polyclonal antisera against the conserved region of CLCs, and Hip1R (1:100; Millipore, number AB9882) were also used. Secondary labeling was done with Alexafluor-488 (1:500; Life Technologies, number A-11001) or 555-conjugated secondary antibodies (1:500; Life Technologies, number A-21422). Alexafluor 647-phalloidin (1:100; Life Technologies, number A-22287) was used to stain F-actin. The following antibodies were used for immunoblotting: anti-CHC17 (1:1000; TD.1), Hip1R (1:500; Millipore, number AB9882) , β1 integrin (1:1000; BD Biosciences, number 610467), TfR (1:1000; BD Biosciences, number 612124), HA (1:1000; Covance, number MMS-101P), Hip1 (1:500; Sigma, number HPA013606), anti-β-actin (1:2000; Sigma, number A5441) and α-tubulin (1:5000; Sigma, number T6199) (Brodsky 1985; Acton et al. 1993; Nathke et al. 1992).

Immunoblotting

Cells were lysed in a buffer containing 50 mM Tris (pH 7.2), 1% Triton X-100, 150mM NaCl, and 20 mM EDTA. Protease inhibitors (Roche) were added to the buffer prior to lysis. Protein content was determined using Bradford reagent (Bio-Rad). Equal amounts of cell lysates were resolved on pre-cast SDS-PAGE gels (Invitrogen) and transferred onto nitrocellulose membranes (Bio-Rad), followed labeling with primary and secondary antibodies.

Migration assays

HeLa or H1299 cells treated with 20 nM siRNA for 48 hours were plated at $2X10^5$ cells ml^{-1} in culture inserts (Ibidi GmbH) affixed to wells in glass-bottom (MatTek) or tissue culture plastic (BD Falcon) 24-well plates and allowed to adhere for 24 hours. Prior to imaging, culture inserts were removed to create the wound, and the cells were washed in culture medium with 1% FBS. Migration across the wound was imaged once every 10 minutes for 24 (HeLa) or 10-15 hours (H1299) using a 10X objective on a Leica TCS SP5 microscope. Cells were maintained at 37°C and 5% CO_2 for the duration of the experiment. Cells were tracked using the MTrackJ plugin of ImageJ. 20 cells were tracked per condition for each experiment. Wound-healing assays for parent HeLa and H1299 cell lines were performed on glass, while migration of CLC transfectants was assessed on plastic, which better supported migration.

Chemotaxis assays were performed using the Dunn chamber (Hawksley DCC100). 2400 H1299 cells transfected with either DsR or CLCa-DsRed1, or mCherry and either control or CLCab siRNA, were plated on 2% matrigel-coated coverslips and allowed to adhere for 6 hours in complete medium. Cells were then starved overnight in medium containing 0.01% serum. The coverslip was placed onto the Dunn chamber in which both inner and outer wells were filled with control medium (medium containing 0.01% serum) and 3 sides were sealed with wax. Media from the outer well was drained using filter paper and control media containing 1 ng ml^{-1} EGF was inserted into the outer well and the fourth side was then sealed with wax. To assess migration in the absence of a gradient, all 4 sides of the coverslip were sealed with wax once the coverslip was placed onto the chamber containing control medium. The Dunn chamber was then placed on a heated stage at 37°C. Time-lapse images were taken every 5 minutes for 3 hours using a 10X objective on a Leica TCS SP5 microscope. Migration of non-dividing DsR, CLCa-DsRed1, or mCherry expressing cells were tracked using the MtrackJ plugin of ImageJ.

Immunofluorescence

Cells grown on coverslips were fixed using 4% PFA (Ted Pella, Inc.) for 10 min. When viewing HA-tagged CLCa with other proteins stained by a monoclonal antibody, Alexafluor 594-conjugated monoclonal antibody to HA (1:500; Covance, number A594-101L) was applied after incubation with secondary antibody. Images were collected with an API DeltaVision DV3 restoration or a Leica TCS SP5 confocal microscope. To determine the percent of cell periphery occupied by focal adhesions, the sum of edges stained for paxillin along the cell perimeter were divided by the cell perimeter, with both measured using ImageJ.

Paraffin-embedded serial placental sections from a de-identified normal human sample were deparaffinized in xylene and rehydrated in reducing concentrations of ethanol (100-70%). Following washes with water and PBS, antigen epitopes were unmasked by boiling slides in 10 mM sodium citrate for 10 min. Cooled slides were washed in PBS, and sections were permeabilized in blocking buffer (PBS, 5% BSA and 2% goat serum) with 0.1% Triton X-100 for 30 min. Sections were incubated in the following primary antibodies diluted in the blocking buffer for 1 hour at room temperature: 5 µg ml^{-1} of LCB.1 (for CLCb) (Brodsky et al. 1987), X16 (for CLCa) (Brodsky 1985) and X22 (for CHC17) (Brodsky 1985), 10 µg ml^{-1} of anti-HLA-G (MEM-G/1, SantaCruz, number sc-51674), or 0.2 µg ml^{-1} of anti-cytokeratin (Clone MNF116, Dako Cytochromation, number M082101-2). Following washes in PBS with 0.1% Tween-20, secondary antibodies (10 µg ml^{-1}) and TO-PRO (Life Technologies, number T3605) were incubated with 10% human AB serum for 30 minutes. After 30 min room temperature incubation, the slides were washed in PBS with 0.1% Tween-20 and mounted. Images in Fig. 7 were cropped to depict the same area using Adobe Photoshop CS3. The intensity of all channels was adjusted equally across all images. The difference in protein expression between the villous trophoblast (V), trophoblast columns (C), and the extravillous trophoblast (EV) within an image was quantified as follows. A line was drawn within the boxed regions in the mosaic image and the plot profile function in ImageJ was used to calculate pixel intensities along the

line. Approval to use these tissues was obtained by the UCSF Committee on Human Research and the Cambridge Local Research Ethics Committee.

MTT assay

To measure cell proliferation, MTT assays (Molecular Probes) were performed according to the manufacturer's protocol. Briefly, 10,000 cells were plated in triplicate in each well of a 96 well plate. After 24 or 48 hours, fresh media was added to the cells followed by 12 mM MTT reagent for 4 hours at 37°C. After the incubation period, DMSO was added to the cells to dissolve the formazan and absorbance was read at 540 nM.

Expression profiling by microarray

RNA expression levels in primary trophoblasts were determined as previously described (Apps et al. 2011). Briefly, biotinylated cRNA was synthesized from total RNA isolated from primary trophoblasts using the Illumina RNA amplifcation kit (Ambion). Labeled cRNA was hybridized to Illumina Human HT-$_{12}$ V$_3$ BeadArrays according to the manufacturer's protocol. Data was processed by converting signal intensities to log$_2$ expression units. Differential gene expression between two groups of samples was determined using the output of a moderated t-test. P values were converted to corrected q values using the previously published FDR method and probe-sets with q<0.01 (FDR 1%) were regarded as having significant differential expression between groups (Smyth 2004).

Antibody-based internalization and recycling assays

Cells plated on glass coverslips were treated with siRNA for 72 hours, then serum starved for 1 hour, followed by labeling with 5 μg ml^{-1} antibody to inactive (mAb13) β1 integrin on ice for 15 minutes. Cells were washed to remove excess antibody and incubated in pre-warmed culture

medium supplemented with 10% FBS at 37°C for 30 minutes to start integrin internalization. To determine surface levels of integrins, cells were placed on ice, washed with ice-cold PBS, fixed in ice-cold 4% PFA, then blocked with 0.2% fetal goat serum and incubated with Alexafluor-555 secondary antibody for 1 hour. To determine internal levels, surface integrins were stripped with ice-cold PBS (pH 2.5) before fixation, followed by permeabilization with 0.2% Triton X-100. The cells were blocked and incubated with Alexafluor-555 secondary antibody as above. To measure recycling, labeled integrins were allowed to internalize at 37°C as above, followed by stripping of surface integrins with ice-cold PBS (pH 2.5). Cells were washed with ice-cold PBS, then incubated in pre-warmed medium (10% FBS) for 30 minutes at 37°C to chase internal integrins to the surface. Surface and internal integrins were determined as above. Images sections were acquired every 0.5 µm in a 2.5 µm slice through the middle of the cell and merged into maximum projections. The mean fluorescent intensity for each image was obtained by measuring total fluorescence, followed by mean background subtraction using ImageJ. This value was then divided by the total number of cells in each image.

Surface biotinylation and biotinylation-based recycling assays

siRNA-treated cells were washed twice in ice-cold PBS (pH 8) and surface proteins were biotinylated with 0.5 mg ml^{-1} Sulfo-NHS-SS Biotin (Thermo Fisher Scientific) in ice-cold PBS (pH 8) for 30 min at 4°C. Excess biotin was quenched by washing cells twice with ice-cold 5mM Tris (pH 7.4), followed by two washes with ice-cold PBS (pH 8) and one wash with PBS (pH 7.4). Cells were lysed in PBS with 1% NP-40 containing protease inhibitors (Roche). Protein concentrations in the samples were determined using Bradford reagent and equal amounts of total protein were loaded onto streptavidin beads (Thermo Fisher Scientific) and incubated at 4°C for 1 hour. After washing the beads, proteins were eluted by boiling the beads in SDS

sample buffer, followed by immunoblotting. Blots were quantified using ImageJ, and the level of surface receptors were normalized to the α-tubulin signal from each sample.

For biotinylation-based recycling assays, serum starved siRNA-treated cells were labeled with biotin and the excess washed as above. The cells were then placed at 37°C in media containing 10% FBS for 30 min to allow internalization of surface proteins. Surface biotin was then reduced with two 10 min washes with 50 mM MesNa (pH 8.6) in TBS, followed by one 10 min wash with 20 mM iodoacetamide in TBS, all at 4°C. Cells were then rinsed with ice-cold PBS and placed at 37°C in media containing 10% FBS for indicated time points to chase internalized proteins to the cell surface. Surface biotin was then reduced again as described, and the cells were lysed, equal amounts of protein loaded onto streptavidin beads, eluted and blotted as mentioned above. The fraction of internalized receptor remaining for each protein was determined from the signal intensity of internalized protein at each time point relative to control cells that had not been placed at 37°C after the first surface reduction.

Quantification of G-clathrin by GGA1 movement

Hela-M cells were transfected with either control or CLC-targeting siRNA, and then co-transfected with YFP-GGA1 48 hours later, or they were transfected with either YFP-GGA1 alone or YFP-GGA1 plus CLCa-DsRed1. The cells were then imaged 24 hours post DNA transfection by spinning disk confocal microscopy using streaming 30 msec exposures to collect 30 frame image stacks as previously described (Luo, Zhan, and Keen 2013). For quantification of G-GGA1, we used a modified assay based on movement area (Zhao and Keen 2008). Briefly, stacks were background corrected using a rolling ball filter (r=5) in ImageJ. Using MetaMorph (Molecular Devices, Inc.), a maximum projection (comprising both highly mobile G-GGA1 and unwavering structures) and sum projection (emphasizing unwavering structures) of each stack were prepared. Each stack was thresholded (using mean+1SD) and binarized.

Regions 100 pixels on edge were randomly selected near the periphery of the cell and maximum projection pixels that did not overlap with the corresponding sum projection were retained, yielding an estimate of "G-GGA1 area". Approximately 80 regions from 20 cells for each condition in three independent experiments were analyzed, and mean G-GGA1 area in control cells was set to 100%. Data were analyzed by a two-tailed unpaired t-test.

Statistical Analysis

Statistical analysis of directionality for Dunn chamber assays was carried out using Oriana (Kovach Computing Services, Anglesey, Wales). All other analyses were carried out using GraphPad Prism software (GraphPad Software, Inc). Parametric data were analyzed using two-tailed Student t-tests, one-way or two-way ANOVA, followed by Newman-Keuls or Bonferroni post hoc tests for multiple comparisons as appropriate (95% confidence interval).

References

Acton, S. L., and F. M. Brodsky. 1990. 'Predominance of clathrin light chain LCb correlates with the presence of a regulated secretory pathway', *J Cell Biol*, 111: 1419-26.

Acton, S. L., D. H. Wong, P. Parham, F. M. Brodsky, and A. P. Jackson. 1993. 'Alteration of clathrin light chain expression by transfection and gene disruption', *Mol Biol Cell*, 4: 647-60.

Aghamohammadzadeh, S., and K. R. Ayscough. 2009. 'Differential requirements for actin during yeast and mammalian endocytosis', *Nat Cell Biol*, 11: 1039-42.

Anitei, M., C. Stange, I. Parshina, T. Baust, A. Schenck, G. Raposo, T. Kirchhausen, and B. Hoflack. 2010. 'Protein complexes containing CYFIP/Sra/PIR121 coordinate Arf1 and Rac1 signalling during clathrin-AP-1-coated carrier biogenesis at the TGN', *Nat Cell Biol*, 12: 330-40.

Apps, R., A. Sharkey, L. Gardner, V. Male, M. Trotter, N. Miller, R. North, S. Founds, and A. Moffett. 2011. 'Genome-wide expression profile of first trimester villous and extravillous human trophoblast cells', *Placenta*, 32: 33-43.

Arjonen, A., J. Alanko, S. Veltel, and J. Ivaska. 2012. 'Distinct recycling of active and inactive beta1 integrins', *Traffic*, 13: 610-25.

Baird, G. S., D. A. Zacharias, and R. Y. Tsien. 2000. 'Biochemistry, mutagenesis, and oligomerization of DsRed, a red fluorescent protein from coral', *Proc Natl Acad Sci U S A*, 97: 11984-9.

Boettner, D. R., R. J. Chi, and S. K. Lemmon. 2012. 'Lessons from yeast for clathrin-mediated endocytosis', *Nat Cell Biol*, 14: 2-10.

Boettner, D. R., H. Friesen, B. Andrews, and S. K. Lemmon. 2011. 'Clathrin light chain directs endocytosis by influencing the binding of the yeast Hip1R homologue, Sla2, to F-actin', *Mol Biol Cell*, 22: 3699-714.

Bonazzi, M., A. Kuhbacher, A. Toledo-Arana, A. Mallet, L. Vasudevan, J. Pizarro-Cerda, F. M. Brodsky, and P. Cossart. 2012. 'A common clathrin-mediated machinery co-ordinates cell-cell adhesion and bacterial internalization', *Traffic*, 13: 1653-66.

Bonazzi, M., L. Vasudevan, A. Mallet, M. Sachse, A. Sartori, M. C. Prevost, A. Roberts, S. B. Taner, J. D. Wilbur, F. M. Brodsky, and P. Cossart. 2011. 'Clathrin phosphorylation is required for actin recruitment at sites of bacterial adhesion and internalization', *J Cell Biol*, 195: 525-36.

Bottcher, R. T., C. Stremmel, A. Meves, H. Meyer, M. Widmaier, H. Y. Tseng, and R. Fassler. 2012. 'Sorting nexin 17 prevents lysosomal degradation of beta1 integrins by binding to the beta1-integrin tail', *Nat Cell Biol*, 14: 584-92.

Boulant, S., C. Kural, J. C. Zeeh, F. Ubelmann, and T. Kirchhausen. 2011. 'Actin dynamics counteract membrane tension during clathrin-mediated endocytosis', *Nat Cell Biol*, 13: 1124-31.

Bradley, S. V., M. R. Smith, T. S. Hyun, P. C. Lucas, L. Li, D. Antonuk, I. Joshi, F. Jin, and T. S. Ross. 2007. 'Aberrant Huntingtin interacting protein 1 in lymphoid malignancies', *Cancer Res*, 67: 8923-31.

Bridgewater, R. E., J. C. Norman, and P. T. Caswell. 2012. 'Integrin trafficking at a glance', *J Cell Sci*, 125: 3695-701.

Brodsky, F. M. 1985. 'Clathrin structure characterized with monoclonal antibodies. I. Analysis of multiple antigenic sites', *J Cell Biol*, 101: 2047-54.

Brodsky. 2012. 'Diversity of clathrin function: new tricks for an old protein', *Annu Rev Cell Dev Biol*, 28: 309-36.

Brodsky, F. M., C. J. Galloway, G. S. Blank, A. P. Jackson, H. F. Seow, K. Drickamer, and P. Parham. 1987. 'Localization of clathrin light-chain sequences mediating heavy-chain binding and coated vesicle diversity', *Nature*, 326: 203-5.

Brodsky, F. M., and P. Parham. 1983. 'Polymorphism in clathrin light chains from different tissues', *J Mol Biol*, 167: 197-204.

Chao, W. T., and J. Kunz. 2009. 'Focal adhesion disassembly requires clathrin-dependent endocytosis of integrins', *FEBS Lett*, 583: 1337-43.

Chen, C. Y., and F. M. Brodsky. 2005. 'Huntingtin-interacting protein 1 (Hip1) and Hip1-related protein (Hip1R) bind the conserved sequence of clathrin light chains and thereby influence clathrin assembly in vitro and actin distribution in vivo', *J Biol Chem*, 280: 6109-17.

Cureton, D. K., R. H. Massol, S. P. Whelan, and T. Kirchhausen. 2010. 'The length of vesicular stomatitis virus particles dictates a need for actin assembly during clathrin-dependent endocytosis', *PLoS Pathog*, 6: e1001127.

Duleh, S. N., and M. D. Welch. 2012. 'Regulation of integrin trafficking, cell adhesion, and cell migration by WASH and the Arp2/3 complex', *Cytoskeleton (Hoboken)*, 69: 1047-58.

Engqvist-Goldstein, A. E., R. A. Warren, M. M. Kessels, J. H. Keen, J. Heuser, and D. G. Drubin. 2001. 'The actin-binding protein Hip1R associates with clathrin during early stages of endocytosis and promotes clathrin assembly in vitro', *J Cell Biol*, 154: 1209-23.

Esk, C., C. Y. Chen, L. Johannes, and F. M. Brodsky. 2010. 'The clathrin heavy chain isoform CHC22 functions in a novel endosomal sorting step', *J Cell Biol*, 188: 131-44.

Ezratty, E. J., C. Bertaux, E. E. Marcantonio, and G. G. Gundersen. 2009. 'Clathrin mediates integrin endocytosis for focal adhesion disassembly in migrating cells', *J Cell Biol*, 187: 733-47.

Fang, Z., N. Takizawa, K. A. Wilson, T. C. Smith, A. Delprato, M. W. Davidson, D. G. Lambright, and E. J. Luna. 2010. 'The membrane-associated protein, supervillin, accelerates F-actin-dependent rapid integrin recycling and cell motility', *Traffic*, 11: 782-99.

Ferreira, F., M. Foley, A. Cooke, M. Cunningham, G. Smith, R. Woolley, G. Henderson, E. Kelly, S. Mundell, and E. Smythe. 2012. 'Endocytosis of G protein-coupled receptors is regulated by clathrin light chain phosphorylation', *Curr Biol*, 22: 1361-70.

Foraker, A. B., S. M. Camus, T. M. Evans, S. R. Majeed, C. Y. Chen, S. B. Taner, I. R. Correa, Jr., S. J. Doxsey, and F. M. Brodsky. 2012. 'Clathrin promotes centrosome integrity in early mitosis through stabilization of centrosomal ch-TOG', *J Cell Biol*, 198: 591-605.

Gautier, J. J., M. E. Lomakina, L. Bouslama-Oueghlani, E. Derivery, H. Beilinson, W. Faigle, D. Loew, D. Louvard, A. Echard, A. Y. Alexandrova, B. Baum, and A. Gautreau. 2011. 'Clathrin is required for Scar/Wave-mediated lamellipodium formation', *J Cell Sci*, 124: 3414-27.

Gottfried, I., M. Ehrlich, and U. Ashery. 2010. 'The Sla2p/HIP1/HIP1R family: similar structure, similar function in endocytosis?', *Biochem Soc Trans*, 38: 187-91.

Hinrichsen, L., J. Harborth, L. Andrees, K. Weber, and E. J. Ungewickell. 2003. 'Effect of clathrin heavy chain- and alpha-adaptin-specific small inhibitory RNAs on endocytic accessory proteins and receptor trafficking in HeLa cells', *J Biol Chem*, 278: 45160-70.

Hsu, V. W., M. Bai, and J. Li. 2012. 'Getting active: protein sorting in endocytic recycling', *Nat Rev Mol Cell Biol*, 13: 323-8.

Huang, F., A. Khvorova, W. Marshall, and A. Sorkin. 2004. 'Analysis of clathrin-mediated endocytosis of epidermal growth factor receptor by RNA interference', *J Biol Chem*, 279: 16657-61.

Humphries, A. C., M. P. Dodding, D. J. Barry, L. M. Collinson, C. H. Durkin, and M. Way. 2012. 'Clathrin potentiates vaccinia-induced actin polymerization to facilitate viral spread', *Cell Host Microbe*, 12: 346-59.

Hynes, R. O. 2002. 'Integrins: bidirectional, allosteric signaling machines', *Cell*, 110: 673-87.

Jacquemet, G., M. J. Humphries, and P. T. Caswell. 2013. 'Role of adhesion receptor trafficking in 3D cell migration', *Curr Opin Cell Biol*, 25: 627-32.

Jones, M. C., P. T. Caswell, and J. C. Norman. 2006. 'Endocytic recycling pathways: emerging regulators of cell migration', *Curr Opin Cell Biol*, 18: 549-57.

King, A., and Y. W. Loke. 1997. 'Placental vascular remodelling', *Lancet*, 350: 220-1.

Legendre-Guillemin, V., M. Metzler, J. F. Lemaire, J. Philie, L. Gan, M. R. Hayden, and P. S. McPherson. 2005. 'Huntingtin interacting protein 1 (HIP1) regulates clathrin assembly through direct binding to the regulatory region of the clathrin light chain', *J Biol Chem*, 280: 6101-8.

Li, J., P. J. Peters, M. Bai, J. Dai, E. Bos, T. Kirchhausen, K. V. Kandror, and V. W. Hsu. 2007. 'An ACAP1-containing clathrin coat complex for endocytic recycling', *J Cell Biol*, 178: 453-64.

Luo, Y., Y. Zhan, and J. H. Keen. 2013. 'Arf6 regulation of Gyrating-clathrin', *Traffic*, 14: 97-106.

Moffett-King, A. 2002. 'Natural killer cells and pregnancy', *Nat Rev Immunol*, 2: 656-63.

Nathke, I. S., J. Heuser, A. Lupas, J. Stock, C. W. Turck, and F. M. Brodsky. 1992. 'Folding and trimerization of clathrin subunits at the triskelion hub', *Cell*, 68: 899-910.

Nishimura, T., and K. Kaibuchi. 2007. 'Numb controls integrin endocytosis for directional cell migration with aPKC and PAR-3', *Dev Cell*, 13: 15-28.

Parachoniak, C. A., Y. Luo, J. V. Abella, J. H. Keen, and M. Park. 2011. 'GGA3 functions as a switch to promote Met receptor recycling, essential for sustained ERK and cell migration', *Dev Cell*, 20: 751-63.

Poupon, V., M. Girard, V. Legendre-Guillemin, S. Thomas, L. Bourbonniere, J. Philie, N. A. Bright, and P. S. McPherson. 2008. 'Clathrin light chains function in mannose phosphate receptor trafficking via regulation of actin assembly', *Proc Natl Acad Sci U S A*, 105: 168-73.

Rao, D. S., S. V. Bradley, P. D. Kumar, T. S. Hyun, D. Saint-Dic, K. Oravecz-Wilson, C. G. Kleer, and T. S. Ross. 2003. 'Altered receptor trafficking in Huntingtin Interacting Protein 1-transformed cells', *Cancer Cell*, 3: 471-82.

Rao, D. S., T. S. Hyun, P. D. Kumar, I. F. Mizukami, M. A. Rubin, P. C. Lucas, M. G. Sanda, and T. S. Ross. 2002. 'Huntingtin-interacting protein 1 is overexpressed in prostate and colon cancer and is critical for cellular survival', *J Clin Invest*, 110: 351-60.

Rappoport, J. Z., A. Benmerah, and S. M. Simon. 2005. 'Analysis of the AP-2 adaptor complex and cargo during clathrin-mediated endocytosis', *Traffic*, 6: 539-47.

Rappoport, J. Z., and S. M. Simon. 2003. 'Real-time analysis of clathrin-mediated endocytosis during cell migration', *J Cell Sci*, 116: 847-55.

Reig, G., E. Pulgar, and M. L. Concha. 2014. 'Cell migration: from tissue culture to embryos', *Development*, 141: 1999-2013.

Saffarian, S., E. Cocucci, and T. Kirchhausen. 2009. 'Distinct dynamics of endocytic clathrin-coated pits and coated plaques', *PLoS Biol*, 7: e1000191.

Serio, A. W., R. L. Jeng, C. M. Haglund, S. C. Reed, and M. D. Welch. 2010. 'Defining a core set of actin cytoskeletal proteins critical for actin-based motility of Rickettsia', *Cell Host Microbe*, 7: 388-98.

Shieh, J. C., B. T. Schaar, K. Srinivasan, F. M. Brodsky, and S. K. McConnell. 2011. 'Endocytosis regulates cell soma translocation and the distribution of adhesion proteins in migrating neurons', *PLoS One*, 6: e17802.

Smyth, G. K. 2004. 'Linear models and empirical bayes methods for assessing differential expression in microarray experiments', *Stat Appl Genet Mol Biol*, 3: Article3.

Steinberg, F., K. J. Heesom, M. D. Bass, and P. J. Cullen. 2012. 'SNX17 protects integrins from degradation by sorting between lysosomal and recycling pathways', *J Cell Biol*, 197: 219-30.

Teckchandani, A., E. E. Mulkearns, T. W. Randolph, N. Toida, and J. A. Cooper. 2012. 'The clathrin adaptor Dab2 recruits EH domain scaffold proteins to regulate integrin beta1 endocytosis', *Mol Biol Cell*, 23: 2905-16.

Teckchandani, A., N. Toida, J. Goodchild, C. Henderson, J. Watts, B. Wollscheid, and J. A. Cooper. 2009. 'Quantitative proteomics identifies a Dab2/integrin module regulating cell migration', *J Cell Biol*, 186: 99-111.

Vassilopoulos, S., C. Esk, S. Hoshino, B. H. Funke, C. Y. Chen, A. M. Plocik, W. E. Wright, R. Kucherlapati, and F. M. Brodsky. 2009. 'A role for the CHC22 clathrin heavy-chain isoform in human glucose metabolism', *Science*, 324: 1192-6.

Wilbur, J. D., C. Y. Chen, V. Manalo, P. K. Hwang, R. J. Fletterick, and F. M. Brodsky. 2008. 'Actin binding by Hip1 (huntingtin-interacting protein 1) and Hip1R (Hip1-related protein) is regulated by clathrin light chain', *J Biol Chem*, 283: 32870-9.

Wilbur, J. D., P. K. Hwang, J. A. Ybe, M. Lane, B. D. Sellers, M. P. Jacobson, R. J. Fletterick, and F. M. Brodsky. 2010. 'Conformation switching of clathrin light chain regulates clathrin lattice assembly', *Dev Cell*, 18: 841-8.

Ybe, J. A., S. N. Fontaine, T. Stone, J. Nix, X. Lin, and S. Mishra. 2013. 'Nuclear localization of clathrin involves a labile helix outside the trimerization domain', *FEBS Lett*, 587: 142-9.

Ybe, J. A., B. Greene, S. H. Liu, U. Pley, P. Parham, and F. M. Brodsky. 1998. 'Clathrin self-assembly is regulated by three light-chain residues controlling the formation of critical salt bridges', *EMBO J*, 17: 1297-303.

Zech, T., S. D. Calaminus, P. Caswell, H. J. Spence, M. Carnell, R. H. Insall, J. Norman, and L. M. Machesky. 2011. 'The Arp2/3 activator WASH regulates alpha5beta1-integrin-mediated invasive migration', *J Cell Sci*, 124: 3753-9.

Zech, T., S. D. Calaminus, and L. M. Machesky. 2012. 'Actin on trafficking: could actin guide directed receptor transport?', *Cell Adh Migr*, 6: 476-81.

Zhao, Y., and J. H. Keen. 2008. 'Gyrating clathrin: highly dynamic clathrin structures involved in rapid receptor recycling', *Traffic*, 9: 2253-64.

Figure legends

Figure 1. CLC-depleted HeLa cells display disorganized actin fibers and reduced focal adhesions. (a) HeLa cells treated with siRNA against CHC17, CLCab or control siRNA and transiently transfected with siRNA-resistant HA-tagged-CLCa or HA-tagged-CLCa mutant were labeled for cortactin (green in merge), actin (red), and HA (blue). In all panels, the overlap of green and red signals is shown in yellow, scale bars, 10 μm. **(b)** HeLa cells transfected with siRNAs against CHC17, CLCab or control siRNA were stained for paxillin (green in merge) and CLC (red). The cell border is outlined in the second panel from the top (yellow dashed line). **(c)** The cell periphery occupied by focal adhesions of cells in (b) was measured using ImageJ to outline cells and quantify paxillin staining at the border (mean; n=12 cells from two independent experiments; *$P<0.05$, ***$P<0.005$; P values, One-way ANOVA followed by Newman-Keuls post test). **(d)** HeLa cells were treated with the indicated siRNA for 72 hours, harvested and subjected to immunoblotting analysis. Control, scrambled siRNA; KD, knockdown. A representative blot of many experiments is shown. Migration positions of molecular mass markers are indicated in kDa at the right of the immunoblots shown.

Figure 2. CHC17 or CLC depletion decreases HeLa and H1299 cell migration. Wound-healing assays were performed in cells transfected with siRNA against CHC17, CLCab, Hip (Hip1 and Hip1R) or control siRNA. Migration across the wound was imaged in the presence of medium containing 1% serum on glass-bottomed plates using live-cell time-lapse microscopy. **(a)** Representative HeLa cell trajectories at end time points (24 hours) are shown. The MtrackJ plugin of ImageJ was used to manually trace cell tracks, marked in color. **(b)** Quantitative analysis of HeLa cell relative net displacement (net displacement from the origin relative to control; left) and average speed (distance migrated per minute relative to control; right) were quantified from track plots (mean ± s.e.m. of at least 230 cells analyzed from eleven

44

independent experiments; *$P<0.05$, ***$P<0.005$; P values, One-way ANOVA followed by Newman-Keuls post test) in (a). **(c)** Representative immunoblots of siRNA treatments of HeLa cells in (a). **(d)** H1299 cell trajectories at end time points (15 hours) are shown. The MtrackJ plugin of ImageJ was used to manually trace cell tracks as in (a). **(e)** Representative immunoblots of siRNA treatments in (d). **(f)** Quantitative analysis of H1299 cell relative net displacement (left) and average speed (right) were quantified from track plots (mean ± s.e.m. of at least 100 cells analyzed from five independent experiments; *$P<0.05$, **$P<0.01$, ***$P<0.005$; P values, One-way ANOVA followed by Newman-Keuls post test) in (d). Migration positions of molecular mass markers are indicated in kDa at the right of the immunoblots shown. Scale bars, 100 µm.

Figure 3. Hip-binding by CLC is required to rescue the migration defect induced by CLC depletion. Wound-healing assays were performed in H1299 clones that stably expressed either empty vector, siRNA-resistant WT CLCa, siRNA-resistant WT CLCb, siRNA-resistant mutant CLCa or siRNA-resistant mutant CLCb after 72 hours of treatment with siRNA targeting CLCab to deplete endogenous CLCs. Mutant (mut) CLCs are defective for Hip-binding. Migration across the wound was imaged in the presence of medium containing 1% serum using live-cell time-lapse microscopy on plastic tissue culture plates for 10 hours. **(a)** Representative cell trajectories at end time points are shown. The MtrackJ plugin of ImageJ was used to manually trace cell tracks, marked in color. Scale bars, 250 µm. **(b)** Quantitative analysis of relative net displacement (left) and relative average speed (right; mean ± s.e.m. of at least 40 cells analyzed from two independent experiments; **$P<0.01$; P value, Two-way ANOVA followed by Bonferroni post test) in (a). **(c)** Representative immunoblots of siRNA treatments in (a). Migration positions of molecular mass markers are indicated in kDa at the right of the immunoblots shown.

Figure 4. CLC depletion reduces constitutive recycling of β1 integrin and steady state levels of other surface molecules. **(a)** HeLa cells transfected with the indicated siRNAs were biotinylated for 30 min and surface biotinylated proteins were isolated using streptavidin beads, followed by immunoblotting for the indicated proteins. **(b and c)** Quantification of surface levels of **(b)** β1 integrin and **(c)** transferrin receptor (TfR) from (a) and replicate experiments (mean ± s.e.m.; n=3; *$P<0.05$, **$P<0.01$ P value, One-way ANOVA followed by Newman-Keuls post test). **(d)** Recycling of internalized β1 integrin in control and CLCab-siRNA treated HeLa cells. Cells were biotinylated and allowed to internalize surface proteins for 30 min at 37°C. Surface biotin was removed by reduction and internalized proteins were chased back to the cell surface for the indicated times at 37°C. Surface biotin was reduced again, and cells were lysed. Above: Biotinylated proteins were bound to streptavidin beads, followed by immunoblotting for β1 integrin. Below: Immunoblots of indicated proteins in total cell lysate at each time point. Representative immunoblots of one experiment (n=6). **(e)** Quantification of β1 integrin recycling assays in (d) (mean ± s.e.m.; n=6; *$P<0.05$, **$P<0.01$ P value, Two-way ANOVA followed by Bonferroni post test). Migration positions of molecular mass markers are indicated in kDa at the right of the immunoblots shown.

Figure 5. CLC depletion decreases recycling of inactive β1 integrin. **(a)** siRNA treated HeLa cells were allowed to internalize antibody specific for inactive β1 integrin for 30 min at 37°C. Cells were fixed and stained with Alexafluor-conjugated secondary antibody to visualize surface integrins. For analysis of internal integrins, surface antibody was stripped by acid wash before fixation, followed by permeabilization. Quantification of surface (bottom left) and internal (bottom right) fluorescent labeling of inactive β1 integrin antibody following internalization, which are presented as raw mean fluorescent intensities (mean ± s.e.m.; n=3; $P=$ not significant; P value, Student's t-test). **(b)** Cells were treated as in (a), followed by surface antibody stripping by acid washing after the 30 min internalization period. Cells were then placed at 37°C for 30

minutes to chase integrins back to the cell surface. Cells were fixed and processed as in (a). Quantification of surface (bottom left) and internal (bottom right) fluorescent labeling of inactive β1 integrin antibody following recycling (mean ± s.e.m.; n=3; ***$P<0.005$, P value, Student's t-test). **(c)** HeLa clones expressing the vector, siRNA-resistant WT CLCb or siRNA-resistant mutant (mut) CLCb were treated with control or CLCab-targeting siRNA and immunostained for CLC.   **(d)** Internalization of inactive β1 integrin antibody was assessed as in (a) in siRNA treated HeLa clones that expressed the vector, siRNA-resistant WT CLCb or siRNA-resistant mutant CLCb.   Quantification of surface (top right) and internal (bottom right) fluorescent labeling of inactive β1 integrin antibody following internalization (mean ± s.e.m.; n=3; *$P<0.05$; P value, Two-way ANOVA followed by Bonferroni post test). **(e)** Recycling of inactive β1 integrin antibody was assessed as in (b) in siRNA treated HeLa clones that stably expressed the vector, siRNA-resistant WT CLCb or siRNA-resistant CLCb. Quantification of surface (top right) and internal (bottom right) fluorescent labeling of inactive β1 integrin antibody following recycling (mean ± s.e.m.; n=3; *$P<0.05$, **$P<0.01$, ***$P<0.005$; P values, Two-way ANOVA followed by Bonferroni post test). Scale bars for all panels, 7.5 µm.

Figure 6. Expression of CLCa-DsRed1 or CLC depletion causes loss of G-clathrin structures and CLCa-DsRed1 reduces recycling and cell migration. (a,b and c) HeLa-M cells transfected with YFP-GGA1, and with either **(a)** control siRNA or **(b)** CLCab siRNA, or with **(c)** CLCa-DsRed1 were imaged using continuous 30 ms exposures (~1 s total). A single image from each sequence is shown on the left. Combined maximum projections (red), which reveal both dynamic and stationary GGA1 structures and sum projections (green), which report stationary structures, are shown at the right, with overlap in yellow (54 µm square panels). Dynamic G-clathrin appears red. Boxed areas are magnified (right) and pixel intensities binarized for clarity. **(d)** Percent of G-clathrin relative to controls in HeLa-M cells transfected with CLCab siRNA or CLCa-DsRed1 in (a,b and c). G-clathrin for each condition was calculated

as the difference between the maximum projection and sum projection of YFP-GGA1 signals (see Methods for details) (mean $\pm$ s.e.m.; n=4 for CLCab KD, n=2 for DsRed-CLCa, ****$P<0.0001$, P values, Student's unpaired t-test). **(e)** Recycling of β1 integrin (left) and TfR (right), assessed by biotinylation as in Fig. 4d, in DsRed1 (DsR)- or CLCa-DsRed1-transfected HeLa cells (mean $\pm$ s.e.m.; n=7; *$P<0.05$, **$P<0.01$ P value, Two-way ANOVA followed by Bonferroni post test). **(f)** Representative immunoblots from one recycling experiment in (e). Lysate samples are shown in Supplementary Fig. 5a. **(g and h)** Dunn chamber migration tracks of H1299 cells transfected with **(g)** DsR or CLCa-DsRed1 or **(h)** mCherry plus control or CLCab siRNA in the presence of an EGF gradient (source at 90°). Tracks in the absence of a gradient are shown in Supplementary Fig. 5b,c. All tracks were set to a common origin (intersection of x-[red] and y-axes). Circular histograms depict proportion of cells whose final position lies within each of 18 20° sectors (mean and 95% confidence interval indicated by black line; at least 50 cells analyzed from 4 independent experiments for each condition, P values, Raleigh uniformity test). **(I and j) (i)** Average speed and **(j)** displacement of DsR- and CLCa-DsRed1-transfected gradient-exposed cells. **(k and l) (k)** Average speed and **(l)** displacement of control-treated and CLCab-depleted gradient-exposed cells. (i,j,k, and l: mean $\pm$ s.e.m.; n=4 *$P<0.05$, **$P<0.01$, P values, Student's paired t-test).

Figure 7. CLCb is upregulated in invasive extravillous trophoblast cells. (a) Microarray analysis of mRNA in human trophoblast cells showing relative gene expression levels in extravillous trophoblast (EVT) cells compared to villous trophoblast (VT) cells. Genes encoding clathrin subunits and their transcript levels are indicated in red. *CLTB* encodes CLCb, *CLTA* encodes CLCa, *CLTC* encodes CHC17 and *CLTCL1* encodes CHC22. For three genes encoding clathrin subunits more than one probe was used to detect splice variants and these are numbered. Probes *CLTB-1, CTLA-2, CLTA-3* and *CLTCL1-1* detect all variants, *CLTB-2* and *CLTA-1* detect the neuronal splice variants of CLCs and *CLTCL1-2* detects a second splice

variant encoded by this gene. **(b)** Serial sections of normal, non-cancerous human placental tissue were stained for CLCb, CLCa, CHC17 and trophoblast markers, as indicated. Cytokeratin staining depicts columnar trophoblast and invading extravillous cells developing from placental villi. Extravillous trophoblast was distinguished from villous trophoblast based on HLA-G expression. Arrowheads depict extravillous trophoblast cells with high CLCb expression. Intensities of the staining are quantified as arbitrary units (a.u.) and illustrated on the right as line profiles across each box shown at the far left. V, villous; C, columnar; EV, extravillous trophoblast. Scale bars, 500 µm.

Figure 8. Model for the roles of clathrin in inactive β1 integrin membrane traffic during cell migration.   Clathrin is involved in both endocytosis from the plasma membrane (PM) and recycling of inactive β1 integrin from endosomes. CLC is required for the recycling of β1 integrin back to the cell surface via G-clathrin structures, but not needed for clathrin-mediated endocytosis (CME). Loss of the total clathrin by CHC17 depletion inhibits all pathways, but manifests itself as an endocytosis defect. We note that non-clathrin mediated endocytic routes can also contribute to integrin uptake[22].

Supplemental Figure Legends

Figure S1. Acute inactivation of CHC17 but not depletion of the CHC22 isoform of CHC affects cell migration. (a) HeLa-SNAP-CLCa cells were treated for 2 hours with either DMSO (mock) as a control, or with BG-GLA-BG (crosslinker), which acutely inactivates CHC17 by crosslinking the associated SNAP-tagged CLCa, and cell migration across a wound was assessed. Representative images of cell trajectories at end time points (24 hours) are shown in top panels. Quantitative analysis of net displacement (bottom left) and average speed relative to control, which were calculated as relative to the average control value (bottom right; mean ± s.e.m. of 60 cells analyzed from three independent experiments; *P=0.0491; P value, Student's

t-test). **(b-e)** Wound-healing assays were performed after 72 hours of the indicated siRNA treatment in HeLa or H1299 cells. Migration across the wound was imaged in the presence of medium containing 1% serum on tissue culture plastic plates using live-cell time-lapse microscopy. **(b)** Representative images of cell trajectories at end time points (24 hours) for migration analyses performed in control and CHC22 siRNA-treated HeLa cells in top panels. Quantitative analysis of relative net displacement (bottom left) and average speed (bottom right; mean ± s.e.m. of 60 cells analyzed from three independent experiments; *P*=not significant; *P* value, Student's t-test). **(c)** Representative immunoblots of siRNA treatments in (b). **(d)** Representative images of cell trajectories at end time points (15 hours) for migration assays performed in control and CHC22 siRNA treated H1299 cells in top panels. Quantitative analysis of net displacement (bottom left) and average speed relative to control (bottom right; mean ± s.e.m. of 60 cells analyzed from three independent experiments; *P*=not significant; *P* value, Student's t-test). **(e)** Representative immunoblots of siRNA treatments in (d). Migration positions of molecular mass markers are indicated at the right of immunoblot panels in kDa. Scale bars, 100 µm.

Figure S2. CLCab or CHC17 depletion does not cause significant changes in cell proliferation after 24 or 48 hours. (a) HeLa cells treated with the indicated siRNA for 72 hours were plated in triplicate and allowed to adhere for 24 hours (left), or were treated with media containing 1% serum for an additional 24 hours (right), after which cell proliferation was measured by uptake of MTT (3-(4,5-dimethylthiazol-2-yl)-2,5-diphenyltetrazolium bromide) (mean ± s.d.; n=3; P= not significant; *P* value, One-way ANOVA). **(b)** Cell proliferation was measured by MTT assay in H1299 cells treated with the indicated siRNA as described above at 24 hours (left) and 48 hours (right) (mean ± s.d.; n=3; P= not significant; *P* value, One-way ANOVA). **(c)** Cell proliferation was measured by MTT assay in a HeLa cell subclone in which

clathrin was acutely inactivated after 24 hours (right) and 48 hours (left) (mean ± s.d.; n=3; P= not significant; *P* value, Student's t-test).

Figure S3. Hip binding by CLC is required to rescue the migration defect induced by CLC depletion in HeLa cells. Wound-healing assays were performed in HeLa clones that stably expressed empty vector, siRNA-resistant WT CLCb or siRNA-resistant mutant CLCb after 72 hours of control or CLCab siRNA treatment to deplete endogenous CLCs. Migration across the wound was imaged in the presence of medium containing 1% serum using live-cell time-lapse microscopy for 24 hours. **(a)** Representative cell trajectories at end time points are shown. The MtrackJ plugin of ImageJ was used to manually trace cell tracks, marked in color. **(b)** Quantitative analysis of relative net displacement (left) and relative average speed (right) were quantified from track plots (mean ± s.e.m. of 60 cells from three independent experiments; **P<0.01; *P* value, Two-way ANOVA followed by Bonferroni post test) in (a). **(c)** Representative immunoblots of siRNA treatments in (a). Migration positions of molecular mass markers are indicated at the right in kDa. Scale bars, 100 µm. We note that the track lengths suggest that over-expression of mutant CLCb in this particular clone reduces the cells' migratory capacity, even under control conditions.

Figure S4. CLC depletion reduces recycling of β1 integrin at 15 and 30 min. (a) Recycling of β1 integrin in control and CLCab-siRNA treated HeLa cells assessed by biotinylation as in Fig. 4d (mean ± s.e.m.; n=3; *P<0.05, **P<0.01 *P* value, Two-way ANOVA followed by Bonferroni post test). **(b)** Representative immunoblot of one experiment in (a). Migration positions of molecular mass markers are indicated at the right in kDa.

Figure S5. Control experiments for Fig 6 showing protein levels in cell lysate and migration tracks of transfected H1299 cells in the absence of a chemotactic gradient. (a)

Immunoblot of lysate from samples analyzed in Fig 6f. Migration positions of molecular mass markers are indicated at the right in kDa. **(b)** The Dunn chamber migration tracks (over 3 hours) of H1299 cells transiently transfected with DsR or CLCa-DsRed1 in the presence of control media with circular histograms (below) depicting the proportion of cells whose final position was within each of 18 equal 20° sectors, generated as in Fig. 6g. **(c)** The Dunn chamber migration tracks (over 3 hours) of H1299 cells transfected with mCherry plus either control or CLCab-targeting siRNA in the presence of control media with circular histograms (below) as in (b) In b and c: mean and 95% confidence interval are indicated by black line; at least 50 cells were analyzed from 4 independent experiments for each condition, *P* values, Raleigh uniformity test).
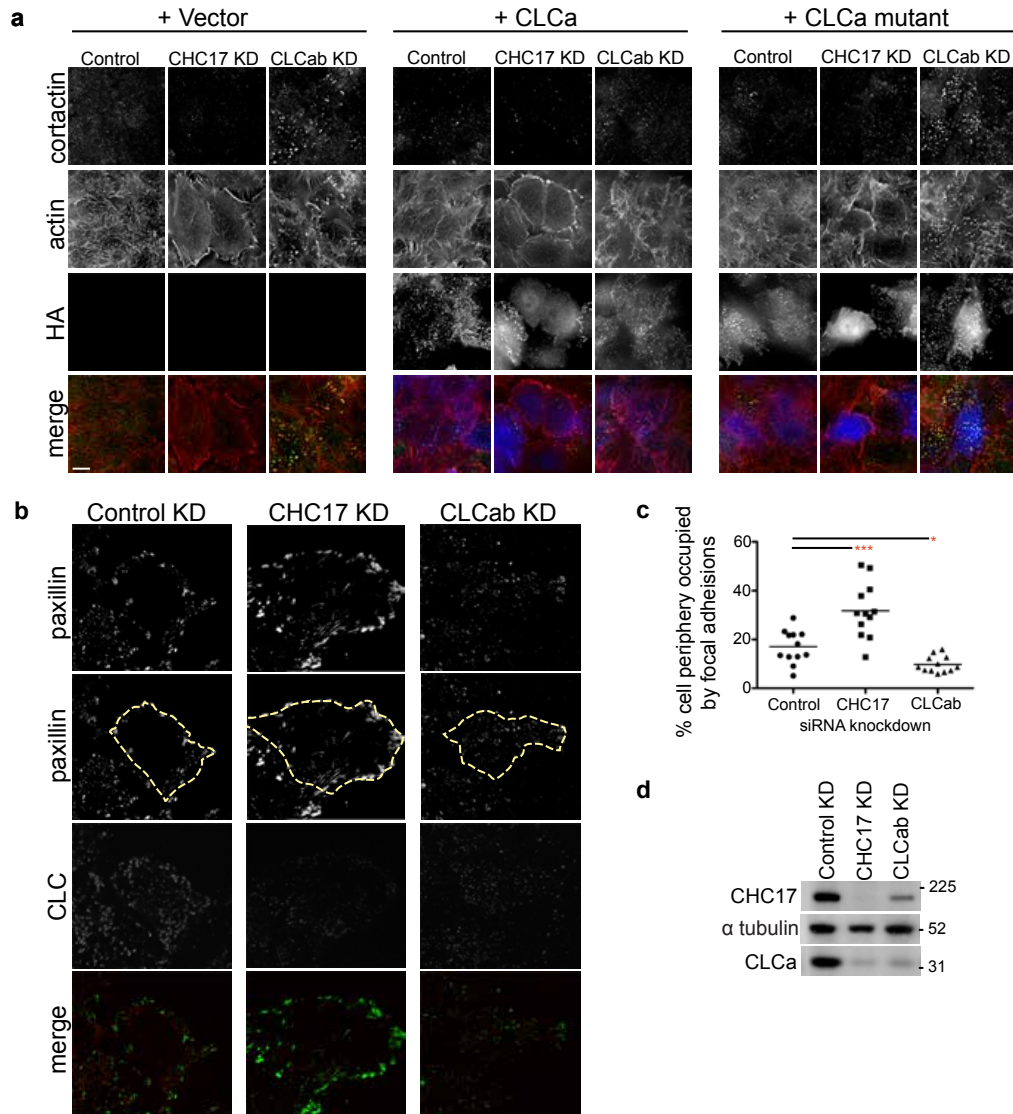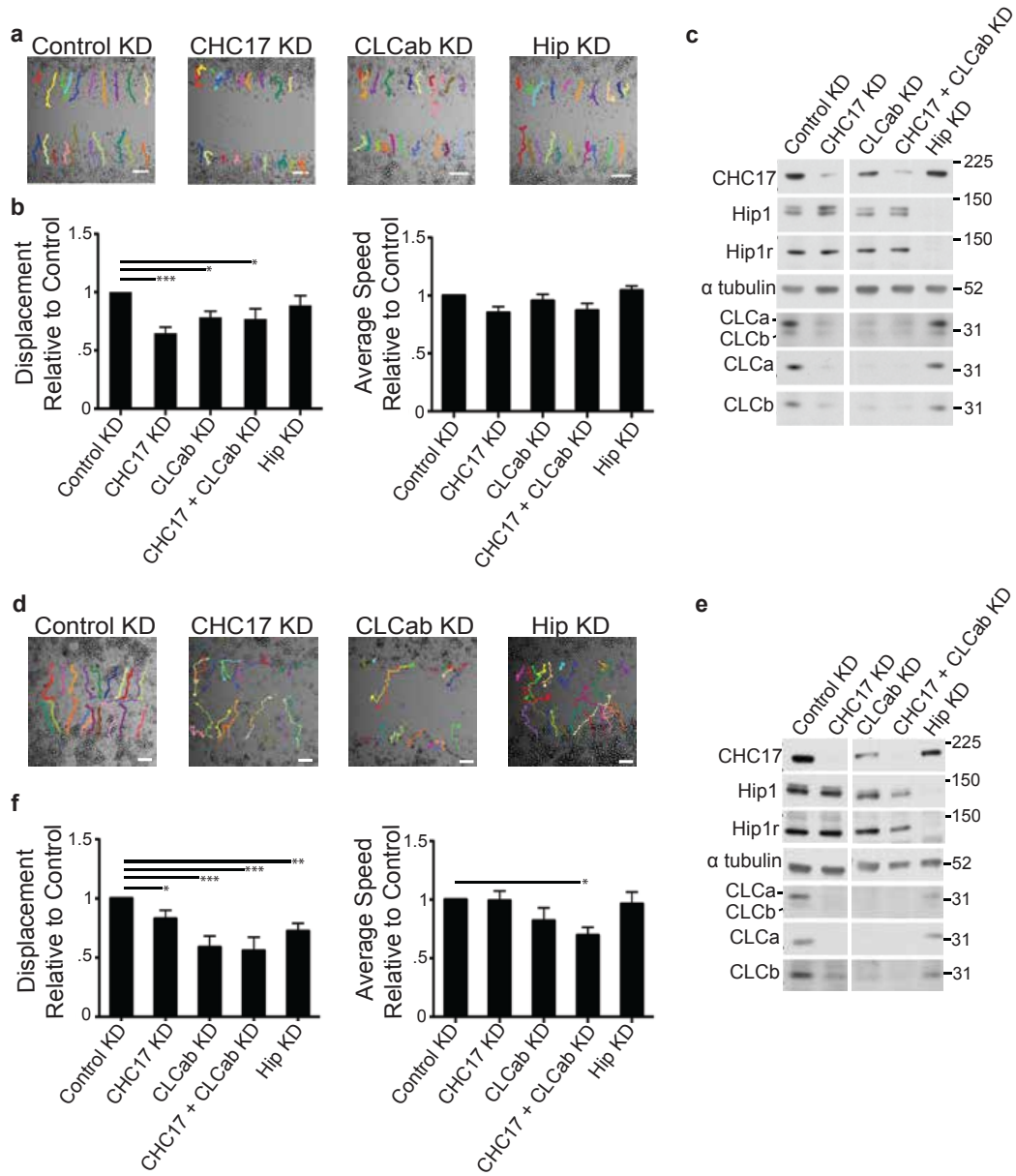
Figure 2-1

Figure 2-2

Figure 2-3
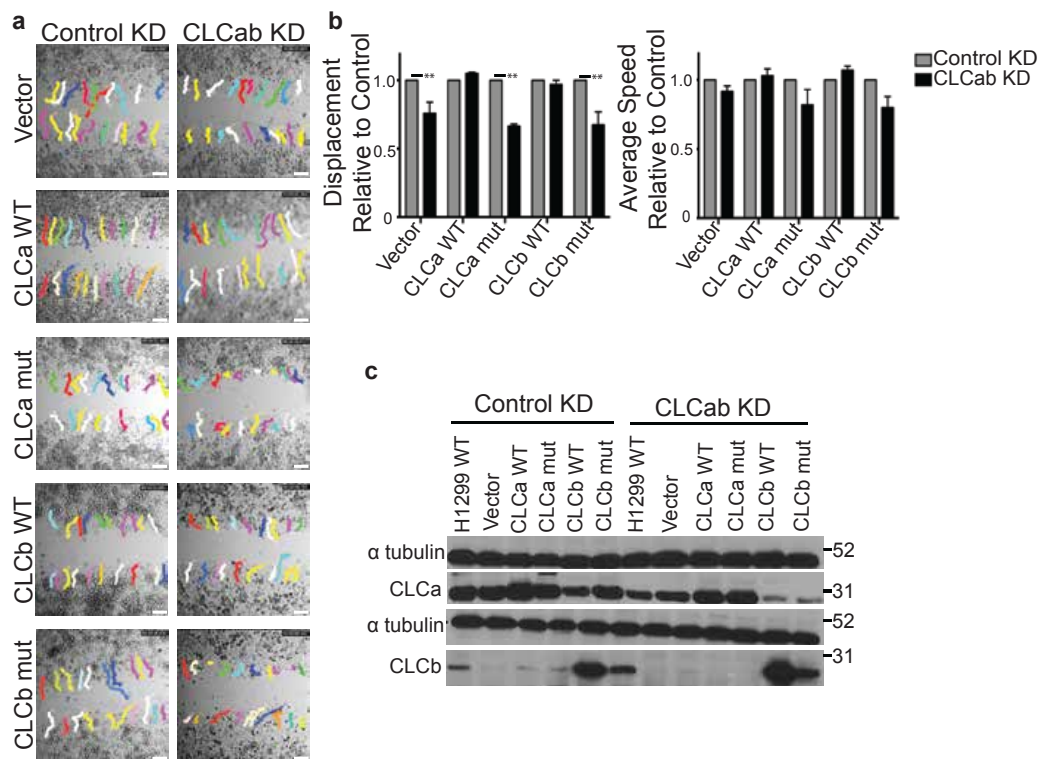
Figure 2-4
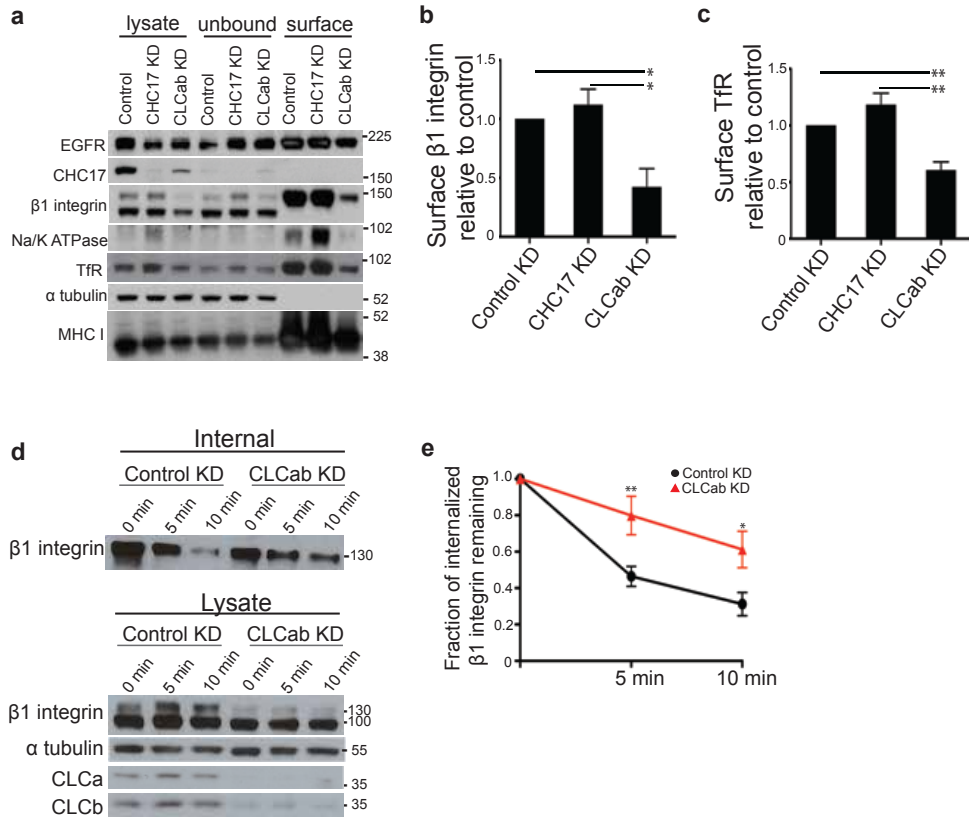
Figure 2-5
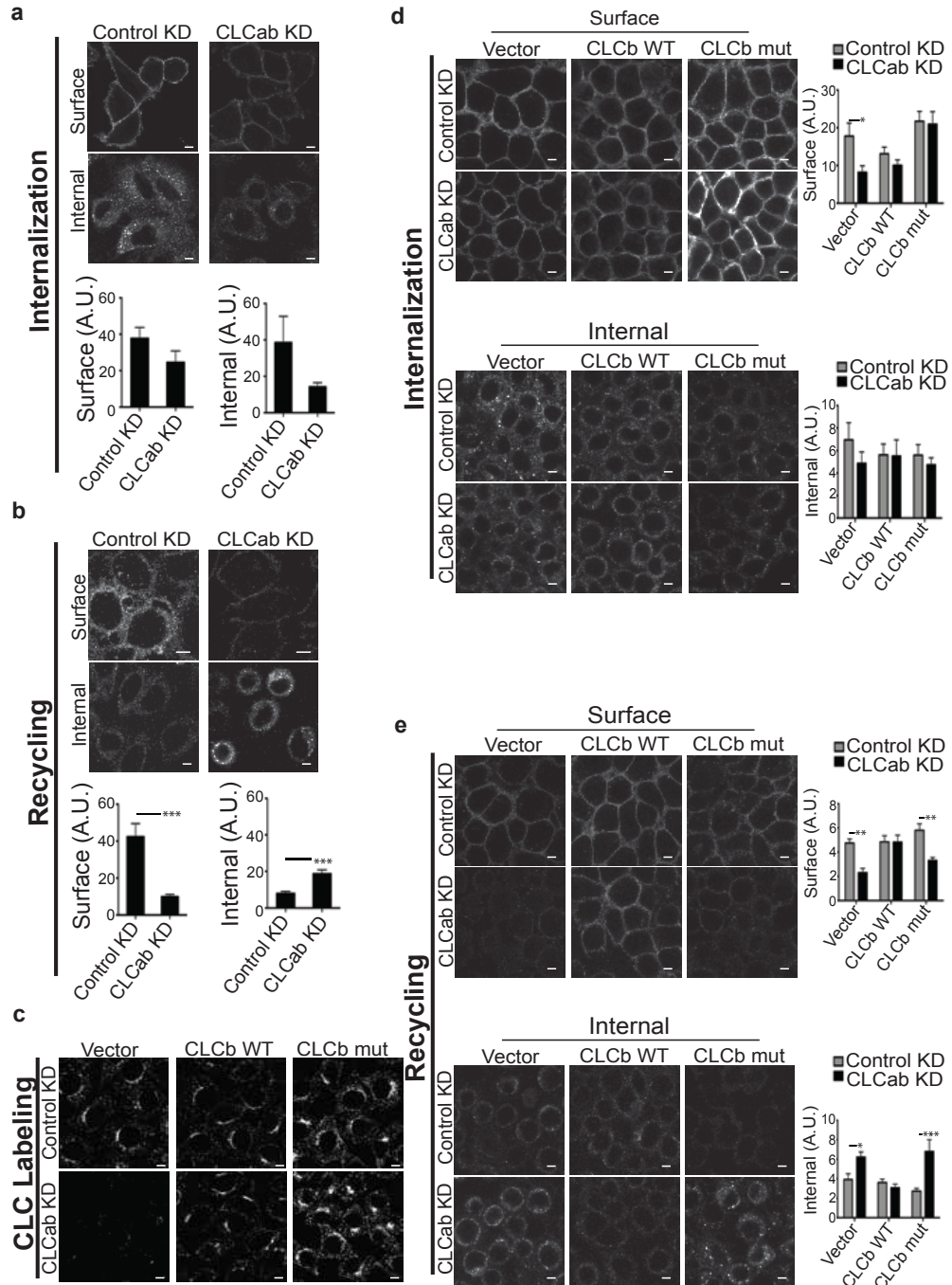
Figure 2-6
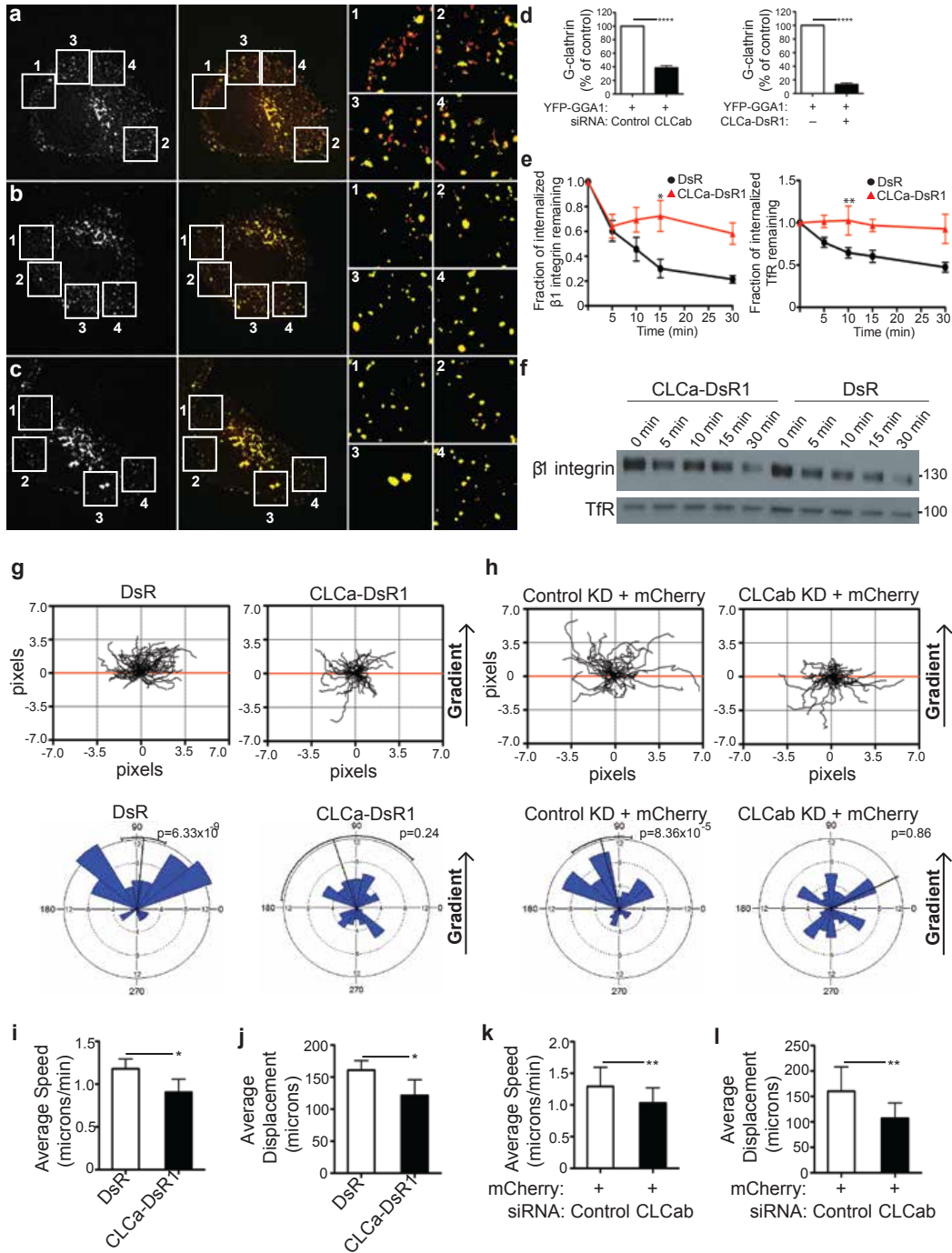
Figure 2-7

Figure 2-8

Figure S 1

a

Mock　　Crosslinker

b

Control KD　　CHC22 KD

c

CHC22 — 170
α tubulin — 52
CHC17 — 170
α tubulin — 52

d

Control KD　　CHC22 KD

e

CHC22 — 170
α tubulin — 52
CHC17 — 170
α tubulin — 52
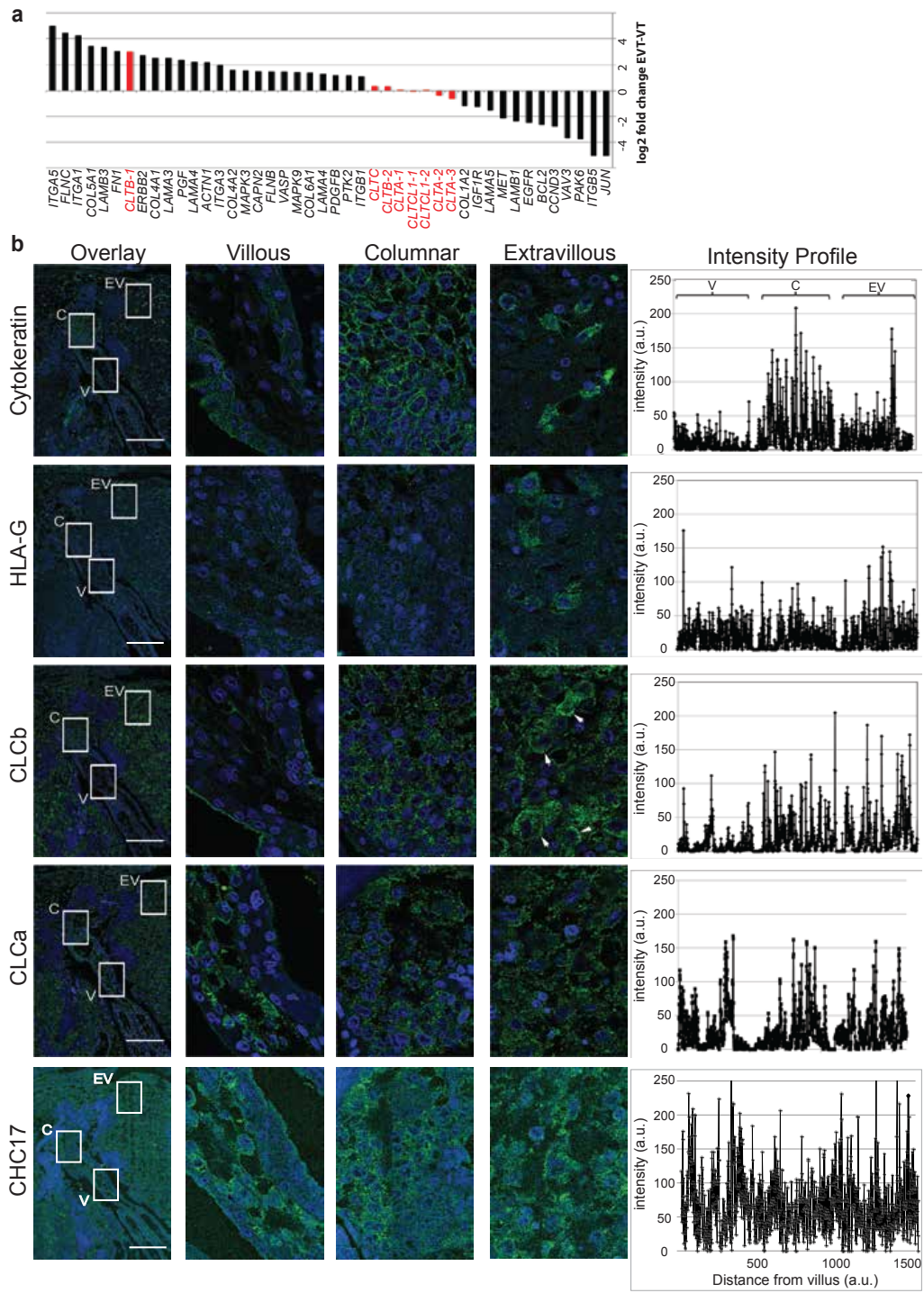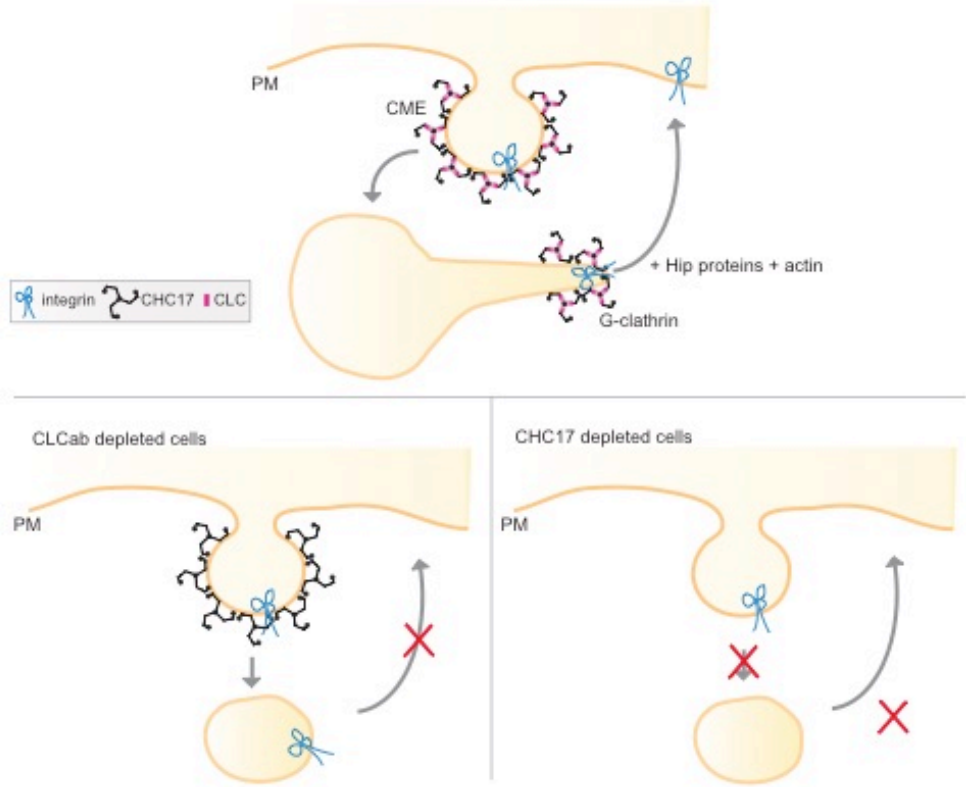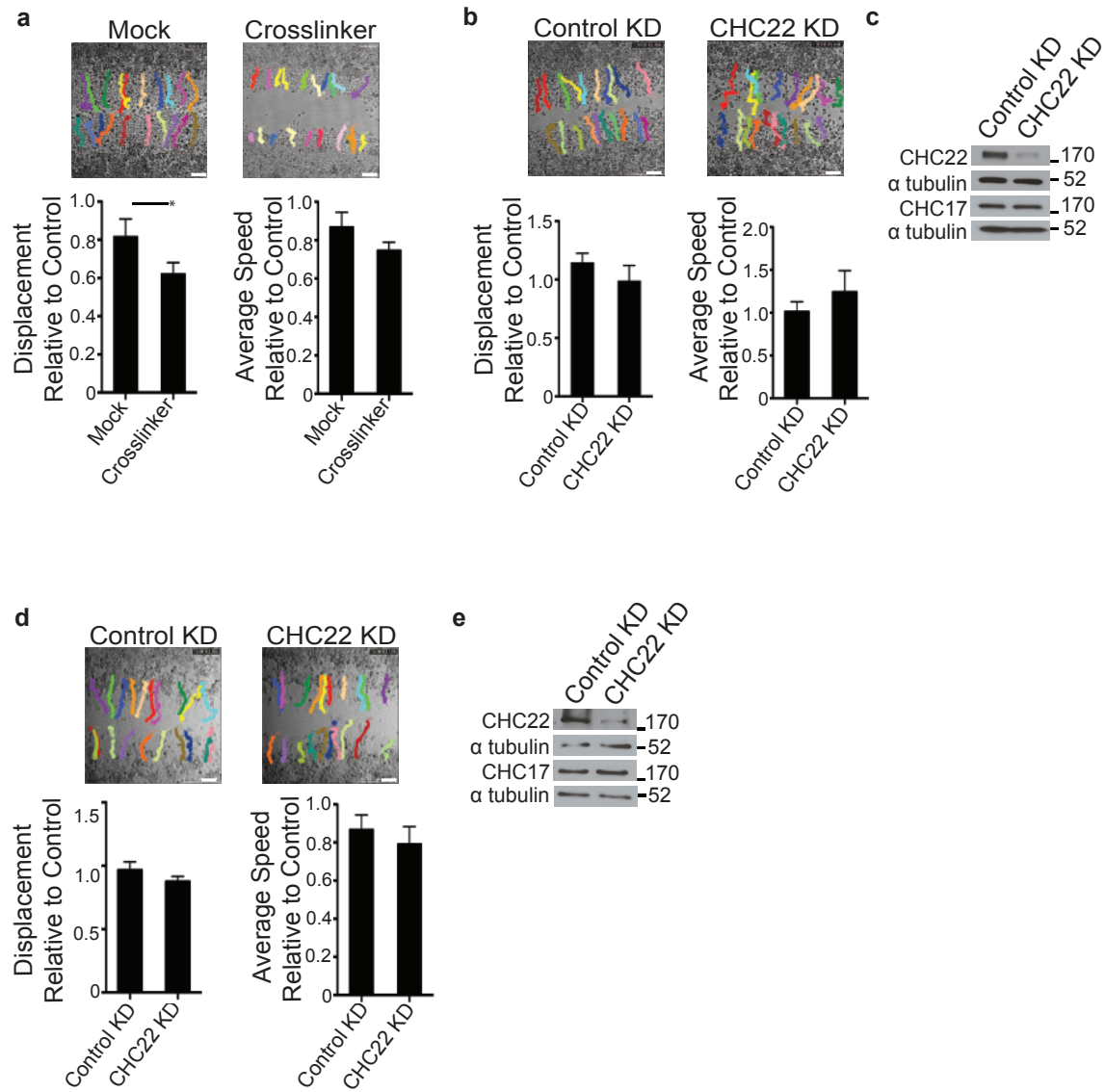
Figure S 2

Figure S 3

a

b

c
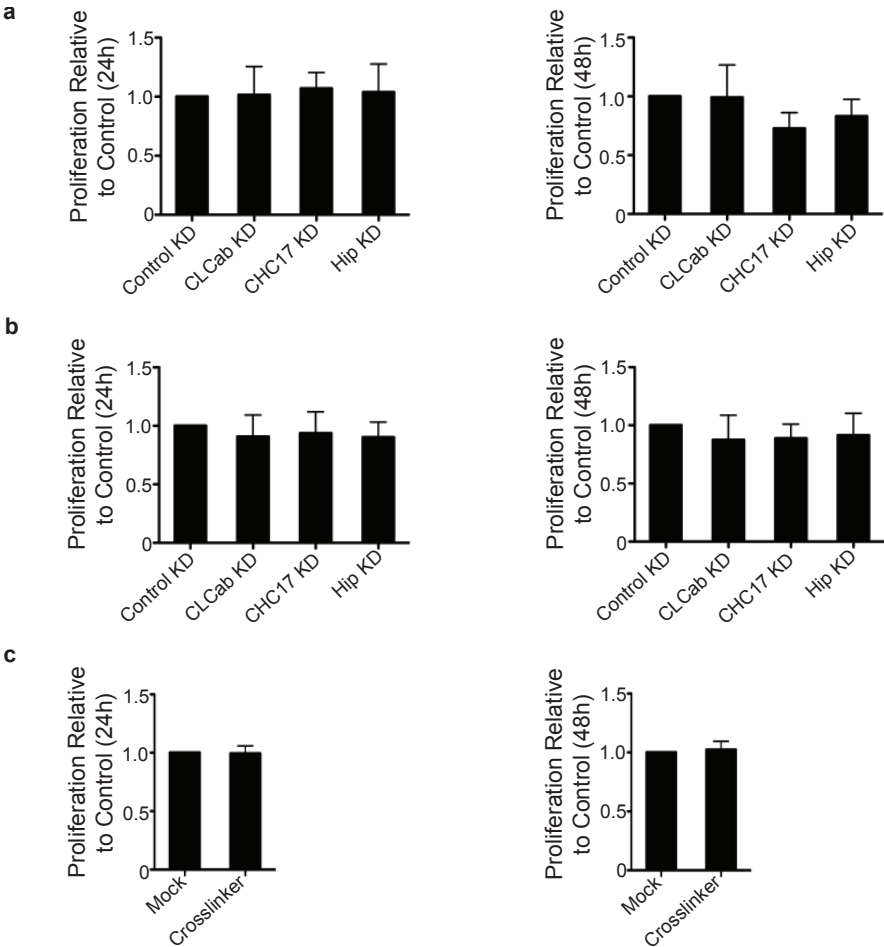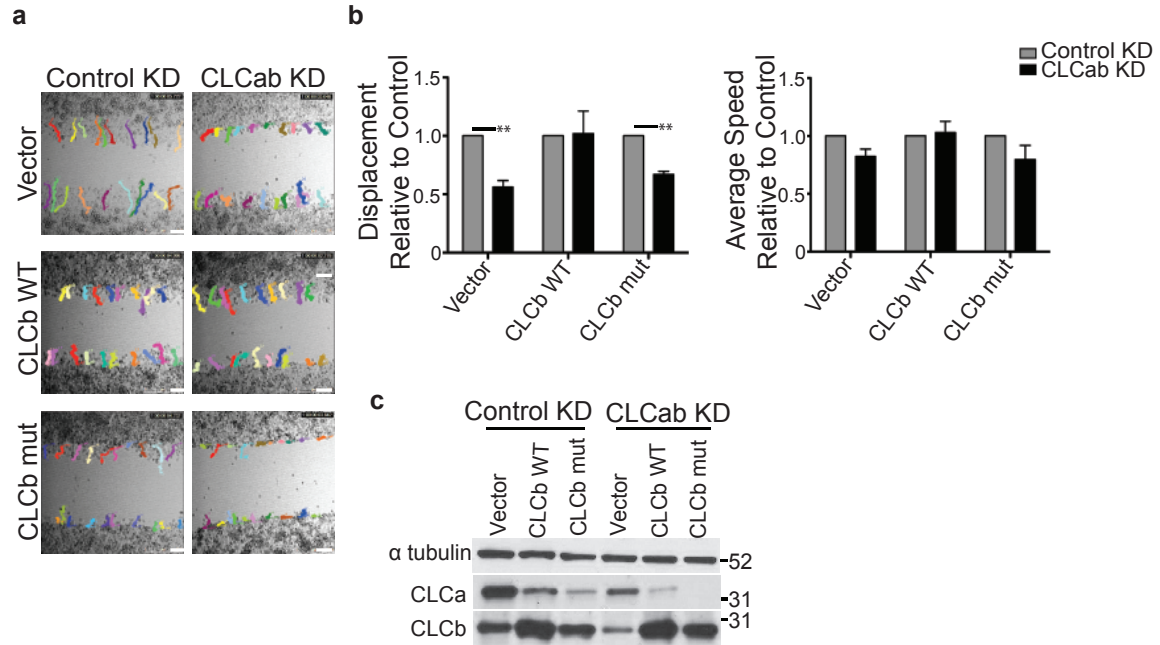
Figure S 4

a

b
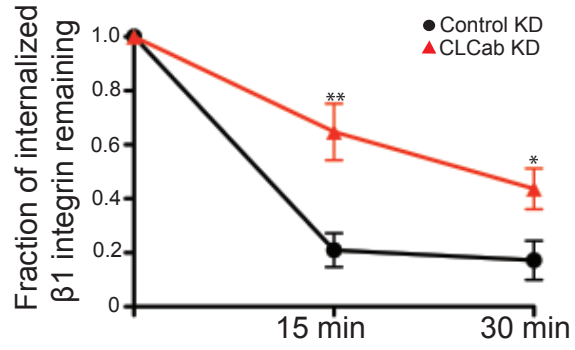
Figure S 5
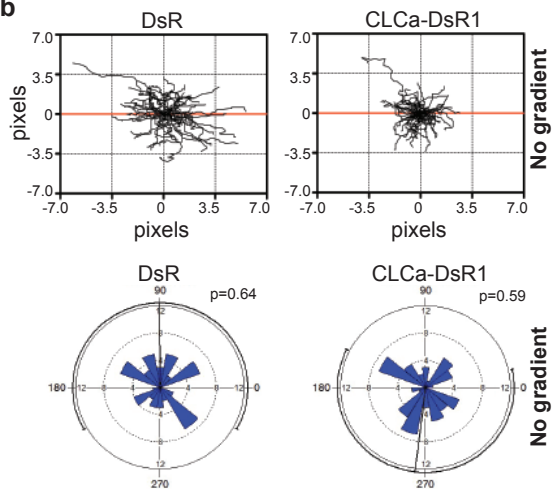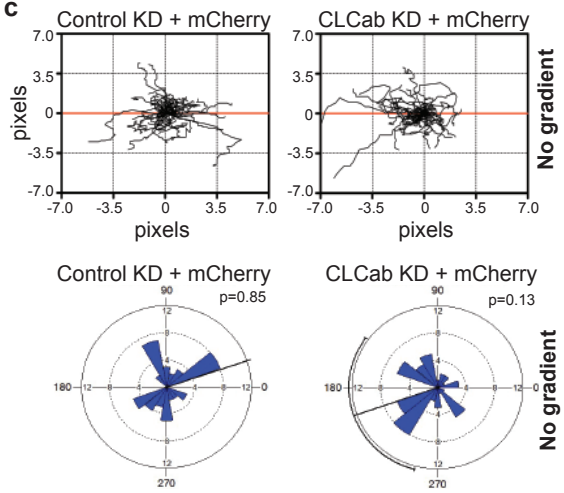
3. Chapter 3: Elevated IgA phenotype resulting from clathrin light chains' role in cargo selection

The clathrin light chain subunits mediate several important clathrin functions that are relevant to development, reproduction and disease as noted in chapter 2. The majority of these functions involve CLCs ability to mobilize actin polymerization through Hip protein binding, including clathrin-mediated recycling, CME from membranes under tension and Rac1 activation on endosomes during Drosophila eye development (Boulant et al., 2011; Majeed et al., 2014; Schreij et al., 2015). Bacteria and large virus particles can also exploit the CLC-Hip pathway to gain entry into the cell (Bonazzi et al., 2011; Cureton et al., 2010). While CME of many cargoes can occur in the absence of CLCs, they are required for uptake of three G-protein coupled receptors (GPCRs; (Ferreira et al., 2012; Huang et al., 2004; Poupon et al., 2008).

To assess whether CLCs are required for these clathrin-mediated pathways in vertebrates, we generated mice lacking the CLCa isoform. We analyzed CLC murine tissue-expression and observed that CLCa is the predominant CLC in lymphoid tissues, including B cells. To understand the contribution of CLCs to B cell function, we analyzed surface expression of several receptors important for B cell function in the mutant mice, followed by internalization studies in both murine B cells and cell lines. These studies demonstrate tha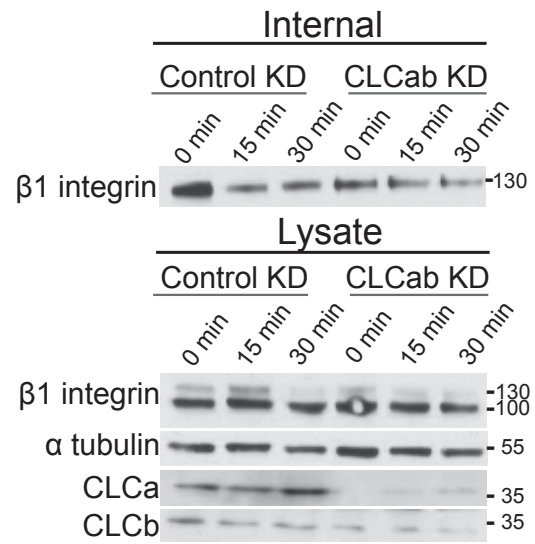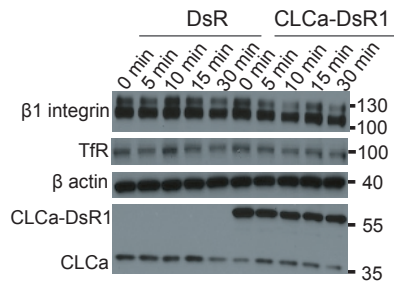t CLCs' contributions to CME are physiologically important. They identify a role for CLCs in CCV cargo selection of TGFβR2, which influences immunoglobulin class switch recombination between IgA and IgG1. These results broaden the role of CLCs in CME and demonstrate that CLCs can influence adaptive immune responses in addition to other physiologically significant pathways.

The rest of this chapter describes studies carried out in the CLCa knockout mice to determine its function *in vivo*. Below is the manuscript that is in preparation for submission to the Journal of Experimental Medicine. This is the first draft and the final submitted version is likely to change.

ELEVATED IgA PHENOTYPE RESULTING FROM CLATHRIN LIGHT CHAINS' ROLE IN CARGO SELECTION

Shuang Wu*[1,2,3,4], Sophia R. Majeed*[1,2,3,4], Timothy M. Evans[1,2,3,4], Marine Camus+[1,2,3,4], Nicole M.L. Wong+[1,2,3,4], Yvette Schollmeier[1,2,3,4], Minjong Park[1,2,3,4], Jagen R. Muppidi[3], Peter Parham[5], Jason G. Cyster#[3] and Frances M. Brodsky#[1,2,3,4]

*equal contribution, +equal contribution, #co-corresponding author

[1]Department of Bioengineering and Therapeutic Sciences, [2]Department of Pharmaceutical Chemistry, [3]Department of Microbiology and Immunology, [4]The G.W. Hooper Foundation, University of California San Francisco, San Francisco, CA 94143, USA,

[5]Departments of Structural Biology and Microbiology and Immunology, Stanford University, Stanford, CA 94305, USA

Corresponding author addresses:

Frances M. Brodsky

The G. W. Hooper Foundation, HSW 1529, Box 0552

University of California San Francisco

513 Parnassus Avenue

San Francisco, CA 94143-0552, USA

Phone: +1-415-476-6406; Fax: +1-415-476-6185

Email: Frances.Brodsky@ucsf.edu

Present address: Division of Biosciences, University College London, UK W1U 6QX

Jason G. Cyster

Microbiology and Immunology, UCSF, San Francisco, CA 94143

Phone: 415-502-6638

Email: Jason.Cyster@ucsf.edu

Abstract

Clathrin, a coat protein composed of heavy and light chain subunits, assembles into lattices on membranes of budding vesicles involved in receptor-mediated endocytosis and organelle biogenesis. Recent studies have elucidated various clathrin light chain (CLC) functions in cell lines, including endocytosis from villous membranes under tension, uptake of large bacterial and virus particles, and a subset of GPCRs. However, the physiological function of the CLCs in the context of a vertebrate model has not yet been addressed. Therefore we generated CLCa-deficient mice to elucidate the function of this CLC isoform *in vivo.* Although CLCa-deficient mice were viable at birth, a significant proportion died within the first month of life, and the mice that did survive had motor-coordination defects. Analysis of murine lymphoid tissues revealed that they express predominantly CLCa, and CLCa deficiency dysregulated isotype switch between IgA and IgG in germinal center B cells, stemming from CLCs role in mediating TGFβR2 endocytosis. Additionally, we found that CLCs are also necessary for efficient endocytosis of CXCR4 and delta opioid receptor, but not β2 agonist receptor or CXCR5, indicating that CLCs exhibit differential cargo selectivity. Thus, our results indicate that CLCs selectively mediate endocytosis of a broad range of receptors, which influences B-lymphocyte function *in vivo.*

Clathrin-coated vesicles (CCVs) select membrane cargo for transport during endocytosis, recycling and organelle biogenesis (Brodsky, 2012; Brodsky et al., 2001; Majeed et al., 2014), thereby influencing cell signaling, migration and metabolism. Clathrin consists of three clathrin heavy chain (CHC17) subunits with associated clathrin light chains (CLCs) configured into a three-legged triskelion. Adaptor molecules stimulate self-assembly of clathrin triskelia into a latticed coat on membranes that captures the adaptors and their associated membrane cargo for sequestration into a CCV for transport to intracellular destinations. In vitro studies have shown that clathrin self-assembly depends on CHC17 interactions but is regulated by CLCs, which span the central hub of the triskelion and impede spontaneous assembly (Wilbur et al., 2010a). CLC depletion by siRNA treatment of tissue culture cells showed that this negative regulation of clathrin assembly is not required for clathrin-mediated uptake of classic CCV cargo such as transferrin receptor, epidermal growth factor receptor or LDL-receptor (Huang et al., 2004; Majeed et al., 2014; Poupon et al., 2008), but CLCs have been implicated in several other aspects of clathrin function (Brodsky, 2012). Through binding actin-organizing proteins (Huntingtin-interacting protein1 (Hip1), the related Hip1R and Sla2p in yeast) at the N-terminus and leucine-rich repeat kinase 2 (LRRK2) at the C-terminus, CLCs facilitate clathrin-mediated endocytosis from membranes under tension (Aghamohammadzadeh and Ayscough, 2009; Boulant et al., 2011), clathrin-mediated recycling in cell migration (Majeed et al., 2014) and endosome function during Drosophila eye development (Schreij et al., 2015). The CLC-Hip interaction also facilitates uptake of large particles including virus and bacteria requiring coordination of clathrin and actin (Bonazzi et al., 2011; Cureton et al., 2010), and organizes the clathrin-actin interfaces during cell adhesion and bacterial pathogenesis (Bonazzi et al., 2012). A further role for CLCs in cargo uptake has been demonstrated for three G-protein coupled receptors (GPCRs), including the mu-opioid receptor (MOR), and the $P2Y_1$ and $P2Y_{12}$ purinergic receptors (Ferreira et al., 2012). Here we address which of these CLC functions has physiological significance for vertebrates, by genetic deletion from mice.

69

There are two CLC isoforms in vertebrates, CLCa and CLCb, encoded by separate genes. Both undergo alternate splicing that removes one or two exons encoding inserts of 12 (CLCa only) and 18 residues (CLCa and CLCb), generating four forms of CLCa and two forms of CLCb. Neurons express the highest molecular weight forms of both CLCs and the lowest molecular weight forms predominate in non-neuronal tissue. The intermediate splice variants of CLCa are present in brain (18 residue insert) (Kirchhausen et al., 1987) and in cardiac tissue (12 residue insert) (Giudice et al., 2014). In mammals, CLCa and CLCb are ~60% identical in protein sequence (Jackson and Parham, 1988), with two conserved regions, a 22-residue sequence near the N-terminus responsible for Hip-binding (Chen and Brodsky, 2005; Legendre-Guillemin et al., 2005) and a 10-residue sequence responsible for LRKK2-binding near the C-terminus (Schreij et al., 2015). Here we report that genetic deletion of CLCa reduces postnatal survival and compromises motor-coordination in mice. Characterization of the CLC composition of murine tissues indicates that lymphoid tissues express predominantly CLCa and do not compensate for CLCa deletion by CLCb expression, so are effectively CLC-negative. Analysis of B-lymphocytes in the CLCa knockout mice revealed that the mutant mice had elevated levels of IgA-expressing germinal center B cells. We were able to attribute this phenotype to CLCs' role in regulating surface levels of the transmembrane serine/threonine kinase, transforming growth factor-β receptor 2 (TGFβR2), through endocytosis. We also showed that CLCs regulate C-X-C chemokine receptor 4 (CXCR4) surface levels through their endocytic function, and we found that CLCs exhibit differential cargo selectivity for GPCRs during clathrin-mediated endocytosis (CME) in additional studies of cell lines. Our results establish TGFβR2 internalization dynamics as a key regulator of isotype switching to IgA in B cells *in vivo.* In addition, these studies of CLC function in vertebrates demonstrate that *in vivo*, CLCs play a significant role in CCV cargo selection by influencing uptake of a subset of signaling receptors in clathrin-mediated pathways.

Results

Genetic loss of CLCa reduces survival and impairs motor-coordination in mice

We generated a CLCa-deficient mouse in order to investigate the physiological function of CLCa *in vivo.* We silenced the *CLTA* gene, which spans ~30kb on mouse chromosome 4, by targeting exon 1 for excision by flanking it with LoxP sites (Fig. 1 A). The *CLTA* [flox/flox] mice were crossed with mice expressing *Cre* recombinase under the transcriptional control of the *ACTB* gene promoter, which resulted in deletion of CLCa from all tissues. Loss of CLCa was confirmed at both the genomic and protein levels by PCR and western blotting of *CLTA* [flox/flox] mice (designated as CLCa KO; Fig. 1 B and C). Deletion of CLCa did not affect protein levels of the CHC17 subunit, which were similar in WT and CLCa KO animals (Fig. 1 D). When heterozygous mutant mice were crossed with each other, the homozygous CLCa KO mice were born in the expected ratio and were viable at birth (Fig. 1 E). However, 50% CLCa KO pups died within the first week of life. We assessed the motor behavior of the mutant mice that survived to adulthood (Fig. 1 F). We evaluated their motor-coordination and balance by performing a rotarod test. CLCa KO mice fell off sooner compared to their WT littermates (Fig. 1 G). We also tested their locomotor activity by subjecting them to a grid-crossing test. CLCa KO mice took nearly twice as long to cross the grid compared to WT mice (Fig. 1 H). Taken together, these data suggest that genetic deletion of CLCa reduces survival and causes defects in motor-coordination in mice.

Murine CLC expression varies by tissue type and CLCa is the predominant light chain in the spleen.

The CLC isoforms have characteristic expression patterns with tissue-specific variation in cows and humans (Acton and Brodsky, 1990; Brodsky and Parham, 1983). Since the ratio of CLCs in mouse tissue was unknown, we quantified the amount of each CLC isoform in brain, heart, liver and spleen tissue in WT and CLCa KO mice by western blot analysis (Figs. 2 A, B

71

and C). Tissue homogenates were run next to dilutions of purified human CLCs of known concentration in order to produce a linear standard curve, and the amount of CLC in each tissue was then assessed using this standard curve. Similar to bovine brain tissue, WT murine brain tissue also expresses neuronal splice variants of both CLCa and CLCb, in addition to the ubiquitous forms of these CLCs (Fig. 2 A). Interestingly, our analysis indicated the presence of two types of tissues, those that express CLCa and CLCb at similar levels such as the heart and liver, and those that express predominantly CLCa, such as the spleen (Fig 2 C). We did not see compensatory increase of CLCb protein levels in the CLCa KO mice, except in liver tissue.

An assessment of CLCa transcript levels in WT mouse tissue correlated with the protein analysis, showing increased levels of CLCa mRNA in lymphoid tissues including the spleen, Peyer's patches (Pp) and mesenteric lymph node (mLN; Fig. 2 D). We also looked at mRNA levels of CLCb and CHC17 in the WT and CLCa KO mice (Fig. 2 E). Similar to what we observed at the protein level, expression of CLCb and CHC17 transcripts were comparable between WT and KO mice, with the exception of decreased CLCb mRNA in the cortex, which correlated with a similar decrease at the protein level. Thus, our results suggest that there are two types of tissue, one type with clathrin coats that contain a mixture of CLCa and CLCb triskelia, and another type in which CLCa is the predominant light chain in coated vesicles.

Genetic loss of CLCa results in an increased proportion of germinal center (GC) B cells that express IgA, and a reduction in the proportion of GC B cells expressing IgG1.

Our observation that the spleen expresses predominantly CLCa and negligible amounts of CLCb led us to further analyze this lymphoid compartment in the mice. We purified B and T lymphocytes from the spleens of WT mice and assessed the amounts of CLCs present in these cell types by western blotting (Fig. 3 A). Consistent with our analysis of total spleen tissue, both B and T cells expressed primarily CLCa. CLCb was undetectable in our samples, as the small yield of purified lymphocytes from each mouse did not allow boiling of the lysates, which

concentrates boil-resistant light chains as was done in Figs. 1 C and 2 A. Interestingly, B cells showed higher levels of total clathrin (CHC17 and CLCa) compared to T cells, which was also consistent at the mRNA level (Fig. 3 B).

Because B cells express more total clathrin, and are nearly absent of CLCs in the CLCa KO mice, we further analyzed these cells to define the role of CLCs *in vivo.* To ensure that our results were directly attributable to CLC levels and not due to changes in CHC17, we assessed CHC17 protein levels in the WT and KO mice by western blot (Fig. 3 C). Indeed, heavy chain levels in B cells in the WT and KO mice were similar. B cells are largely situated in follicles within lymphoid organs such as the spleen, Peyer's patches and lymph nodes (Cyster, 2010). After the first specific antibodies are produced during a T-dependent antibody response, germinal centers (GC), where B cells undergo proliferation, differentiation, antibody affinity maturation and isotype switching, form in B cell follicles (Green and Cyster, 2012; Zhang et al., 2013). Interestingly, we found that CLCa KO mice had an increased frequency of IgA-expressing GC B cells in Peyer's patches (Fig. 3 D, E and F). The mutant mice also showed a two-fold reduction in IgG1-expressing GC B cells (Fig. 3 E and F). To determine whether this was an intrinsic B cell defect or caused by changes in the stroma, we generated mixed bone marrow (BM) chimeras. To do this, sub-lethally irradiated C57BL/6 mice were reconstituted with a 1:1 mixture of WT or CLCa KO BM cells (CD45.2$^+$) and WT C57BL/6 (B6) (CD45.1$^+$CD45.2$^+$) BM cells. Similar to the CLCa KO mice, mixed CLCa KO/B6 mixed chimeras showed both an increase in IgA-expressing GC B cells, and a reduction in IgG1-expressing GC B cells derived from CLCa KO mice than those derived from WT B6 cells (Fig. 3 G, H and I). In contrast, CLCa WT/B6 mixed chimeras had similar proportions of IgA and IgG1-expressing GC B cells derived from WT CD45.2$^+$ or WT B6 cells. Moreover, the ratio of GC B cells to follicular (Fo) B cells was reduced in the mLN, Pp and spleen in cells derived from CLCa KO in CLCa KO/B6 mixed chimeras compared to CLCa WT/B6 mixed chimeras (Fig. 3 J). The data from mixed BM chimeras indicates that anomalies in GC B cell IgA and IgG1 isotype switching are intrinsic

defects. Furthermore, these results indicate that CLCa is required for regulation of GC B cell development and isotype class switching between IgA and IgG1.

CLCa regulates transforming growth factor β receptor 2 (TGFβR2) surface expression and downstream signaling in B cells

Selective deletion of TGFβR2 in B cells was shown to reduce IgA-expressing cells, and increase IgG1-positive B cells in mice, and notably, CHC17 has been implicated in TGFβR2 endocytosis (Cazac and Roes, 2000; Di Guglielmo et al., 2003; Mitchell et al., 2004). This led us to examine surface levels of TGFβR2 on B cells in the CLCa-deficient mice. We found that the CLCa KO mice expressed higher surface levels of TGFβR2 in B cells from Peyer's patches and spleen compared to WT controls (Fig. 4 A and B). In contrast, surface expression of the transmembrane B cell marker, B220, was similar between WT and KO mice. We confirmed that this increase in TGFβR2 surface levels was not the result of increased mRNA or protein expression (Fig. 4 C and D).

To rule out the possibility that up-regulation of surface TGFβR2 was caused by changes in TGF-β cytokines in the stromal environment in the lymphoid tissues, we assessed TGFβR2 surface expression in the mixed BM chimeras. Surface levels of TGFβR2 were increased in the B cells derived from CLCa KO cells in the CLCa KO/B6 mixed chimeras, but not in the CLCa WT/B6 mixed chimeras, demonstrating that the dysregulation of TGFβR2 surface expression is a cell-intrinsic defect (Fig. 5 A and B). We then asked whether there were functional consequences of increased surface TGFβR2 levels. TGFβR2 forms a heteromeric complex with TGFβR1 when the type I receptor is bound by members of the TGFβ superfamily. TGFβR2 then activates TGFβR1, which initiates Smad signaling by phosphorylating R-Smad2 and R-Smad3 (Di Guglielmo et al., 2003). TGFβ signaling through Smad2 was previously shown to be critical for the class switch to IgA in B cells; therefore we investigated this pathway in the CLCa KO

mice (Klein et al., 2006). Indeed we observed higher levels of phospho-Smad2/3 in splenic B cells and total splenocytes from CLCa KO mice (Fig. 5 C and D), suggesting that higher surface levels of TGFβR2 correlate with increased signaling of the receptor.

Since CLCs have been implicated in the endocytosis of a subset of GPCRs, we hypothesized that increased TGFβR2 surface levels in CLCa-deficient B cells were the result of impaired receptor uptake (Ferreira et al., 2012). We were unable to address this in B cells from the mutant mice since the TGFβR2 antibody signal was not sensitive enough to assess receptor internalization, so we tested this hypothesis in HEK293T cell lines transiently co-transfected with TGFβR2-IRES-GFP and siRNA. As expected, TGFβR2 endocytosis was impaired in CHC17-depleted cells (Di Guglielmo et al., 2003). Consistent with our hypothesis, TGFβR2 uptake was also significantly reduced in CLC-depleted cells compared to control cells (Fig. 5 E and G). We assessed uptake of endogenous transferrin receptor (TfR) in TGFβR2-IRES-GFP transfected cells as a control. CHC17 depletion blocked CME of TfR, while CLC depletion had no affect on CME of TfR as previously reported (Fig 5 F and G; (Huang et al., 2004). Thus, our data demonstrate that loss of CLCs causes increased surface levels and signaling of TGFβR2 in GC B cells through the role of CLCs in endocytosis, which in turn impairs isotype class switching between IgA and IgG1.

CLCa is necessary for efficient ligand-induced uptake of CXCR4 in B cells

Since we observed increased surface expression of TGFβR2 in B cells, we investigated surface levels of other receptors critical for GC B cell function (Bannard et al., 2013). We found that GC B cells from CLCa KO mice expressed higher surface levels of CXCR4 compared to WT cells, whereas levels of B220 remained the same between the two groups as noted earlier (Fig. 6 A and B). Experiments in mixed BM chimeras revealed that this was a GC B cell intrinsic defect (Fig. 6 C and D). Since CLCs were required for endocytosis of TGFβR2, we asked if

increased CXCR4 surface levels in CLCa-deficient B cells were the result of impaired internalization of the receptor. Stromal cell-derived factor 1 (SDF)-induced internalization of CXCR4 in B cells isolated from the mLNs of WT and CLCa KO mice revealed that endocytosis of this receptor was reduced in the CLCa-deficient Fo and GC B cells (Fig 7 A and B). Consistent with these findings, SDF-mediated uptake of CXCR4 was also reduced in the cells derived from CLCa KO mice in CLCa KO/B6 mixed chimeras compared to controls (Fig. 7 C). In contrast, surface expression of CXCR5 in Fo and GC B cells was similar between WT and CLCa KO animals (Fig, 8 A). In keeping with this observation, there was no difference in B lymphocyte chemoattractant (BLC)-induced internalization of CXCR5 in B cells isolated from WT or CLCa KO mice, or from B cells from mixed chimera mice (Fig. 8 B, C and D). This data demonstrates that CLCs are required for CME of CXCR4 in B cells, while being dispensable for CME of other cargo such as CXCR5. More broadly, these results suggest that CLCs play an important role in CCV cargo selection.

CLC depletion in cell lines reveals differential affects of CLCs on CCV cargo selection

Our finding that CLCa regulates surface levels of TGFβR2 and CXCR4, but not CXCR5 and B220 in B cells, prompted to us to broaden our investigation to other cargoes in cell lines. We depleted CHC17 or both CLCs from HEK293 cells that stably expressed either N-terminally Flag-tagged β2 agonist receptor (F-β2AR), or N-terminally Flag-tagged delta-opioid receptor (F-DOR) and performed ligand-induced internalization experiments on these cells (Fig. 8 A and B). These studies revealed that CLC depletion impaired ligand-induced CME of F-DOR. (Fig. 8 C). Uptake of endogenous TfR in these cells showed that CLC depletion was dispensable for this receptor's CME (Fig. 8 D). In contrast, CLC depletion had no effect on ligand-induced CME of F-β2AR, indicating that CLCs exhibit cargo selectivity (Fig. 8 E). Depletion of CLCs did not affect uptake of endogenous TfR in these cells as expected (Fig. 8 F). This data reveals that CLCs are

required for CME of a subset of signaling receptors, such as HA-TGFβR2, CXCR4 and F-DOR, but are dispensable for other receptors, such as F-β2AR and CXCR5.

Discussion

In this study, we define the physiological function of the CLCs in endocytosis in the context of a mouse model, and we further show that CLCs' role in cargo selection is critical for B cell function. During the course of an antigen-driven response, B cells first express a low-affinity functional antibody, and then undergo positive selection to produce antigen-specific immunoglobulin (Ig) of increasing affinity (Rajewsky, 1996). TGFβR2 induces IgA expression in B cells, and this isotype switch is mediated by TGFβ signaling through Smad2 (Cazac and Roes, 2000; Klein et al., 2006). We establish a role for CLCs in isotype switching between IgA and IgG1 in B cells, stemming from their role in regulation of TGFβR2 endocytosis and signaling. The frequency of IgA-expressing GC B cells is increased in the CLCa KO mice, whereas IgG1-expressing GC B cells are reduced. Consistent with this phenotype, surface levels of TGFβR2 and downstream signaling through Smad2 are both elevated in CLCa-deficient B cells. Our results demonstrate that CLCs are required for mediating uptake of TGFβR2, which is necessary to achieve the appropriate Ig response.

TGFβR2 can internalize through a clathrin-dependent route, or through a caveloae-dependent pathway. CME of TGFβR2 is believed to promote signaling of the receptor through phosphorylation of Smad2 and Smad3, while clathrin-independent pathways lead to degradation of ligand-bound TGFβ receptors and attenuation of signaling (Di Guglielmo et al., 2003; Huang and Huang, 2005; Le Roy and Wrana, 2005). TGFβR2 signaling was further found to occur at the coated pit stage, as the dynamin inhibitor Dynasore increased TGFβ receptor signaling through Smad2 both in cells and *in vivo* (Chen et al., 2009). Our results support these findings

77

as genetic loss of CLCa increased TGFβR2 surface levels and levels of pSmad2/3 *in vivo*. These results also suggest that CLCs are necessary for TGFβR2 CCV formation and further studies will be needed to address this.

A recent study implicated CLCs in endocytosis of three GPCRs, while others have found them to be dispensable for CME of other types of cargo including TfR, the epidermal growth factor receptor (EGFR), the low-density lipoprotein (LDL) receptor, and the cation-independent-mannose-6-phosphate receptor (CIMPR;(Ferreira et al., 2012; Huang et al., 2004; Poupon et al., 2008). Here, we extend the types of cargo that require CLCs for CME beyond GPCRs to include the serine/threonine kinase TGFβR2. Our finding that TGFβR2, CXCR4 and F-DOR, but not F-β2AR and CXCR5, require CLCs for CME suggests that CLCs are needed for coated pit formation and maturation depending on the type of cargo present in the clathrin-coated pit (CCP). Previous studies have demonstrated that the Sec13 component of the COPII vesicle coat, which mediates cargo transport from the endoplasmic reticulum, confers structural rigidity onto the coat. Thus, Sec13 is necessary to promote membrane curvature in the presence of asymmetric or rigid cargo, such as collagen (Copic et al., 2012; Townley et al., 2008). Structural models of CLCs predict that they influence lattice curvature by regulating rigidity of clathrin triskelia at the "knee," and several CLC-Hip dependent functions have been characterized which rely on CLCs' ability to regulate actin (Bonazzi et al., 2011; Boulant et al., 2011; Majeed et al., 2014; Wilbur et al., 2010b). Therefore, we propose that some cargo, such as TGFβR2, CXCR4 and F-DOR, require CLCs to provide tensile strength to bend the membrane for CME by influencing nearby actin assembly. Ubiquitination of cargo can mediate the recruitment of ubiquitin-binding endocytic adaptors to promote clustering of cargo into CCPs, including MOR and CXCR4, which require CLCs for CME (Ferreira et al., 2012; Henry et al., 2012; Hicke and Dunn, 2003; Marchese et al., 2003; Shih et al., 2002; Torrisi et al., 1999; Toshima et al., 2009). Interestingly, ubiquitin has also been implicated in regulating COPII coat size in the biosynthetic

pathway (Jin et al., 2012). Therefore, it is possible that some cargoes, which increase membrane rigidity or vesicle size by accumulation or some other mechanism, require CLCs for uptake. Further studies will be needed to dissect the precise membrane dynamics of coated pits that require CLCs for CME.

The ratio of CLCa to CLCb expression is different depending on the tissue type, and we show here that mice contain tissues that either express roughly equal amounts of CLCa and CLCb, or predominantly CLCa, hinting that there may be some functional differences between the two CLC isoforms which have yet to be characterized (Acton and Brodsky, 1990; Brodsky and Parham, 1983). The impaired survival of CLCa KO mice, paired with their loco-motor defects further suggests that the CLCa isoform may play an important role in brain and muscle function. Indeed, expression of alternative splice variants of CLCa during postnatal mouse heart development was recently reported, suggesting that CLCa may have additional specialized tissue functions which need to be investigated in future biochemical studies (Giudice et al., 2014).

Notably, the present study reveals that CLCa is the dominant CLC in lymphoid tissues, which prompted us to investigate the function of CLCs in B cells. A recent study described a role for the endocytic scission protein, dynamin-2, in mediating T cell egress from lymphoid organs through regulation of sphingosine-1-phosphate (S1P) receptor 1 internalization, demonstrating that endocytic proteins can influence lymphocyte function by cargo regulation (Willinger et al., 2014). Previous studies involving the role of clathrin in lymphocytes have shown that CHC17 regulates endocytosis of the B-cell receptor and recruits proteins that mediate actin polymerization to the immunological synapse in T cells (Calabia-Linares et al., 2011; Stoddart et al., 2002). However, the contribution of CLCs was not addressed in these studies. In this study, we define a new function for CLCs in regulating TGFβ-directed isotype class switching to IgA in B-lymphocytes *in vivo* through their role in endocytic cargo selection. Our work reveals that

CLCs are required for CME of a broad range of cargoes, which likely influences their function in other specialized tissue types, including brain and muscle.

Materials and Methods

Mice and mixed bone Marrow chimeras

C57BL/6 mice were purchased from The Jackson Laboratory. CD45.1$^+$ congenic mice were obtained from the National Cancer Institute (01B96; B6-LY5.2/Cr). CD45.1$^+$CD45.2$^+$ mice were generated by crossing B6 and Boy/J (Jackson Laboratory, 002014; B6.SJL-Ptprc a Pepc b/BoyJ) mice.

Mixed bone marrow chimeras were generated by intravenously transferring 3 x 10^6 to 5 x 10^6 cells from the following mixes into lethally irradiated (2 x 450 rads 3 hours apart) CD45.1$^+$ congenic mice: Clta$^{-/-}$ mice(CD45.2$^+$): WT B6(CD45.1$^+$CD45.2$^+$); Clta$^{+/+}$(CD45.2$^+$): WT B6 (CD45.1$^+$CD45.2$^+$), at a 50:50 ratio. Mice were analyzed at least of 8 weeks after reconstitution. Mice were bred and maintained at the Laboratory Animal Research Center at UCSF. The UCSF Institutional Animal Care and Use Committee approved all animal experiments.

Generation of CLCa-deficient mutant mice

The entire mouse CLCa gene was inserted into a bacterial artificial chromosome (BAC). Using BAC-based homologous recombination in E. coli, we produced a BAC targeting construct containing a PGK*neo* cassette flanked by FRT sites and a loxP site in intron 1. A second loxP site was cloned into the 5' UTR. The PGK*neo* cassette was excised by Flpe-recombinase mediated deletion. This recombinant BAC was transfected into ES cells and transfectants were selected for recombination of the floxed CLCa gene. These ES cells were transfected with Cre recombinase to ensure that the loxP sites were functional and exon excision was confirmed by PCR. The ES cells were then injected into C57BL/6 mouse blastocysts and transferred into foster mothers. Chimeras were mated with C57BL/6 females and germ line transmission of the floxed CLCa gene was confirmed by Southern blotting of tail DNA. CLCa^{flox}/+ heterozygous mice were mated to *ACTB-Cre* deleter mice to excise the CLCa gene between the LoxP sites in

order to generate the CLCa null mutation. Excision of the CLCa gene was confirmed using PCR using the following primers: LCa-GTF1 (TGTGTTGAGTAGTCGGGAAGAG) and LCa-FRT-R (ACTTACACGAATTCCGAAGTTCC).

Behavioral tests

Accelerating rotarod. Mice were placed onto the rotarod (Ugo Basile) facing the opposite direction of rotation. Initially, the rotarod moved at a speed of 2 rpm and after 10 seconds the speed was incrementally increased to 20 rpm per minute over 5min. The time it took for the mice to fall once acceleration had begun was recorded.

Grid-walking test. Mice were placed onto a grid-walking apparatus and were trained to cross the grid 3 times over 2 days prior to the test. The time it took for each mouse to cross the grid was noted.

siRNAs and plasmids

siRNA duplexes were synthesized by Qiagen. Targeting sequences were published as follows, CHC17, CLCa and CLCb (Huang et al., 2004). Human TGFβR2 (sub-cloned from pCMV5B-TGFbeta receptor II wt (N-term HA), Addgene plasmid # 24801) was cloned into IRES-GFP in the vector PCL6IEGWO (Bosch et al., 2013).

Tissue Culture and Transfections

HEK293 cells were cultured in DMEM, supplemented with 10% FBS (Hyclone) and antibiotics. Cells were plated at ~70% confluency, and were transfected with siRNA using the Jetprime reagent (VWR), the following day according to the manufacturer's protocol. Cells were analyzed 72 hours post-siRNA treatments. For TGFβR2 internalization assays, HEK293T cells were co-transfected with siRNA and TGFβR2-IRES-GFP using Jetprime reagent (VWR).

Splenic B cells and T cells purification

Splenic B cells were purified by negative selection using anti-CD43 magnetic beads (MACS, Miltenyl Biotech). T cells were purified by negative selection by using a biotin conjugated antibody cocktail (anti-Ter119, anti-B220, anti-CD19, anti-CD11b, anti-Gr1, anti-CD11c) followed by binding to Streptavidin MicroBeads (MACS, Miltenyl Biotech). Cell purity was confirmed by FACs.

Antibodies and other reagents

The following antibodies were used for FACS-based internalization: Flag M1 (1:1000, Sigma, number F-3040), TfR (1:300, BD, number 555534), human TGFβR2 (1:250, AF241, R&D systems), Alex Fluor-555 (1:500, Life Technologies, number A-22287), Alex Fluor-568 (1:500, life Technologies, A-11057), Alexa Fluor-647 antibody labeling kit (Life Technologies, A-20186).

The following antibodies were used for western blotting: anti-CHC17 (2μg/ml, TD.1), anti-CLCa (5μg/mL, X16), CLTA (1:1000, Proteintech, number 10852-1-AP), CLTB (1:1000, Proteintech, number 10455-1-AP), anti-CLCb (2μg/mL, LCb.1), anti-β-actin (1:5000, Sigma, number A5441) and α-tubulin (1:10,000, Sigma, number T6199), biotin-conjugated anti-TGFβR2 (1:1000, BAF532, R&D). Biotin conjugated anti α-tubulin (1:3000, clone DM1A, eBiosciences), pSMAD2/3 (1:1000, clone D27F4, Cell Signaling Tech), SMAD2 (1:1000, number 51-1300, Life Technologies)

The following secondary antibodies were used for western blotting: Donkey anti-rabbit IRDye700DX (1:1000, Rockland, number 611-730-127), Donkey anti-mouse IRDye800 (1:1000, Rockland, 610-732-124), Streptavidin IRDye 800(1:10,000, 926-32230, LiCor). For pSMAD2/3 detection, stabilized goat anti-rabbit HRP-conjugated antibody (1:4000, number 1A110693, Pierce) was used.

Immunoblotting

Cells were lysed in a buffer containing 50mM Tris (pH 7.2), 150mM NaCl, 20mM EDTA, 1% Triton X-100, and EDTA-free protease inhibitors (Roche, number 11836170001). Protein content was determined using the Pierce BCA Protein Assay kit (Thermo Scientific, number 23225). Equal amounts of proteins were resolved on pre-cast SDS-PAGE gels (Invitrogen) and then transferred onto nitrocellulose membranes (Bio-Rad), Proteins were detected by labeling with primary and secondary antibodies. Blots were scanned using the Odyssey Infrared Imaging System (LI-COR Biosciences, Lincoln, NE), or by using the ECL system (Amersham Biosciences) according to the manufacturers protocols.

CLC isoform levels in tissues were determined by western blotting using a previously described protocol (Acton and Brodsky 1990). Briefly, murine tissues were homogenized in lysis buffer (150mM NaCl, 1mM EGTA, 10mM Hepes, 0.5mM $MgCl_2$, 0.02% NaN_3, 0.05% PMSF, pH 7.2) containing EDTA-free protease inhibitors (Roche) on ice and centrifuged at 1,000 g for 30 min at 4°C. The supernatants were then boiled for 10 min and centrifuged at 10,000 g for 10 min at 4°C, which left boiling-resistant CLCs in solution and causes CHC and the majority of other proteins to precipitate. Protein levels in boiled homogenates were quantified, then reduced in 4x sample buffer and alkylated by addition of 20mM iodoacetamide for 1 hour at room temperature. Both tissue homogenates and purified human His-tagged CLC proteins of known concentration were run next to one another on 12% polyacrylamide gels, and then transferred onto nitrocellulose membranes (Bio-Rad). Membranes were blocked with Odyssey blocking buffer (LI-COR Biosciences, number 927-40000) diluted 1:1 in PBS for 1 hour at room temperature, and then incubated in primary antibodies overnight, followed by incubation with secondary antibodies after several washes.

CLC isoform in splenic B cells and T cells were determined by western blotting of directly lysed purified B and T cells with the lysis buffer mentioned above.

Band intensities were quantified using ImageJ by plotting signal intensities and measuring the areas under each peak. For tissue samples, band intensities were titrated against known concentrations of purified His-tagged CLCa and CLCb in order to determine their concentrations. Plots were generated for each tissue type and titrations were only accepted if the linear fit had an R^2 value of at least 0.9, except in the case for spleen where values of 0.73 were used due to the limited availability of tissue sample for titrations. For pSmad2/3, the pSmad2/3 band intensities were normalized with CHC17 band intensities.

Flow cytometry.

Spleen, mesenteric lymph nodes and Peyer's patches cells were isolated and stained as previously described (Bannard et al., 2014). For GC B cell staining, cells were stained with APC-cy7 or PercPCy5.5 conjugated B220 (clone RA3-6B2, Biolegend), PercPCy5.5 or Pacific Blue-conjugated anti-IgD (clone IA6-2, number 11-26c.2a, Biolegend), PE-Cy7–conjugated anti-CD95 (clone Jo2; BD Biosciences), FITC or Alexa Fluor647-conjugated anti GL7 antigen (T&B cell activation antigen or Ly-77, clone GL7, Biolegend). To analyze mixed bone marrow chimera, Pacific Blue, PE, FITC, BV605 conjugated anti-CD45.1 (clone A20, Biolegend) or anti-CD45.2 (clone 104, Biolegend) antibodies were used. For TGFβR2 staining, PE (number FAB532P, R&D) or biotin (number BAF532, R&D) conjugated anti-mouse TGFβR2 antibodies were used. For CXCR4 and CXCR5 staining, biotin labeled anti-CXCR4 (number 551968, BD Biosciences) and anti-mouse CXCR5 (number 551960, BD Biosciences) antibodies were used. Data was acquired on LSRII (BD Biosciences) and analyzed with FlowJo (Tree Star).

Internalization assays

Stably transfected HEK293 cells grown in 12-well plates were first washed with serum-free media, and then serum starved in serum-free media for 15 minutes at 37°C. Ligand diluted at the appropriate concentration in serum-free media was then added to the cells at the

appropriate time points, after which cells were placed back at 37°C and allowed to internalize the receptor for the indicated times. Control cells were left untreated and remained at 37°C. Then, all cells were immediately placed on ice and washed once with cold PBS, after which they were stained with M1 antibody conjugated to Alexa Fluor-647 for 30 min at 4°C. Next, the cells were lifted into tubes by gentle pipetting and washed once with cold PBS. The cells were then suspended in 0.2% BSA in PBS and analyzed by FACS.

For analysis of transferrin receptor internalization, stably transfected HEK293 cells grown in 12-well plates were serum starved and then labeled with anti-TfR antibody diluted in 0.2% BSA in PBS for 30 min at 4°C. Cells were then placed on ice, washed twice with cold PBS, and then maintained in 0.2% BSA in PBS for the remainder of the experiment. Cells were removed from ice and placed at 37°C for the appropriate time points to allow labeled receptor to internalize, after which cells were placed back on ice. Next, cells were incubated with Alexa Fluor-555 secondary antibody for 30 min at 4°C. Cells were then lifted into tubes by gentle pipetting, washed once with cold PBS, and then re-suspended in 0.2% BSA in PBS and analyzed by FACS.

For CXCR4 or CXCR5 internalization of mesenteric B cells, the mLNs were harvested into pre-warmed migration buffer (RPMI supplemented with 0.5% fatty acid-free BSA, 10mM Hepes, glutamine and antibiotics), and then lymphocytes were isolated by mechanical disaggregation through a 80-µm nylon sieve at room temperature. After two washes with migration buffer, cells were re-suspended in migration buffer at 10^7/ml. Cells were incubated in a 37°C water bath for 30 min. Cells suspensions were added to tubes containing migration buffer only (PBS), SDF (1µg/ml) or BLC (10 µg/ml) to reach the working concentration of SDF (100ng/ml), or BLC (1 µg/ml). Cells were incubated for indicated times, and then ice-cold migration buffer was added to the tubes, which were immediately placed on ice. After

internalization, cells were washed, pelleted, and stained with Bio-CXCR4 or Bio-CXCR5. After staining with secondary antibodies, the cells were analyzed by FACS.

For TGFβR2 internalization, plasmid and siRNA co-transfected HEK293T cells were grown in 24 well plates for 72 hours. Cells labeled with anti-TGFβR2 antibody diluted in DMEM supplemented with 10mM Hepes for 30 min on ice. Cells were washed with ice cold DMEM + Hepes twice, and then were placed back at 37°C for the appropriate time points to allow labeled receptor to internalize, after which cells were placed back on ice. Next, cells were incubated with Alexa Fluor-568 secondary antibody for 30 min on ice in the dark, and then washed with with ice-cold DMEM + Hepes twice. Cells were then lifted into tubes by gentle pipetting, and re-suspended in 0.2% BSA in PBS + DAPI and analyzed by FACS. GFP-positive cells were gated for the TGFβR2 internalization analysis.

mRNA quantification

Total RNA was isolated with RNeasy Micro Kit or RNeasy Mini Kit (Qiagen, Venlo, The Netherlands). cDNA was synthesized by using MMLV reverse transcriptase and random primers (Life Technologies). Real-time PCR was carried out using a StepOnePlus real-time PCR system (Applied Biosystems, Foster City, CA) with SYBR Green PCR Master Mix (Applied Biosystems) and the appropriate primer pairs. For *CLTA*, forward 5'-ATGCTGTTGACGGAGTGATGA-3', and reverse 5'-CCACTTACGGATACTTTCAGGCT-3'. For *CLTB*, forward 5'-GAAAGCGAGATTGCTGGCATC-3' and reverse 5'-CGTTAGCCTCCTGAAACACATC-3'. For *CLTC*, forward 5'- AGATTCTGCCCATTCGCTTTC-3' and reverse 5'-TCAGTGCAATCACTTTGCTGG-3'; For *Hprt1* forward 5'-AGGTTGCAAGCTTGCTGGT-3' and reverse 5'-TGAAGTACTCATTATAGTCAAGGGCA-3', synthesized by Integrated DNA Technologies. Relative mRNA abundance of target genes was determined by subtracting the threshold cycle for the internal reference (*Hprt1*) from that of the target.

Statistical Analysis

Statistical analyses were performed using GraphPad Prism (GraphPad Software, Inc). Parametric data were analyzed using two-tailed Student t-tests, one-way or two-way ANOVA, followed by Bonferroni post hoc tests for multiple comparisons as appropriate (95% confidence interval).

Acknowledgements

Author Contributions

S.W., S.R.M., T.E., P.P., J.M., J.G.C., and F.M.B. designed the experiments. S.W., S.R.M., M.C., N.M.L.W., T.E., Y.S., and M.P. performed the experiments. S.R.M. and F.M.B. wrote this draft version of the manuscript with input from S.W.

References

Acton, S., and F.M. Brodsky. 1990. Predominance of clathrin light chain LCb correlates with the presence of a regulated secretory pathway. *J. Cell Biol.* 111:1419-1426.

Aghamohammadzadeh, S., and K.R. Ayscough. 2009. Differential requirements for actin during yeast and mammalian endocytosis. *Nat Cell Biol* 11:1039-1042.

Bannard, O., R.M. Horton, C.D. Allen, J. An, T. Nagasawa, and J.G. Cyster. 2013. Germinal center centroblasts transition to a centrocyte phenotype according to a timed program and depend on the dark zone for effective selection. *Immunity* 39:912-924.

Bonazzi, M., A. Kuhbacher, A. Toledo-Arana, A. Mallet, L. Vasudevan, J. Pizarro-Cerda, F.M. Brodsky, and P. Cossart. 2012. A common clathrin-mediated machinery co-ordinates cell-cell adhesion and bacterial internalization. *Traffic* 13:1653-1666.

Bonazzi, M., L. Vasudevan, A. Mallet, M. Sachse, A. Sartori, M.C. Prevost, A. Roberts, S.B. Taner, J.D. Wilbur, F.M. Brodsky, and P. Cossart. 2011. Clathrin phosphorylation is required for actin recruitment at sites of bacterial adhesion and internalization. *J Cell Biol* 195:525-536.

Bosch, J., A.P. Houben, T. Hennicke, R. Deenen, K. Kohrer, S. Liedtke, and G. Kogler. 2013. Comparing the gene expression profile of stromal cells from human cord blood and bone marrow: lack of the typical "bone" signature in cord blood cells. *Stem Cells Int* 2013:631984.

Boulant, S., C. Kural, J.C. Zeeh, F. Ubelmann, and T. Kirchhausen. 2011. Actin dynamics counteract membrane tension during clathrin-mediated endocytosis. *Nat Cell Biol* 13:1124-1131.

Brodsky, F.M. 2012. Diversity of clathrin function: new tricks for an old protein. *Annu Rev Cell Dev Biol* 28:309-336.

Brodsky, F.M., C.Y. Chen, C. Knuehl, M.C. Towler, and D.E. Wakeham. 2001. Biological basket weaving: Formation and function of clathrin-coated vesicles. *Annu. Rev. Cell. Dev. Biol.* 17:517-568.

Brodsky, F.M., and P. Parham. 1983. Polymorphism in clathrin light chains from different tissues. *J. Mol. Biol.* 167:197-204.

Calabia-Linares, C., J. Robles-Valero, H. de la Fuente, M. Perez-Martinez, N. Martin-Cofreces, M. Alfonso-Perez, C. Gutierrez-Vazquez, M. Mittelbrunn, S. Ibiza, F.R. Urbano-Olmos, C. Aguado-Ballano, C.O. Sanchez-Sorzano, F. Sanchez-Madrid, and E. Veiga. 2011. Endosomal clathrin drives actin accumulation at the immunological synapse. *J Cell Sci* 124:820-830.

Cazac, B.B., and J. Roes. 2000. TGF-beta receptor controls B cell responsiveness and induction of IgA in vivo. *Immunity* 13:443-451.

Chen, C.L., W.H. Hou, I.H. Liu, G. Hsiao, S.S. Huang, and J.S. Huang. 2009. Inhibitors of clathrin-dependent endocytosis enhance TGFbeta signaling and responses. *J Cell Sci* 122:1863-1871.

Chen, C.Y., and F.M. Brodsky. 2005. Huntingtin-interacting protein 1 (Hip1) and Hip1-related protein (Hip1R) bind the conserved sequence of clathrin light chains and thereby influence clathrin assembly in vitro and actin distribution in vivo. *J. Biol. Chem.* 280:6109-6117.

Copic, A., C.F. Latham, M.A. Horlbeck, J.G. D'Arcangelo, and E.A. Miller. 2012. ER cargo properties specify a requirement for COPII coat rigidity mediated by Sec13p. *Science* 335:1359-1362.

Cureton, D.K., R.H. Massol, S.P. Whelan, and T. Kirchhausen. 2010. The length of vesicular stomatitis virus particles dictates a need for actin assembly during clathrin-dependent endocytosis. *PLoS Pathog* 6:e1001127.

Cyster, J.G. 2010. B cell follicles and antigen encounters of the third kind. *Nat Immunol* 11:989-996.

Di Guglielmo, G.M., C. Le Roy, A.F. Goodfellow, and J.L. Wrana. 2003. Distinct endocytic pathways regulate TGF-beta receptor signalling and turnover. *Nat Cell Biol* 5:410-421.

Ferreira, F., M. Foley, A. Cooke, M. Cunningham, G. Smith, R. Woolley, G. Henderson, E. Kelly, S. Mundell, and E. Smythe. 2012. Endocytosis of G protein-coupled receptors is regulated by clathrin light chain phosphorylation. *Curr Biol* 22:1361-1370.

Giudice, J., Z. Xia, E.T. Wang, M.A. Scavuzzo, A.J. Ward, A. Kalsotra, W. Wang, X.H. Wehrens, C.B. Burge, W. Li, and T.A. Cooper. 2014. Alternative splicing regulates vesicular trafficking genes in cardiomyocytes during postnatal heart development. *Nat Commun* 5:3603.

Green, J.A., and J.G. Cyster. 2012. S1PR2 links germinal center confinement and growth regulation. *Immunol Rev* 247:36-51.

Henry, A.G., J.N. Hislop, J. Grove, K. Thorn, M. Marsh, and M. von Zastrow. 2012. Regulation of endocytic clathrin dynamics by cargo ubiquitination. *Dev Cell* 23:519-532.

Hicke, L., and R. Dunn. 2003. Regulation of membrane protein transport by ubiquitin and ubiquitin-binding proteins. *Annu. Rev. Cell. Dev. Biol.* 19:141-172.

Huang, F., A. Khvorova, W. Marshall, and A. Sorkin. 2004. Analysis of clathrin-mediated endocytosis of epidermal growth factor receptor by RNA interference. *J Biol Chem* 279:16657-16661.

Huang, S.S., and J.S. Huang. 2005. TGF-beta control of cell proliferation. *J Cell Biochem* 96:447-462.

Jackson, A.P., and P. Parham. 1988. Structure of human clathrin light chains. Conservation of light chain polymorphism in three mammalian species. *J. Biol. Chem* 263:16688-16695.

Jin, L., K.B. Pahuja, K.E. Wickliffe, A. Gorur, C. Baumgartel, R. Schekman, and M. Rape. 2012. Ubiquitin-dependent regulation of COPII coat size and function. *Nature* 482:495-500.

Kirchhausen, T., P. Scarmato, S.C. Harrison, J.J. Monroe, E.P. Chow, R.J. Mattaliano, K.L. Ramachandran, J.E. Smart, A.H. Ahn, and J. Brosius. 1987. Clathrin light chains LC$_a$ and LC$_b$ are similar, polymorphic, and share repeated heptad motifs. *Science* 236:320-324.

Klein, J., W. Ju, J. Heyer, B. Wittek, T. Haneke, P. Knaus, R. Kucherlapati, E.P. Bottinger, L. Nitschke, and B. Kneitz. 2006. B cell-specific deficiency for Smad2 in vivo leads to defects in TGF-beta-directed IgA switching and changes in B cell fate. *J Immunol* 176:2389-2396.

Le Roy, C., and J.L. Wrana. 2005. Clathrin- and non-clathrin-mediated endocytic regulation of cell signalling. *Nat Rev Mol Cell Biol* 6:112-126.

Legendre-Guillemin, V., M. Metzler, J.F. Lemaire, J. Philie, L. Gan, M.R. Hayden, and P.S. McPherson. 2005. Huntingtin interacting protein 1 (HIP1) regulates clathrin assembly through direct binding to the regulatory region of the clathrin light chain. *J. Biol. Chem.* 280:6101-6108.

Majeed, S.R., L. Vasudevan, C.Y. Chen, Y. Luo, J.A. Torres, T.M. Evans, A. Sharkey, A.B. Foraker, N.M. Wong, C. Esk, T.A. Freeman, A. Moffett, J.H. Keen, and F.M. Brodsky. 2014. Clathrin light chains are required for the gyrating-clathrin recycling pathway and thereby promote cell migration. *Nat Commun* 5:3891.

Marchese, A., C. Raiborg, F. Santini, J.H. Keen, H. Stenmark, and J.L. Benovic. 2003. The E3 ubiquitin ligase AIP4 mediates ubiquitination and sorting of the G protein-coupled receptor CXCR4. *Dev Cell* 5:709-722.

Mitchell, H., A. Choudhury, R.E. Pagano, and E.B. Leof. 2004. Ligand-dependent and -independent transforming growth factor-beta receptor recycling regulated by clathrin-mediated endocytosis and Rab11. *Mol Biol Cell* 15:4166-4178.

Poupon, V., M. Girard, V. Legendre-Guillemin, S. Thomas, L. Bourbonniere, J. Philie, N.A. Bright, and P.S. McPherson. 2008. Clathrin light chains function in mannose phosphate

receptor trafficking via regulation of actin assembly. *Proc Natl Acad Sci U S A* 105:168-173.

Rajewsky, K. 1996. Clonal selection and learning in the antibody system. *Nature* 381:751-758.

Schreij, A.M., M. Chaineau, W. Ruan, S. Lin, P.A. Barker, E.A. Fon, and P.S. McPherson. 2015. LRRK2 localizes to endosomes and interacts with clathrin-light chains to limit Rac1 activation. *EMBO Rep* 16:79-86.

Shih, S.C., D.J. Katzmann, J.D. Schnell, M. Sutanto, S.D. Emr, and L. Hicke. 2002. Epsins and Vps27p/Hrs contain ubiquitin-binding domains that function in receptor endocytosis. *Nat Cell Biol* 4:389-393.

Stoddart, A., M.L. Dykstra, B.K. Brown, W. Song, S.K. Pierce, and F.M. Brodsky. 2002. Lipid rafts unite signaling cascades with clathrin to regulate BCR internalization. *Immunity* 17:451-462.

Torrisi, M.R., L.V. Lotti, F. Belleudi, R. Gradini, A.E. Salcini, S. Confalonieri, P.G. Pelicci, and P.P. Di Fiore. 1999. Eps15 is recruited to the plasma membrane upon epidermal growth factor receptor activation and localizes to components of the endocytic pathway during receptor internalization. *Mol Biol Cell* 10:417-434.

Toshima, J.Y., J. Nakanishi, K. Mizuno, J. Toshima, and D.G. Drubin. 2009. Requirements for recruitment of a G protein-coupled receptor to clathrin-coated pits in budding yeast. *Mol Biol Cell* 20:5039-5050.

Townley, A.K., Y. Feng, K. Schmidt, D.A. Carter, R. Porter, P. Verkade, and D.J. Stephens. 2008. Efficient coupling of Sec23-Sec24 to Sec13-Sec31 drives COPII-dependent collagen secretion and is essential for normal craniofacial development. *J Cell Sci* 121:3025-3034.

Wilbur, J., P.K. Hwang, J.A. Ybe, M. Lane, B.D. Sellers, M.P. Jacobson, R.J. Fletterick, and F.M. Brodsky. 2010a. Conformation switching of clathrin light chain regulates clathrin lattice assembly. *Dev. Cell* 18:841-848.

Wilbur, J.D., P.K. Hwang, J.A. Ybe, M. Lane, B.D. Sellers, M.P. Jacobson, R.J. Fletterick, and F.M. Brodsky. 2010b. Conformation switching of clathrin light chain regulates clathrin lattice assembly. *Dev Cell* 18:841-848.

Willinger, T., S.M. Ferguson, J.P. Pereira, P. De Camilli, and R.A. Flavell. 2014. Dynamin 2-dependent endocytosis is required for sustained S1PR1 signaling. *J Exp Med* 211:685-700.

Zhang, Y., M. Meyer-Hermann, L.A. George, M.T. Figge, M. Khan, M. Goodall, S.P. Young, A. Reynolds, F. Falciani, A. Waisman, C.A. Notley, M.R. Ehrenstein, M. Kosco-Vilbois, and K.M. Toellner. 2013. Germinal center B cells govern their own fate via antibody feedback. *J Exp Med* 210:457-464.

Figure Legends

Figure 1. Genetic deletion of CLCa in mice induces postnatal lethality, weight reduction and defects in motor-skills. (A) Recombined *CLTA* genetic construct for targeted deletion of CLCa in all tissues by ACTB-cre-mediated deletion of exon 1 flanked by LoxP sites. Exons are numbered and are indicated by black boxes. White box indicates 5' untranslated region. Primers are designated by orange, blue and black triangles. Black lines below each allele denote PCR products generated from each wildtype (311bp) and CLCa knockout (KO, 682bp). (B) PCR analysis of genomic DNA from wildtype (+/+), heterozygous (-/+) and CLCa homozygous KO (-/-) mice. (C) Indicated tissues from CLCa wildtype (WT) and KO mice were homogenized and analyzed by immunoblotting for CLCa and CLCb using isoform-specific antibodies with CLCa in green and CLCb in red. nCLCa and nCLCb are the neuron-specific splice variants. (D) Indicated tissues from CLCa WT and KO animals were homogenized and immunoblotted for CHC17 and α-tubulin. (E) All pups in multiple litters from heterozygote (CLCa KO/CLCa WT) crosses were genotyped at the indicated time points, and the proportion of CLCa KO homozygotes present compared to expected is shown (mean ± s.e.m. of at least five litters analyzed for each time point *P=0.04, ***P<0.0001; P values, Fisher's exact test). (F) Homozygous CLCa WT and KO male animals were weighed at the indicated time points (mean ± s.e.m. of n=18, ***P<0.001; P values, Two-way ANOVA followed by Bonferroni post test). (G) Homozygous CLCa WT and KO male mice were individually placed on a rotarod and their latency to fall recorded (mean ± s.e.m. of n=12, ***P<0.005; P values, unpaired t-test). (H) Homozygous CLCa WT and KO male mice were assessed for grid-crossing time after being trained to cross the grid 3 times over 2 days prior to the test (mean ± s.e.m. of n=10, *P<0.05; P values, Mann Whitney test).

Figure 2. Murine tissues express characteristic ratios of CLC isoforms and CLCa deletion does not substantially affect CLCb protein or mRNA levels. Concentrations of CLCs per ng of murine tissue from wildtype (WT) and CLCa knockout (KO) animals were determined by quantitative immunoblotting. Dilutions of tissue homogenate were analyzed on the same gel as dilutions of purified human His-tagged CLC proteins of known concentration. Plotted signals in the linear range of each sample were used for comparative quantification.. (A) Immunoblots of brain and spleen tissue homogenates using isoform-specific antibodies are shown as examples, with CLCa in green and CLCb in red. nCLCa and nCLCb are the neuron-specific splice variants. (B) Signals in the linear range generated from characteristic immunoblots for the indicated tissues and purified proteins, used for establishing tissue concentrations of CLCs. (C) The concentrations of each CLC isoform determined for the indicated tissues from WT and KO tissues by comparison to the purified protein standards in each experiment (mean ± s.e.m. of n=3 for each tissue). (D) CLCa mRNA transcript abundance measured by quantitative PCR analysis of indicated tissues from WT mice. Expression is shown relative to levels of hypoxanthine guanine phosphoribosyl transferase (HPRT, mean ± s.e.m. of n=3). (E) CLCb (left) and CHC17 (right) transcript abundance measured by quantitative PCR analysis of the indicated tissues from WT and CLCa KO mice. Expression levels are shown relative to HPRT (mean ± s.e.m. of n=3, except n=2 for brain cortex).

Figure 3. CLCa KO mice have elevated frequency of IgA-expressing B cells. Isolated lymphocytes from wildtype (WT) murine spleens were lysed and analyzed by immunoblotting for expression of the proteins indicated. CLCa and CLCb signals were compared to dilutions of purified human CLCs.. The amount of total protein loaded is indicated above each lane. (B) Abundance of CLCa, CLCb and CHC17 mRNA transcripts in B and T cells isolated from WT spleens determined by quantitative PCR. Expression level is shown relative to HPRT (mean ± s.e.m. of n=3, **P<0.05, unpaired t-test). (C) Total splenocytes and B cells were isolated from

spleens of WT or CLCa knockout (KO) mice were lysed and analyzed by immunoblotting for proteins indicated by arrowheads. (D) Lymphocytes isolated from Peyer's patches of unimmunized WT and CLCa KO animals were immunolabeled for the markers indicated. B220-positive cells were first gated on CD95^{high} and IgD^{low} expression, and then gated on GL7^{high} expression to identify germinal center B cells (GC B). Follicular B cells (Fo B) were identified by CD95^{low} and IgD^{high} expression. (E and F) Flow cytometric analysis (E) and quantification (F) of the frequency of IgA and IgG1-expressing GC B cells in the Peyer's patches of WT and CLCa KO mice, detected by intracellular staining for each antibody isotype. Numbers in (E) indicate the percentage of cells in the respective quadrant (mean ± s.e.m. of n=19, * $P<0.01$, **$P<0.05$, unpaired t-test) (G) Mixed bone marrow chimeras (WT/B6 and CLCa KO/B6) were generated by injection of cells from CLCa WT or KO mice (CD45.2^{+}) mixed in a 1:1 ratio with bone marrow cells from WT C57BL/6 (B6) mice (CD45.1^{+} CD45.2^{+}) into irradiated recipient B6 mice (CD45.1^{+}). Surviving cells from each donor in the GC and Fo B cell populations from Peyer's patches of chimeric animals were analyzed based the gating scheme shown. (H and I) Flow cytometric analysis (H) and quantification (I) of the frequency of IgA and IgG1-producing GC B cells in Peyer's patches of mixed chimera mice (mean ± s.e.m. of n=19 from at least 4 pairs of donors for mixed chimera mice, **$P<0.05$, ns means not significant, one-way ANOVA) (J) Graph depicting the percentage of GC B cells relative to Fo B cell population in mixed bone marrow chimeras. (mean ± s.e.m.; n>26 for mesenteric lymph node (mLN), n=42 for Peyer's patches (PP), n>10 for spleen, **$P<0.05$, *** $P<0.001$, unpaired t-test). Each dot in F, I, and J represents one mouse. X- and Y-axes represent fluorescence intensity in (D, E, G and H).

Figure 4. Loss of CLCa increases surface levels of TGFβR2 in B cells. (A) Surface expression of TGFβR2 and B220 on GC and Fo B cells from Peyer's patches (left) and total B cells from spleen (right) determined by flow cytometry (gating as in Figure 3D). X-axes

represent fluorescence intensities and relative counts indicated by Y-axes are normalized to the maximum cell count. (B) Quantification of TGFβR2 and B220 surface fluorescent labeling from (A) in Peyer's patches (left) and spleen (right). Data is presented as geometric mean fluorescent intensity (MFI; n=11 for PP and n=5 for spleen, * $P<0.01$, unpaired t test). (C) TGFβR1 and TGFβR2 mRNA abundance in wildtype (WT) and knockout (CLCa KO) spleen B cells determined by quantitative PCR. Expression is shown relative to HPRT (mean ± s.e.m. of n=3). (D) B cells purified from WT and CLCa KO were lysed and analyzed by immunoblotting for TGFβR2 and other proteins indicated by arrowheads.

Figure 5. CLCa regulates TGFβR2 signaling and internalization. (A) Surface levels of TGFβR2 and B220 on GC and Fo B cells in Peyer's patches from mixed chimera mice measured by flow cytometry. Background staining is show in tinted coloring. (B) The ratio of the geometric MFI of WT or CLCa KO (CD45.2[+]) to B6 (CD45.1[+]CD45.2[+]) for TGFβR2 and B220 is shown for GC (right) and Fo B (left) cells (mean ± s.e.m. of n=10 from at least 3 pairs of different donors for mixed chimera mice, ** $P<0.05$, *** $P<0.001$, unpaired, t-test). (C) Total splenocytes and purified B cells from WT and CLCa KO spleens were lysed and analyzed by western blot for CHC17, phophorylated Smad2/3 (pSmad2/3), and CLCa. A representative blot of several experiments is shown (D) Quantification of pSmad2/3 levels in WT and CLCa KO mice from western blots in (C). pSmad2/3 levels were normalized to CHC17 protein levels (n=5 for total splenocytes and n=2 for purified spleen B cells, * $P<0.01$, one-way ANOVA). (E) HEK293T cells were treated with the indicated siRNA for 72 hours and transiently transfected with TGFβR2-IRES-GFP, then lysed for western blot analysis. (F) siRNA-treated HEK293T cells transiently transfected with TGFβR2-IRES-GFP were surface labeled with anti-TGFβR2 antibody on ice for 30 minutes, and then allowed to internalize the antibody for the indicated time points at 37°C, after which they were immediately placed on ice. Cells were then labeled with Alexafluor

conjugated secondary antibody and analyzed by flow cytometry. Only GFP-expressing cells were included in the analysis, and TGFβR2 MFI was normalized to GFP MFI. Graph indicates the proportion of TGFβR2 internalized at the indicated time points compared to steady state levels (mean ± s.e.m. of n=5 independent experiments, ***$P<0.001$; P values, Two-way ANOVA followed by Bonferroni post test). (G) siRNA-treated HEK293T cells transiently transfected with TGFβR2-IRES-GFP were surface labeled with transferrin receptor (TfR) antibody on ice for 30 minutes, and then allowed to internalize the antibody for the indicated time points at 37°C, after which they were immediately placed on ice. Cells were then labeled with Alexafluor conjugated secondary antibody and analyzed by flow cytometry. Graph indicates the proportion of TfR internalized at the indicated time points compared to steady state levels (mean ± s.e.m. of n=5 independent experiments, ***$P<0.001$; P values, Two-way ANOVA followed by Bonferroni post test).

Figure 6. CLCa-deficient germinal center B cells have increased CXCR4 surface levels.
(A) Surface levels of CXCR4 or B220 on GC B cells from Peyer's patches of wildtype (WT) and CLCa knockout (KO) mice analyzed by flow cytometry. (B) Quantification of CXCR4 and B220 surface labeling of germinal center (GC) B cells from (A) Peyer's patches (left) and mesenteric lymph nodes (mLN; right). Data is presented as geometric mean fluorescent intensity (MFI; n=5 for PP and n=10 for spleen, * $P<0.01$, unpaired t test). (C) Surface levels of CXCR4 or B220 on germinal center B cells from Peyer's patches in mixed chimera mice, measured by flow cytometry, separated by donor genotype. WT is indicated in black, KO in red and B6 in blue. (D) Ratios of the geometric MFI of labeling for CXCR4 or B220 on WT or CLCa KO donor cells (CD45.2$^+$) to B6 donor cells (CD45.1$^+$CD45.2$^+$) for GC B cells from Peyer's patches (left), mLN (middle) and spleen (right) from mixed bone marrow chimera mice (mean ± s.e.m.; n=26 for mLN, n=42 for PP, n>10 for spleen, from at least 3 pairs of different donors for mixed chimera

mice, ** *P*<0.05, *** *P*<0.001, unpaired, t-test). X-axes represent fluorescence intensities and Y-axes indicate relative count normalized to the maximum cell count in (A and C).

Figure 7. CLCa loss impairs ligand-induced internalization of CXCR4 in B cells. (A) Germinal center (GC) and follicular (Fo) B cells isolated from the mesenteric lymph nodes (mLNs) of wildtype (WT) and CLCa knockout (KO) mice were treated with PBS or 100ng/mL SDF (Stromal cell-derived factor 1) for 10 or 30 minutes at 37°C, then immediately chilled and CXCR4 surface levels assessed by flow cytometry. Plots depict one representative experiment. X-axes represent fluorescence intensities and Y-axes represent cell count normalized to the maximum count (B) Quantitative analysis of the proportion of CXCR4 internalized after addition of SDF relative to PBS-treated controls at the indicated time points is shown for Fo B cells (left) and GC B cells (right) from mLNs (mean ± s.e.m. of n=5 WT and n=6 CLCa KO from 2 independent experiments, ** *P*<0.01, two-way ANOVA with Bonferroni post tests). (C) SDF-induced internalization of CXCR4 on GC and Fo B cells isolated from mLNs of WT/B6 and CLCa KO/B6 mixed chimeras was measured as in (A). Quantitative analysis of the ratio of the proportion of surface CXCR4 remaining on WT or CLCa KO donor cells (CD45.2$^+$) to the proportion remaining on B6 donor cells (CD45.1$^+$CD45.2$^+$) in the mixed bone marrow chimera is shown for the indicated time points, with Fo B cells on the left and GC B cells on the right (mean ± s.e.m. of n=6 WT and n=7 CLCa KO mice from 4 independent experiments, * *P*<0.01, ** *P*<0.05, *** *P*<0.001, two-way ANOVA with Bonferroni post tests).

Figure 8. CLCa is not required for internalization of CXCR5 in B cells.. (A) Mean fluorescence intensity (MFI) for CXCR5 and B220 on wildtype (WT) or CLCa knockout (KO) donor cells (CD45.2$^+$) relative to MFI of B6 donor cells (CD45.1$^+$CD45.2$^+$) in the same mixed bone marrow chimera on Fo (left) and GC B cells (right) from mLNs (mean ± s.e.m.; n=11). (B) GC and Fo B cells isolated from the mLNs of WT and CLCa KO mice were treated with PBS or

1μg/ml B lymphocyte chemoattractant (BLC) for 10 or 30 minutes at 37°C, after which they were

immediately chilled and CXCR5 surface expression assessed by flow cytometry. One

representative experiment is shown. X-axes indicate fluorescence intensities and Y-axes

represent relative cell counts normalized to the maximum count (C) The proportion of CXCR5

internalized after addition of BLC relative to PBS-treated controls at the indicated time points is

shown for Fo B cells (left) and GC B cells (right) from the mLN (mean ± s.e.m. of n= 5 WT and 5

CLCa KO mice, from 2 independent experiments). (D) BLC-induced internalization of CXCR5 on

Fo and GC B cells isolated from WT/B6 and CLCa KO/B6 mixed chimeras was measured as in

(B). The ratio of the proportion of surface CXCR5 remaining on WT or CLCa KO donor cells

(CD45.2$^+$) to B6 donor cells (CD45.1$^+$CD45.2$^+$) in the same mixed bone marrow chimera is

shown for the indicated time points, with Fo B cells on the left and GC B cells on the right

(mean ± s.e.m. of n=2 and n= 3 KO mice from 2 independent experiments).

Figure 9. CLC depletion does not affect uptake of β2-adrenergic receptor, but does impair

internalization of the delta-opioid receptor. (A & B) HEK293 cells that stably expressed (A)

FLAG-tagged β2-adrenergic receptor (FLAG-β2AR) or (B) FLAG-tagged delta-opioid receptor

(FLAG-DOR) were treated with the indicated siRNA for 72 hours and then analyzed by

immunobloting for levels of the indicated proteins. (C-F) HEK293 cells stably expressing the

indicated FLAG-tagged receptor were either treated with control siRNA or siRNA for CHC17 or

CLCab knockdown (KD) for 72 hours, then serum starved for 15 minutes, followed by treatment

with agonist (10μM DPDPE or isoproterenol) at 37°C for the indicated time points. (C & E) Cells

were then surface labeled with anti-FLAG antibody at 4°C and analyzed by flow cytometry.

Graph on the left indicates the proportion of receptor internalized after ligand addition at the

indicated time points compared to untreated controls. The plots on the right depict the

fluorescent surface receptor intensity (x-axis) at each indicated time point from one

representative experiment measured by flow cytometry (mean ± s.e.m. of n=4 independent

experiments, *$P<0.05$, **$P<0.01$, ***$P<0.001$; *P* values, Two-way ANOVA followed by Bonferroni

post test). (D & F) Cells from the same treatments as in C & E were surface labeled with

antibody to transferrin receptor (TfR) at 4°C for 30 minutes, and then allowed to internalize the

antibody for the indicated time points at 37°C. Cells were then analyzed by flow cytometry for

residual surface antibody. Graph on the left indicates the proportion of TfR internalized at the

indicated time points compared to control cells that remained chilled at 4°C. The plots on the

right show the surface receptor fluorescent intensity (x-axis) at each time point from one

representative experiment measured by flow cytometry (mean ± s.e.m. of n=3 independent

experiments, ***$P<0.001$; *P* values, Two-way ANOVA followed by Bonferroni post test).
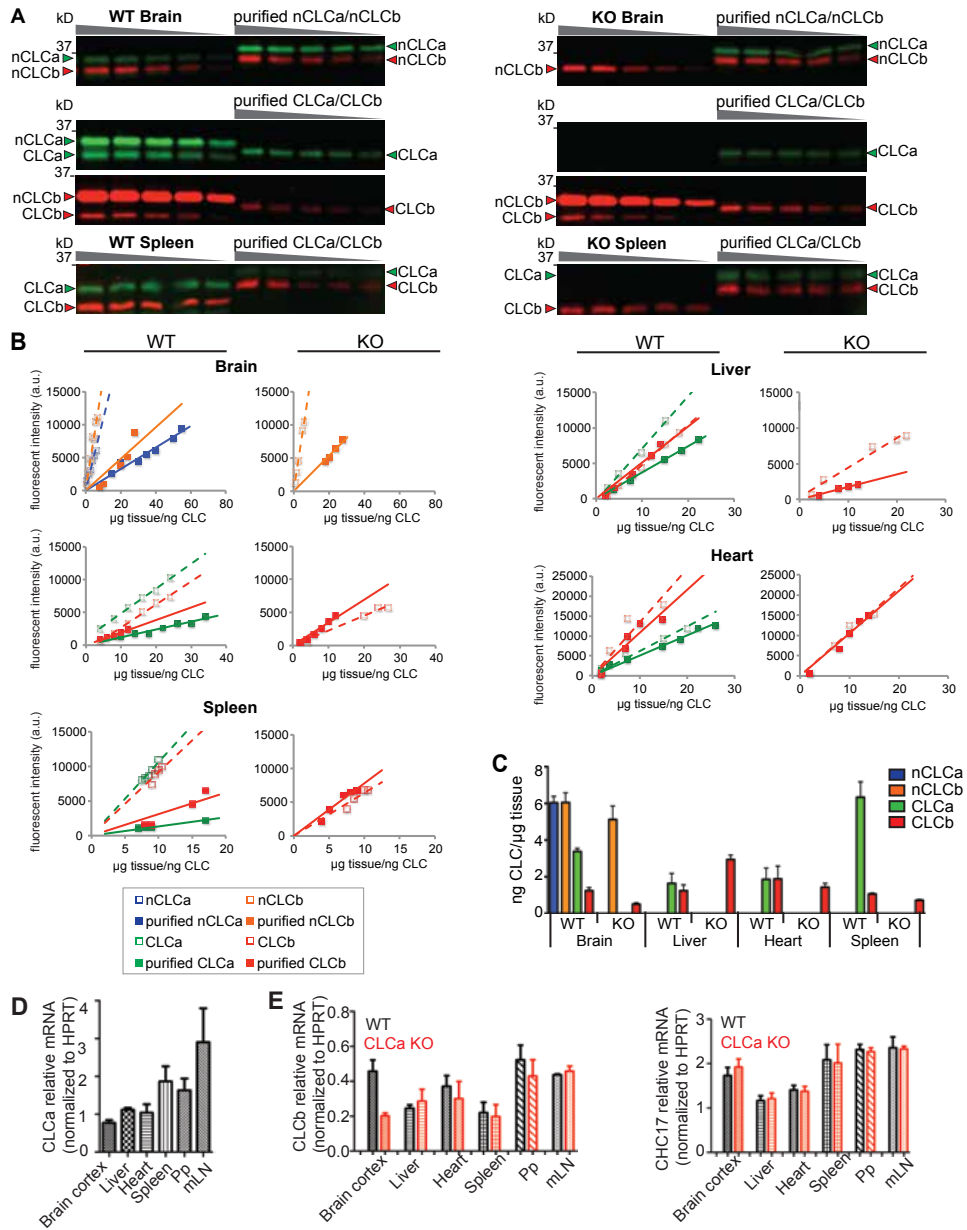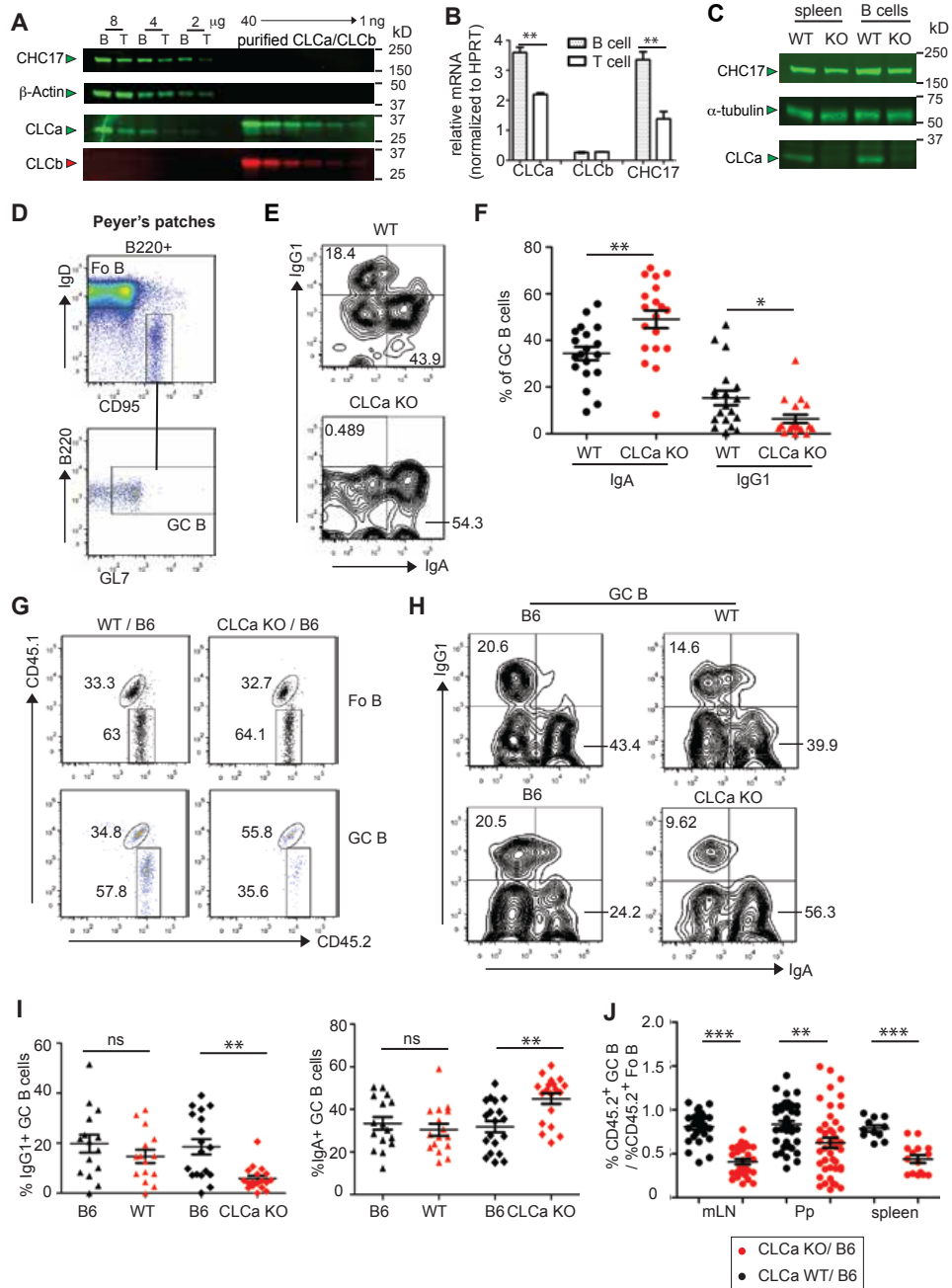
Figure 3-1
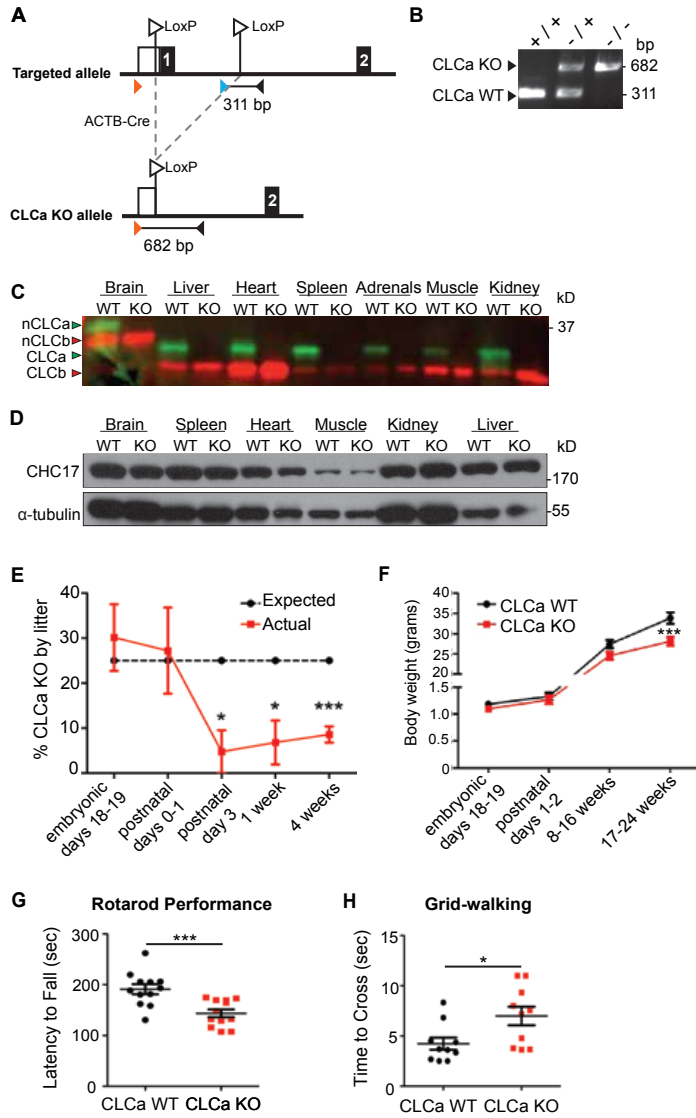
Figure 3-2

Figure 3-3

Figure 3-4
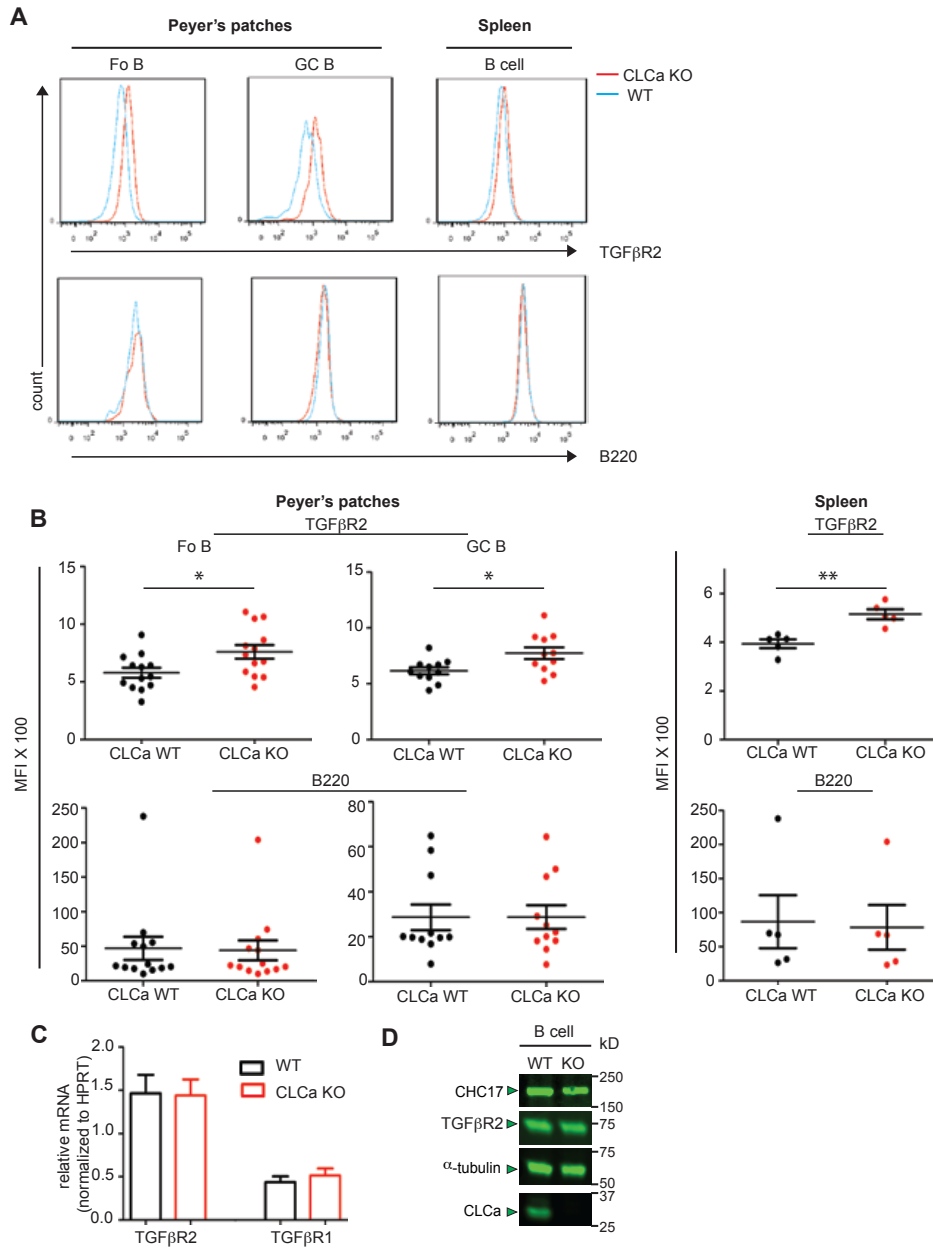
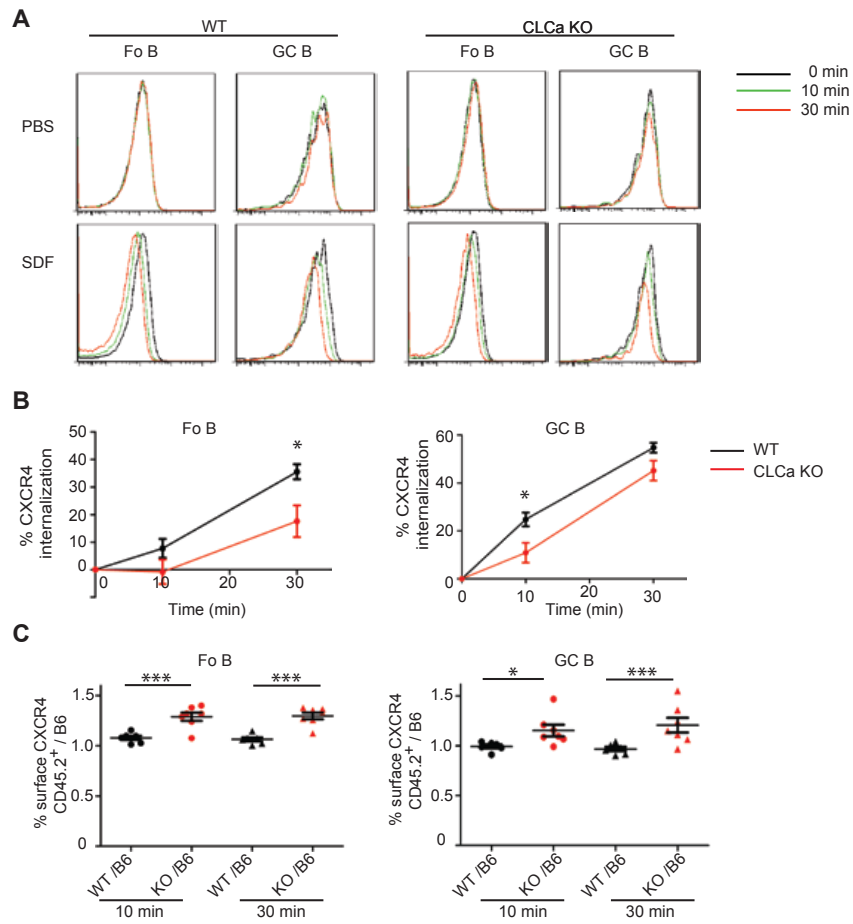**Figure 3-5**
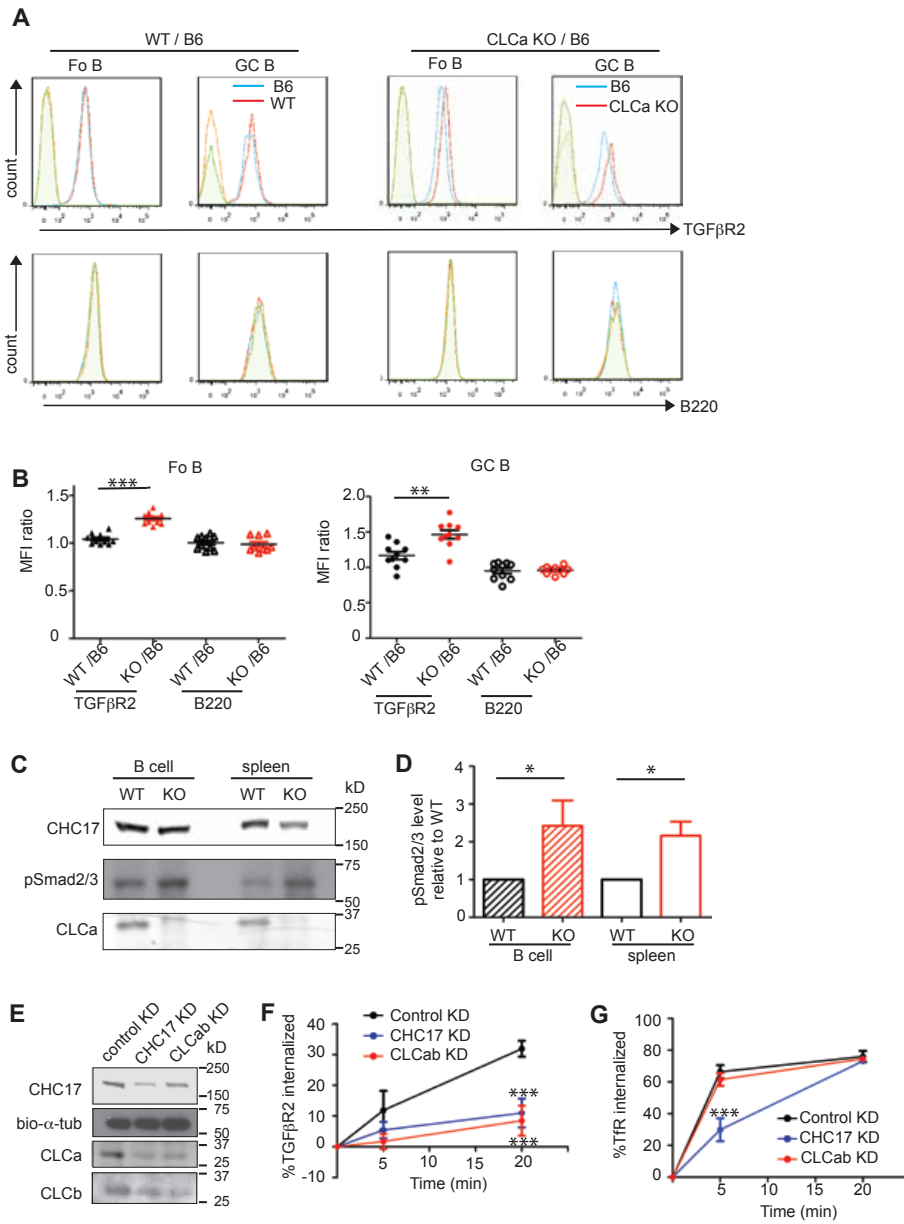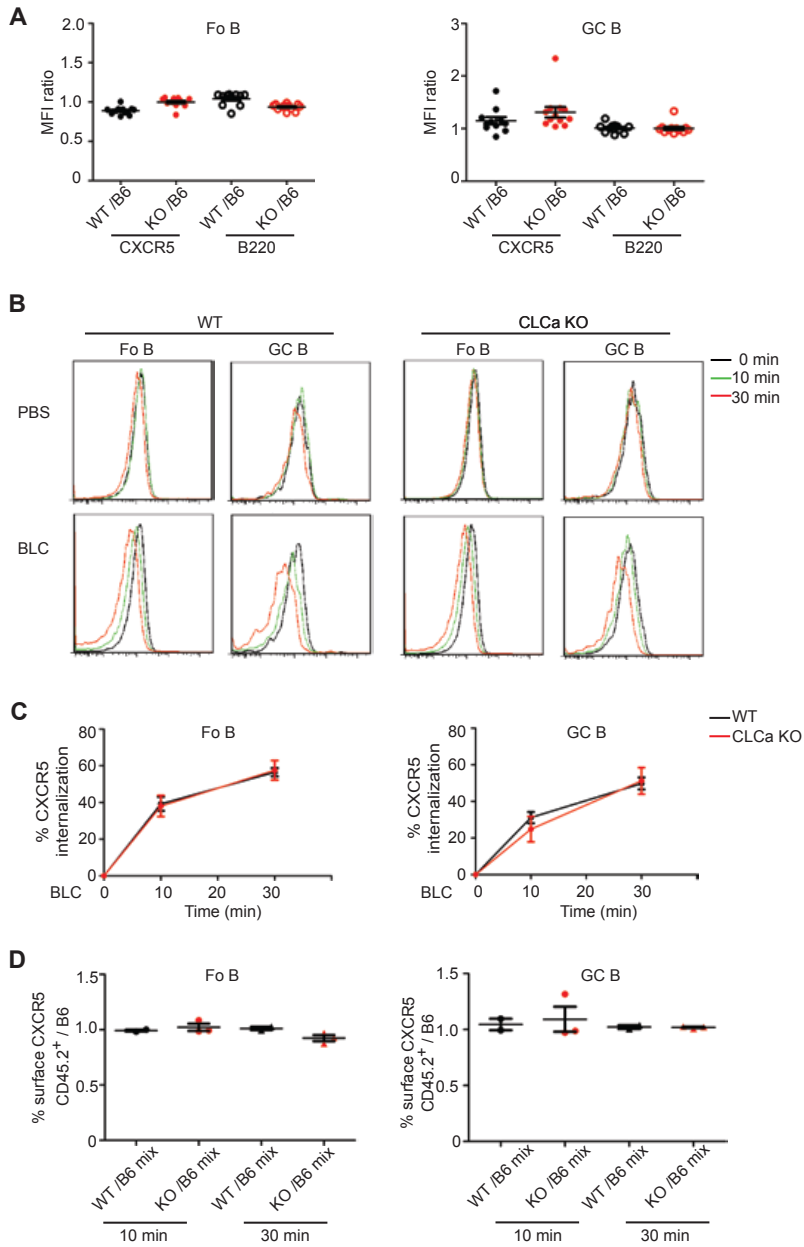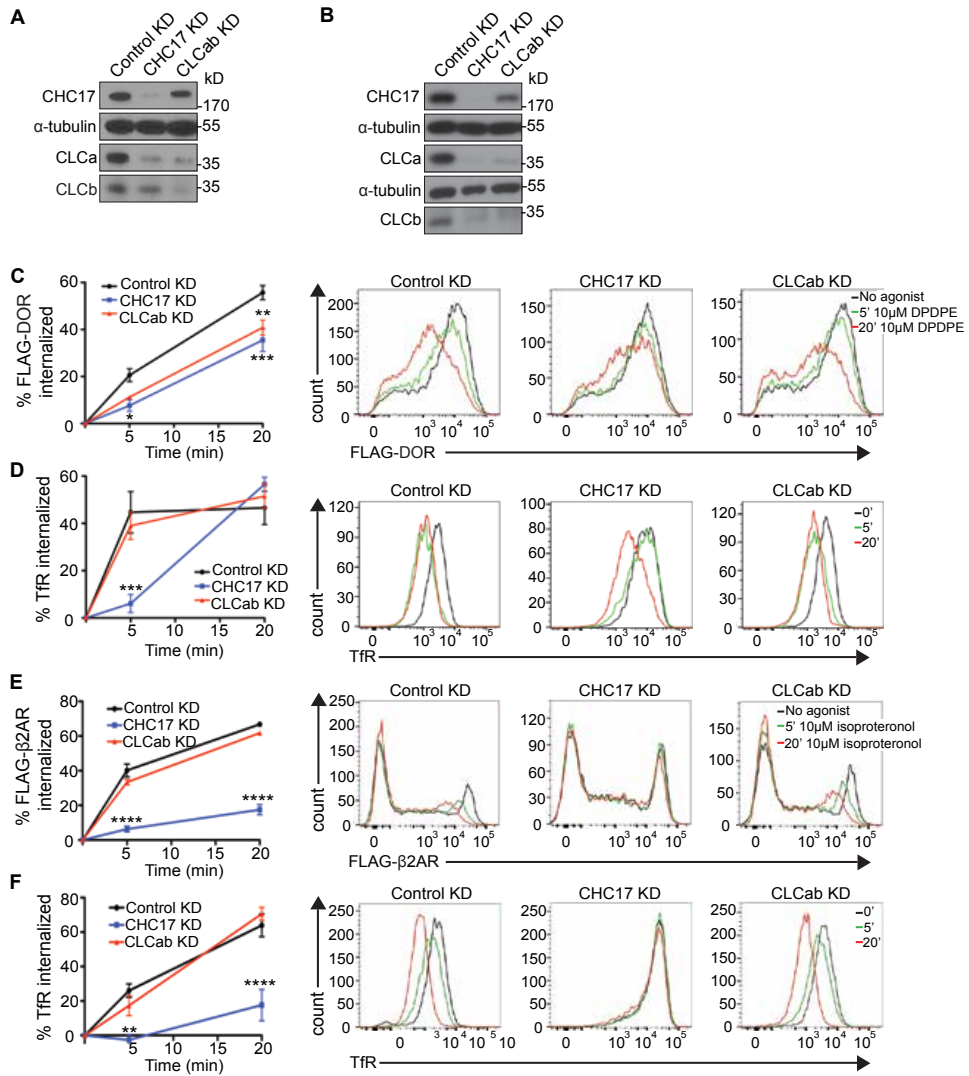
Figure 3-6
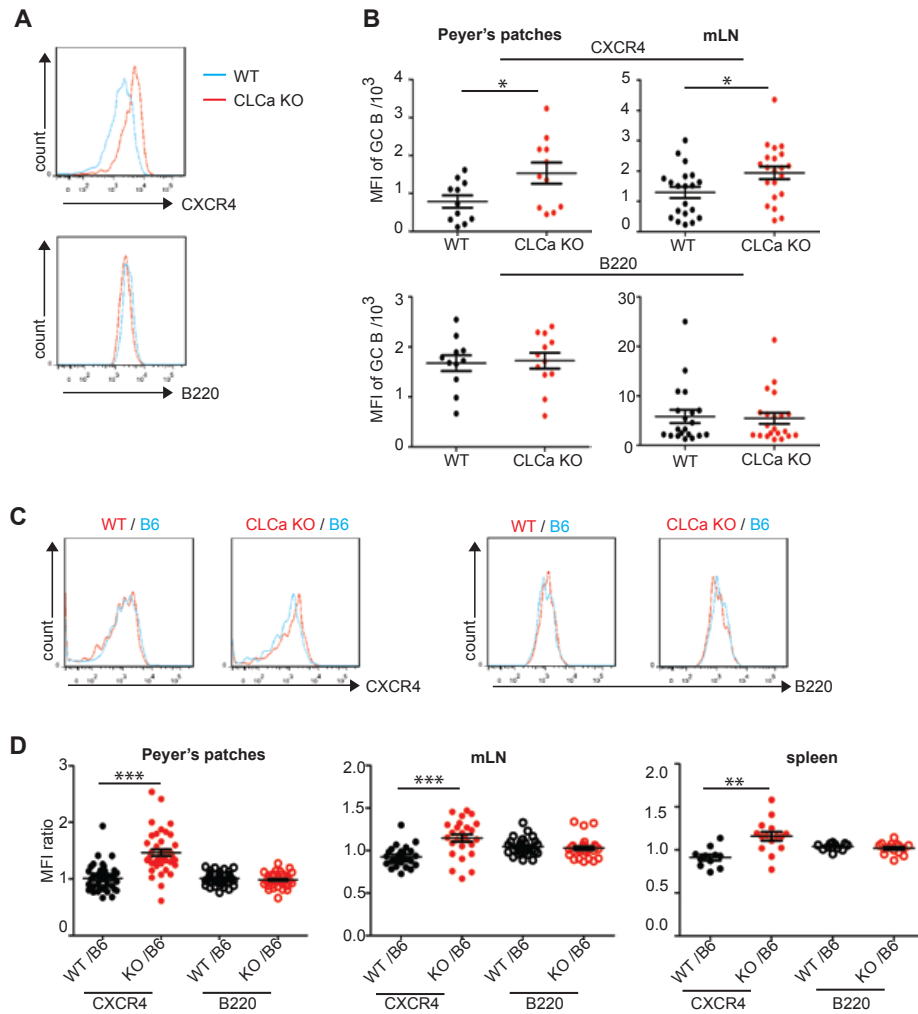
Figure 3-7

Figure 3-8

Figure 3-9

4. Chapter 4: Conclusions and Perspectives

Clathrin was the first coat protein to be identified forty years ago by Pearse, and the cellular functions and biochemistry for the CHC17 heavy chain subunit have since been characterized (Pearse 1976). Clathrin is recruited to membranes by adaptor proteins, where it provides force to bend membranes on budding vesicles for membrane traffic (Stachowiak, Brodsky, and Miller 2013). Recently, several functions for the light chain subunits have been defined. Many of these functions involve CLCs' ability to organize actin through their interaction with Hip proteins (Wilbur et al. 2010; Wilbur et al. 2008; Bonazzi et al. 2011; Bonazzi et al. 2012; Boulant et al. 2011). The goal of this work was to characterize additional CLC functions in cell lines and *in vivo*.

CHC17 plays a critical role in cell migration. It is required for turnover of β1 integrin adhesion proteins (Teckchandani et al. 2012; Teckchandani et al. 2009; Nishimura and Kaibuchi 2007). Since CLCs can coordinate actin assembly through Hip binding, we hypothesized that CLCs have a functional role in cell motility exclusive of CME. In chapter 2, we defined a functional role for CLCs in cell migration using siRNA-mediated depletion of both CLC subunits in studies of cell lines. We observed that CLC-depleted cells had smaller and fewer focal adhesions compared to control and CHC17-depleted cells, in addition to impaired cell migration. We attributed this phenotype to CLCs role in promoting clathrin-mediated recycling of inactive β1 integrins.

Both siRNA-mediated depletion of CLC and inhibition of CLC function through expression of a dominant-negative CLC reduced the appearance of gyrating (G)-clathrin structures, which mediate rapid recycling of transferrin receptor (Zhao and Keen 2008; Luo, Zhan, and Keen 2013). Indeed, expression of the dominant-negative CLC likewise reduced recycling of transferrin receptor. While we were unable to visualize the presence of β1 integrins in G-clathrin structures due to technical difficulties, these results suggest that β1 integrins are

sequestered into G-clathrin coated tubules for recycling. To determine the physiological

relevance of our findings, we performed additional studies examining changes in protein

expression during differentiation of placenta cells from non-invasive villous trophoblasts to

invasive extra-villous trophoblasts. CLCb protein expression was up regulated during this

transition to an invasive phenotype, while levels of CLCa and CHC17 remained unchanged,

indicating that the CLCs are important for cell migration during physiologically significant

processes such as differentiation.

Taken together, these studies define a novel role for the CLCs in cell migration. They

add to the growing list of CLC-Hip dependent functions, strengthening the importance of CLCs

as a link between membrane traffic and the cell's actin machinery. This work also suggests that

the CLCs make significant contributions to both normal developmental and differentiation

programs, in addition to pathologies that require cell migration, including pregnancy and

malignancy. Previous studies in the Brodsky lab have demonstrated that the CLC-Hip protein

interaction can be inhibited by expression of a construct containing the consensus sequence of

CLCs fused to GFP, which contains the binding site for Hip proteins (Chen and Brodsky 2005).

Thus, this interaction can potentially be targeted for therapeutic purposes as an anti-metastatic

strategy. Further work will need to be done to address whether inhibiting CLC-Hip binding is

sufficient to prevent the spread of cancer.

The majority of studies that have characterized CLC functions, including those described

above, have been carried out in cell lines. This led us to ask which of these functions were

physiologically important in an *in vivo* vertebrate model. In chapter 3 we addressed this by

genetically engineering mice lacking the CLCa isoform. Analysis of murine tissue from wild type

mice showed that lymphoid tissues, including the spleen, mesenteric lymph node and Peyer's

patches expressed predominantly CLCa, so we focused our studies on cells from these tissues

in the CLCa knockout mice. We observed that the mutant mice had defects in immunoglobulin

class switching between IgA and IgG, a process regulated by signaling through TGFβR2.

Further analysis of TGFβR2 revealed that surface levels of the receptor and downstream

signaling were increased in the germinal center B cells from the knockout mice compared to

controls. To address whether this phenotype was the result of defects in CME caused by loss of

the CLCa, we performed internalization experiments in cell lines, which indicated that CLCs are

required for CME of TGFβR2. These results define a new role for CLCs in regulating immune

cell function and highlight the importance of CLCs in adaptive immune responses.

In addition to TGFβR2, we investigated surface levels of other cargo important for B cell

function. We observed increased surface expression of CXCR4 on germinal center B cells,

while levels of other cargoes such as CXCR5 and B220 remain unchanged. To address whether

this was a result of defective CME of CXCR4 in the CLCa KO cells, we performed internalization

experiments and found that CLCs were indeed required for CME of CXCR4, but not CXCR5.

These results implicate the CLCs in cargo selection for CME. We further extended our

observations in studies of cell lines and found that CLCs were necessary for CME of F-DOR,

but not F-β2AR. All in all, these data broaden the range of cargo that require CLCs for CME

beyond the initial group of 3 GPCRs that were identified previously (Ferreira et al. 2012).

Furthermore, they demonstrate that CLCs make crucial contributions to CME, possibly through

their actin-organizing function.

Studies of another major coat protein in eukaryotes, COPII, demonstrated that the

Sec13 component of this coat confers structural rigidity and is thus necessary to promote

membrane curvature to form vesicles around asymmetric or rigid cargo such as collagen

(Townley et al. 2008; Copic et al. 2012). Likewise, structural models of CLCs indicate that they

can impact curvature of the clathrin coat by regulating flexibility of the clathrin triskelia,

suggesting that CLCs may be required to generate the necessary force to bend membranes

around certain cargo (Wilbur et al. 2010; Dannhauser et al. 2015). Since CLCs can influence

local actin assembly through Hip binding, it is possible that CLCs can further add tensile

114

strength to the clathrin coat by promoting actin polymerization to extend or pinch the neck of budding vesicles. Additional studies that assess the contributions of Hip proteins and actin assembly for CME of CLC-dependent cargo will be needed to address this hypothesis.

In summary, this work defines a new role for CLCs in cell migration, clathrin-mediated recycling, and immune cell function. It further characterizes the physiological function of the CLCs *in vivo* and broadens their involvement in CME. These studies demonstrate that while the CLCs are dispensable for the CME of many classical cargoes such as transferrin receptor and EGF-receptor, they make significant contributions to other specialized clathrin functions through their influence on actin assembly. This includes clathrin-mediated recycling and possibly cargo selection for CME, which are shared functions for both CLCs. This work demonstrates that these CLC functions impact a diverse range of cellular processes including cell migration and immunoglobulin class switching.

Studies of CLCa KO mice revealed that the CLCs make important contributions to clathrin functions *in vivo* and that they can generally compensate for each other. Since the CLCs only share ~60% sequence similarity at the protein level and have distinct tissue-specific expression patterns, it is likely that they also have some differential functions (Brodsky et al. 2001). Further biochemical and *in vivo* studies will be needed to identify isoform-specific functions. In conclusion, these results exemplify the important role membrane traffic pathways play in a broad range of physiological processes, including maintenance of homeostasis, development and adaptive immune responses.

References

Bonazzi, M., A. Kuhbacher, A. Toledo-Arana, A. Mallet, L. Vasudevan, J. Pizarro-Cerda, F. M. Brodsky, and P. Cossart. 2012. 'A common clathrin-mediated machinery co-ordinates cell-cell adhesion and bacterial internalization', *Traffic*, 13: 1653-66.

Bonazzi, M., L. Vasudevan, A. Mallet, M. Sachse, A. Sartori, M. C. Prevost, A. Roberts, S. B. Taner, J. D. Wilbur, F. M. Brodsky, and P. Cossart. 2011. 'Clathrin phosphorylation is required for actin recruitment at sites of bacterial adhesion and internalization', *J Cell Biol*, 195: 525-36.

Boulant, S., C. Kural, J. C. Zeeh, F. Ubelmann, and T. Kirchhausen. 2011. 'Actin dynamics counteract membrane tension during clathrin-mediated endocytosis', *Nat Cell Biol*, 13: 1124-31.

Brodsky, F. M., C. Y. Chen, C. Knuehl, M. C. Towler, and D. E. Wakeham. 2001. 'Biological basket weaving: formation and function of clathrin-coated vesicles', *Annu Rev Cell Dev Biol*, 17: 517-68.

Chen, C. Y., and F. M. Brodsky. 2005. 'Huntingtin-interacting protein 1 (Hip1) and Hip1-related protein (Hip1R) bind the conserved sequence of clathrin light chains and thereby influence clathrin assembly in vitro and actin distribution in vivo', *J Biol Chem*, 280: 6109-17.

Copic, A., C. F. Latham, M. A. Horlbeck, J. G. D'Arcangelo, and E. A. Miller. 2012. 'ER cargo properties specify a requirement for COPII coat rigidity mediated by Sec13p', *Science*, 335: 1359-62.

Dannhauser, P.N., M. Platen, H. Boning, H. Ungewickell, I.A. Schaap, and E.J. Ungewickell. 2015. Effect of clathrin light chains on the stiffness of clathrin lattices and membrane budding. *Traffic* 16:519-533.

Ferreira, F., M. Foley, A. Cooke, M. Cunningham, G. Smith, R. Woolley, G. Henderson, E. Kelly, S. Mundell, and E. Smythe. 2012. 'Endocytosis of G protein-coupled receptors is regulated by clathrin light chain phosphorylation', *Curr Biol*, 22: 1361-70.

Luo, Y., Y. Zhan, and J. H. Keen. 2013. 'Arf6 regulation of Gyrating-clathrin', *Traffic*, 14: 97-106.

Nishimura, T., and K. Kaibuchi. 2007. 'Numb controls integrin endocytosis for directional cell migration with aPKC and PAR-3', *Dev Cell*, 13: 15-28.

Pearse, B. M. 1976. 'Clathrin: a unique protein associated with intracellular transfer of membrane by coated vesicles', *Proc Natl Acad Sci U S A*, 73: 1255-9.

Stachowiak, J. C., F. M. Brodsky, and E. A. Miller. 2013. 'A cost-benefit analysis of the physical mechanisms of membrane curvature', *Nat Cell Biol*, 15: 1019-27.

Teckchandani, A., E. E. Mulkearns, T. W. Randolph, N. Toida, and J. A. Cooper. 2012. 'The clathrin adaptor Dab2 recruits EH domain scaffold proteins to regulate integrin beta1 endocytosis', *Mol Biol Cell*, 23: 2905-16.

Teckchandani, A., N. Toida, J. Goodchild, C. Henderson, J. Watts, B. Wollscheid, and J. A. Cooper. 2009. 'Quantitative proteomics identifies a Dab2/integrin module regulating cell migration', *J Cell Biol*, 186: 99-111.

Townley, A. K., Y. Feng, K. Schmidt, D. A. Carter, R. Porter, P. Verkade, and D. J. Stephens. 2008. 'Efficient coupling of Sec23-Sec24 to Sec13-Sec31 drives COPII-dependent collagen secretion and is essential for normal craniofacial development', *J Cell Sci*, 121: 3025-34.

Wilbur, J. D., C. Y. Chen, V. Manalo, P. K. Hwang, R. J. Fletterick, and F. M. Brodsky. 2008. 'Actin binding by Hip1 (huntingtin-interacting protein 1) and Hip1R (Hip1-related protein) is regulated by clathrin light chain', *J Biol Chem*, 283: 32870-9.

Wilbur, J. D., P. K. Hwang, J. A. Ybe, M. Lane, B. D. Sellers, M. P. Jacobson, R. J. Fletterick, and F. M. Brodsky. 2010. 'Conformation switching of clathrin light chain regulates clathrin lattice assembly', *Dev Cell*, 18: 841-8.
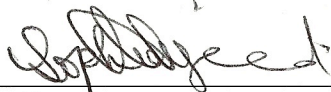
Zhao, Y., and J. H. Keen. 2008. 'Gyrating clathrin: highly dynamic clathrin structures involved in

    rapid receptor recycling', *Traffic*, 9: 2253-64.
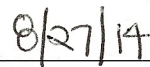
Publishing Agreement

It is the policy of the University to encourage the distribution of all theses, dissertations, and manuscripts. Copies of all UCSF theses, dissertations, and manuscripts will be routed to the library via the Graduate Division. The library will make all theses, dissertations, and manuscripts accessible to the public and will preserve these to the best of their abilities, in perpetuity.

Please sign the following statement:

I hereby grant permission to the Graduate Division of the University of California, San Francisco to release copies of my thesis, dissertation, or manuscript to the Campus Library to provide access and preservation, in whole or in part, in perpetuity.

_____   _____
Author Signature   Date